8/31 Lib. 1041

FOSSIL ENERGY

FE-1770-15
Distribution Category UC-90c

COMPUTER MODELING OF COAL GASIFICATION REACTORS

Annual Progress Report, June 1975—June 1976

1976

Work Performed Under Contract No. E(49-18)-1770

Systems, Science and Software
La Jolla, California

ENERGY RESEARCH AND DEVELOPMENT ADMINISTRATION

NOTICE

TABLE OF CONTENTS

ABSTRACT

General computer models are being developed to provide a theoretical description of gas-solids flows in reactors for coal gasification. These models include representations of fluidized and entrained systems. The first year of research, in a three year project, is described; during this twelve month effort the theoretical formulation of the thermohydrodynamics and chemistry for the fluidized bed flows was developed and incorporated into finite difference computer codes. Calculations, with the thermohydrodynamic code, of nonreactive flows in fluidized beds, were compared with experimental measurements and good qualitative and quantitative agreement was demonstrated. The chemistry code was used to model a homogeneous, constant temperature, steady flow gasifier (CO_2 acceptor process) and good quantitative agreement was obtained between the calculation and pilot plant data. The combination of the thermohydrodynamics and chemistry to provide a model for reactive flows, in the second year of this project, is briefly discussed.

I. OBJECTIVE AND SCOPE OF WORK

The purpose of this program is to develop and apply, over three years, general computer models that will expedite the development and aid in the optimization and scale-up of reactors for coal gasification. Initial applications will be to fluidized bed gasification processes; subsequently both entrained flow reactors and fast fluidized beds will be examined.

During the first year, work will be initiated on the fluidized bed model in the areas of multiphase fluid flow without chemical reactions, and chemical reactions without fluid flow. The computer codes, developed to represent these aspects of gasification processes, will be combined in the second year of the program into a numerical model of reactive flows in fluidized beds. This model will provide a time-dependent field description of fluidized bed flows in two space dimensions. Calculations will be performed with the prototype code during the first and second years to verify the accuracy of the formulations employed and, in the second year, these calculations should provide preliminary results relevant to coal gasification. During the second year a computer model for entrained flow gasifiers will be formulated and the chemistry defined; this model will provide a field description of entrained flows in two space dimensions. Nonreactive flow calculations will be performed for entrained flow processes at the end of the second year.

In the third year the application of the fluidized bed computer model to specific gasifier processes will be extended and a computational model which includes three-dimensional effects will be developed. Also, during this third year the coal chemistry will be combined with the entrained flow computer model and some calculations of such gasifier configurations will be performed.

SECTION 2

SUMMARY OF PROGRESS TO DATE

This was the first year of a three year program to develop and apply general computer models to the gasification processes in fluidized bed and entrained flow reactors. These models are based upon a continuum representation wherein space-averaging techniques are used to describe multiphase transport processes.

In the first year, the research effort was directed to the development of the chemistry and thermohydrodynamic computer models describing fluidized bed gasification processes. To this end, the activities in the first year were organized into five task areas: (1) one-dimensional thermohydrodynamic code development; (2) two-dimensional thermohydrodynamic code development; (3) boundary layer formulation; (4) chemistry code development; and (5) miscellaneous formulations (constitutive representations, interaction functions, mathematical studies). The major efforts were naturally in the second, fourth and fifth task areas with the one-dimensional code development and the boundary layer formulations being adjuncts to the primary development. A brief summary of the progress in these five task areas is presented in the following paragraphs.

- TASK AREA -01: One-Dimensional Thermohydrodynamic Code Development

  This code was developed, tested and sample calculations were compared with existing fluidization data on representative particles, including coals and char. The numerical model represents transient non-reactive flows, with heat exchange in fluidized beds. Test calculations for different flow rates and flow conditions have been performed and we have examined the pressure, temperature and velocity fields in the gas and solid phases. The development of instabilities and the related bubble growth, again in one spatial dimension, have been observed. A comparison of the calculations with existing measurements showed that there was good agreement with data on minimum fluidization, slugging bed velocity correlations and bed expansion measurements.

- TASK AREA -02: Two-Dimensional Thermohydrodynamic Code Development

  This code was developed, tested and qualitative comparisons were made between the calculations and existing data on fluidized bed flows. The numerical model represents transient, non-reactive, fluidized bed flows, in two space dimensions, with heat transfer. A first order, implicit finite difference procedure is used to solve the coupled solid and gas phase equations for conservation of mass, momentum and energy. This numerical method is analogous to that used in the one-dimensional code, but it necessarily includes procedures which are particular to two or more space dimensions. A series of parametric calculations was performed to model the flow from a two-dimensional distributor plate in a shallow bed. The formation and rise of the gas bubbles, together with the interaction of the bubbles with the free surface of the bed were calculated. A motion picture, based upon the computer calculation, shows clearly the transient character of the successive bubble formation at the orifice in the distributor plate. Solid particle convection, including particle entrainment in the wake of the bubbles, was determined from the calculations.

- TASK AREA -03: Boundary Layer Formulation

  A theoretical evaluation of wall effects in gas fluidized beds was undertaken; in addition, a review was conducted of both theoretical models (e.g., the packet model) and experimental data related to heat and mass transfer in fluidized beds. Special classes of flow problems with wall effects were solved analytically to examine the influence of boundary conditions upon the solutions. Conceptual models to treat heat transfer at the walls of the fluidized beds were examined. It is expected that the relative influences of the emulsion and bubble phases upon such transfer will be readily determined from the field description inherent in the numerical formulation of the thermohydrodynamic model (Task Area 02). The quantification of the sub-layer effects (e.g., the particle distribution immediately adjacent to the wall) will be incorporated into an effective heat transfer coefficient.

- TASK AREA -04: Chemistry Code Development

  A chemistry code describing chemical kinetics which occur in coal gasification reactors has been formulated. A particular version of this code, which incorporates the chemistry and kinetics appropriate to the CO_2 acceptor process, was developed and sample calculations were performed. These calculations were shown to be in good agreement with pilot plant data. This code, based upon the assumption of locally uniform spatial distributions of solid particles, gas composition and thermodynamic properties, represents the processes in a single computational zone in the finite difference computer model of a reactor. Alternatively, it can be used to represent the complete reactor during homogeneous operation; in the latter mode, with gas and solid feed rates appropriate to the Conoco Rapid City Pilot Plant, the code has been used to calculate the start-up and time-dependent evolution to steady state of the CO_2 acceptor process. The calculated exit stream flow rates, exit stream compositions and reactor materials inventory, at steady state, are in very good agreement with both direct measurements and estimated data from the pilot plant.

- TASK AREA -05: Miscellaneous Formulations (Constitutive Representations, Interaction Functions, Mathematical Studies)

  Interaction functions which represent the coupled influence of solid particles and gas upon each other, together with constitutive equations for the individual phases were developed based upon theoretical formulations and laboratory data. These representations of drag coefficient, solid viscosity, solid pressure and thermal conductivities include, where appropriate, the influences of the solid particle parameters such as shape, diameter, size distribution and density as well as the properties of the gas phase. These functions have been compared with data for non-reactive flows in fluidized beds of coal and char. The functions provide, through numerical calculations (c.f., Task Area 01) good quantitative agreement with those experiments.

A careful examination of the mathematical character of the equations for fluidized beds was also conducted. This study established that the equations were of the hyperbolic-parabolic type and that initial value problems for these fluidized bed equations were well posed.

The progress in the above task areas is according to the planned schedule for the first year of the present contract and it represents the initial stages in an ordered development of a complex computer model of fluidized bed gasification processes. While the accomplishments are essentially of a theoretical nature we also note that the computer codes discussed in Task Areas 02 and 04 can, in their present state of development, be useful tools in the study of fluidized bed phenomena. For example, the two-dimensional thermohydrodynamic code has already been used (c.f., Section 4.4 of this report) to examine parametric variations in gas flow rate upon fluidized bed behavior. In the next year such calculations will be continued, both to learn more about the phenomenology and to also compare the code with experimental measurements. Such parametric calculations, which can also include reactor geometry and distributor plate design, should provide useful design information relative to non-reactive flows in fluidized beds.

The chemistry code in its present representation of the CO_2 acceptor process chemistry can be used to provide a homogeneous model of the transient and steady performance of such reactors. The influences of different feed rates, system transients and chemical kinetics could be examined. In the second year of this contract, the kinetics appropriate to steam-oxygen gasification will be incorporated into that code and it will be possible to use the code to provide a representation of such gasifier processes. Such a representation should be useful in the examination of these reactors as elements in an overall gasification system.

The details of the code development for the first year of the contract and the comparison of the calculations with experimental measurements are examined in the succeeding sections.

SECTION 3

THEORETICAL BASIS FOR THERMOHYDRODYNAMIC MODEL

In this section we present the theoretical development for the numerical model of gas fluidized beds. This development includes portions of the research effort in Task Areas 01, 02, 03 and 05 as summarized in Section 2.

This thermohydrodynamic model is based upon a continuum mathematical representation wherein space-averaging is introduced to describe multiphase transport processes. With this methodology we obtain a field description of the flow processes in fluidized beds which provides the time histories and spatial distributions of important process variables within the reactor. In this model the important details of the flow processes such as the formation and rise of gas bubbles, the exchange of gas between the bubbles and the emulsion region, the entrainment of solid particles in the wake of the bubble and the distribution of gas composition, evolve naturally from the numerical calculations of the field within the fluidized bed. Further, the important influences of the gas phase properties and the nature of the solid particles, such as shape and particle size distribution, are included in the continuum representation.

In Section 3.1 we derive the differential equations for the gas fluidized bed. The mathematical character of these equations, which is important to the validity of the numerical model, is examined in Section 3.2. These equations require the definition of constitutive relationships and interaction functions; such relationships are derived within the context of laboratory data in Section 3.3.

3.1 DIFFERENTIAL EQUATIONS FOR THERMOHYDRODYNAMIC MODEL

In this section the derivation of the conservation equations expressing mass, momentum, energy and chemical species balance is presented. These differential equations account for both interphase transport and flow field fluctuations. From these equations a first order theory without fluctuations has been developed and incorporated into the numerical model of the thermohydrodynamic transport processes.

A continuum mathematical description of flow through fluidized beds requires the application of appropriate averaging techniques (e.g., Murray, 1965; Anderson and Jackson, 1967; Garg and Pritchett, 1975). The model of Anderson and Jackson is particularly attractive because it provides a mathematical structure for the inclusion of fluctuations in a continuum model. In the present report we extend the methodology of Anderson and Jackson to the case of nonisothermal compressible fluid flow with interphase mass exchange between the gas and the solid particles.*

3.1.1 Mathematical Preliminaries

In the Anderson and Jackson methodology, a formal technique, incorporating the concept of a weighting function, is used to replace point variables by local mean variables. Specifically if ψ' is a point variable in the fluid phase of the flow in a fluidized bed, then a local mean variable ψ is defined by:

$$\psi(x_i,t) \int_f g\,(|x_i - y_i|)\, dV\,(y_i)$$

$$= \int_f \psi'\,(y_i,t)\; g\,(|x_i - y_i|)\, dV\,(y_i) \qquad (3.1)$$

where $g\,(|x_i - y_i|) = g(r)$ is the weighting function and where the integrals are taken over the volume occupied by the fluid phase at time t. In these integrals (3.1), the use of repeated subscripts in the arguments of the indicated functions does not imply summation. This notation will be used throughout; tensorial summation will only apply when repeated subscripts appear on the function itself.

The weighting function has the properties

$$r > 0: \quad g(r) \geq 0, \quad \frac{dg(r)}{dr} \leq 0$$

---

*We will explicitly omit spatial integrals of products of fluctuating components in our first order theory. This theory, then, differs from the results of Anderson and Jackson in that we do not lump these integrals with, say, the space-averaged stress tensor.

and

$$4\pi \int_0^{\infty} g(r)\ r^2 dr = 1$$

Further, we require that g(r) possess derivatives of all orders and that the corresponding volume integrals of these derivatives exist. The radius, R, of the weighting function is defined as

$$4\pi \int_0^{R} g(r)\ r^2 dr = \frac{1}{2}$$

If ℓ is a characteristic local dimension of the fluid phase and L is a characteristic dimension of the complete fluid-solid system, it is assumed that

$$\ell << R << L$$

With this restriction, the actual structure of the weighting function is unimportant; the relationship between the local mean porosity ϕ and the weighting function, satisfying the above restrictions can now be stated. This is expressed as

$$\phi(x_i,t) = 1 - \theta(x_i,t) = \int_f g\ (|x_i - y_i|)\ dV\ (y_i) \qquad (3.2)$$

Further, the spatial variation of the local mean variable is small compared with that of the weighting function and we have, with (3.2) that

$$\int_f \psi(y_i,t)\ g\ (|x_i - y_i|)\ dV\ (y_i) \simeq \psi(x_i,t)\phi(x_i,t) \qquad (3.3)$$

Then, if the point variable ψ' is expressed as the sum of the local mean variable ψ and a fluctuation about that mean value ψ'', namely

$$\psi'(x_i,t) = \psi(x_i,t) + \psi''(x_i,t) \tag{3.4}$$

it follows that the local mean value of the fluctuation is much smaller than (3.3), and it can be neglected; that is

$$\int_f \psi''(y_i,t)\, g\,(|x_i-y_i|)\, dV\,(y_i) << \int_f \psi(y_i,t)\, g\,(|x_i-y_i|)\, dV\,(y_i) \approx \psi(x_i,t)\phi(x_i,t) \tag{3.5}$$

This inequality will permit significant simplifications in the derivation of the conservation equations for the local mean variables. In addition, we will need relationships between the temporal and spatial derivatives of the local mean variables and those respective derivatives of the point variables. These relationships are derived by Anderson and Jackson and are given by

$$\int_f \frac{\partial \psi'}{\partial t}(y_i,t)g(|x_i-y_i|)dV(y_i) = \frac{\partial}{\partial t}\phi(x_i,t)\psi(x_i,t) + \int \psi'(y_i,t)\, n_k v_k^b\,(y_i,t)g(|x_i-y_i|)dA(y_i) \tag{3.6}$$

$$\int_f \frac{\partial \psi'}{\partial y_j}(y_i,t)g(|x_i-y_i|)dV(y_i) = \frac{\partial}{\partial x_j}\phi(x_i,t)\psi(x_i,t) - \int \psi'\,(y_i,t)n_j g(|x_i-y_i|)dA(y_i) \tag{3.7}$$

where the integrals on the right hand side of (3.6) are taken over the fluid-solid interface which is a surface bounding the fluid phase and n_j is a unit normal vector directed into the fluid volume; v_k^b is the local velocity of this bounding surface. Since the solid phase is composed of discrete particles, we may write the surface integrals as a summation over the particles, P

$$\int \psi'(y_i,t) n_j g(|x_i-y_i|) dA(y_i) = \sum_P \int_P \psi'(y_i,t) g(|x_i-y_i|) n_j$$

$$dA_p(y_i) \qquad (3.8)$$

There is a strong analogy between the radius R of the weighting function and the linear dimension of the "representative elementary volume" which is used by Bear, 1972, and others to derive averaged equations for flow through porous media. That is, in both cases, the appropriate dimension is very large compared to a characteristic local dimension of the fluid phase, but it is much smaller than a characteristic dimension of the medium in question. Further, the present definition of the local mean value of a point variable is analogous to the spatial average of a point variable, over the void space of the representative elementary volume. For example, Blake and Garg, 1976, have shown that there is formal agreement between the differential equations for solute transport through porous media (or fluidized beds) derived by the present methodology and that derived by Bear. However, the spatial averaging of Anderson and Jackson provides, perhaps, a more explicit description of the respective influences of flow field fluctuations and transport at the gas-solid interfaces.

3.1.2 Conservation Equations for Local Mean Variables

Consider the gas phase in the fluidized bed. We assume that at a point, y_i, in the gas phase, the principles of conservation of mass, momentum and energy can be described by the following differential equations: where tensorial notation is used,

$$\frac{\partial \rho'}{\partial t} + \frac{\partial \rho' v_i'}{\partial y_i} = 0 \qquad (3.8)$$

$$\frac{\partial \rho' v_i'}{\partial t} + \frac{\partial}{\partial y_j} \rho' v_i' v_j' = \frac{\partial \sigma_{ij}'}{\partial y_j} + \rho' g_i \qquad (3.10)$$

$$\frac{\partial}{\partial t}\rho'\left(e' + \frac{v_i'v_i'}{2}\right) + \frac{\partial}{\partial y_j}\rho'v_j'\left(e' + \frac{v_i'v_i'}{2}\right)$$

$$= \frac{\partial}{\partial y_j} v_i'\sigma_{ij}' + \rho' g_i v_i' - \frac{\partial q_i'}{\partial y_i} + H \qquad (3.11)$$

The point variables ρ', v_i', e', σ_{ij}', q_i', H' are respectively the gas density, velocity, specific internal energy, stress tensor, heat flux vector and volumetric heat source. For the present we shall consider that q_i' represents only heat flux by conduction; however, both radiative transport and diffusional transport of heat may be included in this expression (c.f., Penner, 1957 and Bond, et al., 1965). The equations for a single particle, with the assumptions of constant density, rigidity and uniform intraparticle velocity and temperature fields, are

$$\rho^s \frac{dv'}{dt} = \rho^s \int_P (v_i^b - u_i')\, n_j dA_p \qquad (3.12)$$

$$\rho^s \frac{du_i'v'}{dt} = f_i' + \tilde{f}_i' + \rho^s v' g_i + \int_P \rho^s u_i (v_k^b - u_k')\, n_k dA_p \qquad (3.13)$$

$$\rho^s \frac{d}{dt} v'\left(e^{s'} + \frac{u_i'u_i'}{2}\right) = f_i'u_i' + \tilde{f}_i'u_i' + \rho^s v'u_i'g_i$$

$$+ \int_P \rho^s \left(e^{s'} + \frac{u_i'u_i'}{2}\right)(v_k^b - u_k')\, n_k dA_p$$

$$- \int_P q_i^{s'}\, n_i dA + v'H^{s'} \qquad (3.14)$$

where dA includes surface elements in contact with either gas or solid and where the derivative d/dt is understood to be Lagrangian in character. The variables ρ^s, u_i', $e^{s'}$, v', $q^{s'}$, $H^{s'}$ are, respectively, the solid particle density, velocity, specific internal energy, volume, heat flux and volumetric heat source. The source f_i' represents the gas-particle drag force while the force $\tilde{f}_i'$ represents particle-particle interaction. The velocity v_i^b is the local velocity of the particle boundary; hence the integrals represent mass, momentum and energy exchange between the particle and the gas. In these equations, we assume that the mass exchange is from the particle to the gas and that it is reflected by changes in the particle volume at constant density. This is appropriate to, say, a surface reaction where v_k^b measures the velocity of propagation of the reaction front. For reactions that occur throughout the particle a slightly different form of these equations may be derived. The corresponding equations for the local mean variables are obtained by a spatial average of (3.9)-(3.14). We therefore multiply those equations by the weighting function $g(|x_i-y_i|)$, and by integrating over the fluid volume for (3.9)-(3.11) and taking a summation over the particles for (3.12)-(3.14), we can with (3.1), (3.2), (3.4), (3.6) and (3.7), obtain the spatial averages for conservation of mass, momentum and energy for the gas and solid phases. The interphase exchange of mass, momentum and energy between the gas and the solid is determined by appropriate surface integrals. The influence of the fluctuations upon these conservation equations is represented by volumetric integrals containing second or higher order products of the fluctuations in the field variables. In analogy with the theory of turbulence, it will be necessary to develop specific representations of such surface and volume integrals to provide closure for the system of equations and explicitly describe the flow field.

The interphase exchange is represented by surface integrals for mass flux, S, momentum flux, M_i, and energy flux, N, in the respective spatial averages of the point differential equations (3.9)-(3.14).

$$S = -\sum_P \int_P \rho'(v_j^b - v_j')\, n_j\, g\,(|x_k-y_k|)\, dAp \qquad (3.15)$$

$$M_i = -\sum_P \int_P \left\{\rho' v_i'(v_j^b - v_j') + \sigma_{ij}'\right\} n_j\, g\,(|x_k-y_k|)\, dA_p \qquad (3.16)$$

$$N = -\sum_P \int_P \left\{ \rho' \left(e' + \frac{v_i' v_i'}{2} \right) (v_j^b - v_j') + v_i' \sigma_{ij}' - q_j' \right\} n_j g\,(|x_k - y_k|)\, dA_p \tag{3.17}$$

In analogy to the case of slow combustion fronts in gases (Landau and Lifshitz, 1959) we can assume that the momentum integral, M_i, is dominated by the stress tensor, thereby assuring that continuity of stress occurs at the particle surface. Consistent with that assumption we would also neglect the flux of kinetic energy in the energy integral, N. The surface integrals (3.15)-(3.17) must be defined in terms of averaged variables to provide closure; for the present we only consider the momentum flux M_i, and with the assumption that this integral is dominated by the stress term, we write

$$M_i = -\sum_P \int_P \sigma_{ij}' n_j g\,(|x_k - y_k|)\, dA_p = -\frac{B(\theta)}{(1-\theta)} (v_i - u_i) \tag{3.18}$$

where $B(\theta)$ is the local drag coefficient and it is implicitly a function of particle size, shape and local Reynolds number. This specification means that we are neglecting virtual mass effects (c.f., Anderson and Jackson, 1967; Garg and Pritchett, 1975). In addition to the momentum exchange between the solid particles and the gas, there is a momentum exchange caused by particle to particle interaction, represented in the point equations (3.13) and (3.14) by $\tilde{f}_i'$. In the averaged equation for conservation of solid momentum this term leads to an integral momentum term. We assume that (c.f., Anderson and Jackson, 1967) this integral can be expressed as the divergence of a stress tensor,

$$\sum_P \tilde{f}_i' g\,(|x_k - y_k|) = \frac{\partial \tau_{ij}}{\partial x_j} \tag{3.19}$$

With (3.15)-(3.19) the spatial averages of the conservation equations for the gas and solid phases, derived from (3.9)-(3.14), are

$$\frac{\partial}{\partial t}\left[\rho\ (1-\theta)\right] + \frac{\partial}{\partial x_i}\left[\rho v_i\ (1-\theta)\right] = S + \ldots \tag{3.20}$$

$$\frac{\partial}{\partial t}\left[\rho^s \theta\right] + \frac{\partial}{\partial x_i}\left[\rho^s u_i \theta\right] = -\ S + \ldots \tag{3.21}$$

$$\frac{\partial}{\partial t}\left[\rho v_i (1-\theta)\right] + \frac{\partial}{\partial x_j}\left[\rho v_i v_j (1-\theta)\right] = \frac{\partial}{\partial x_j}\sigma_{ij} + M_i + (1-\theta)\ \rho g_i + \ldots \tag{3.22}$$

$$\frac{\partial}{\partial t}\left[\rho^s u_i\right] + \frac{\partial}{\partial x_j}\left[\rho^s u_i u_j \theta\right] = \frac{\partial \tau_{ij}}{\partial x_j} - M_i + \theta\rho^s g_i + \ldots \tag{3.23}$$

$$\frac{\partial}{\partial t}\left[\rho(1-\theta)\ \left\{e + \frac{v_i v_i}{2}\right\}\right] + \frac{\partial}{\partial x_j}\left[\rho v_j (1-\theta)\ \left\{e + \frac{v_i v_i}{2}\right\}\right] = \frac{\partial}{\partial x_j}\left[v_i \sigma_{ij}\right] - \frac{\partial}{\partial x_j}\left[(1-\theta) q_i\right] + N + (1-\theta) H + (1-\theta)\rho v_i g_i + \ldots \tag{3.24}$$

$$\frac{\partial}{\partial t}\left[\rho^s \theta \left\{e^s + \frac{u_i u_i}{2}\right\}\right] + \frac{\partial}{\partial x_j}\left[\rho^s u_j (1-\theta)\ \left\{e^s + \frac{u_i u_i}{2}\right\}\right] = u_i \frac{\partial \tau_{ij}}{x_j} - \frac{\partial}{\partial x_j}\left[\theta q_i^s\right] - N + \theta H^s + \theta\rho^s u_i g_i + \ldots \tag{3.25}$$

where {+ ...} indicates volumetric integrals representing fluctuations. These integrals are neglected in the first order theory.

For the present study we now introduce important restrictions on the terms in the conservation equations (3.20)-(3.25). First we neglect chemical reactions and interphase mass exchange. Secondly, based upon order of magnitude considerations, we neglect the inertia of the gas phase relative to that of the solid particles and also neglect the viscous dissipation in the energy equation. Third, we assume that the solid and gas phases have the same local temperatures. With these assumptions the conservation equations become

$$\frac{\partial}{\partial t}\left[\rho(1-\theta)\right] + \frac{\partial}{\partial x_j}\left[\rho v_i(1-\theta)\right] = 0 \tag{3.26}$$

$$\frac{\partial \theta}{\partial t} + \frac{\partial}{\partial x_i}\theta u_i = 0 \tag{3.27}$$

$$\frac{\partial \sigma_{ij}}{\partial x_j} - \frac{B(\theta)}{1-\theta}(v_i - u_i) = 0 \tag{3.28}$$

$$\rho^s\left\{\frac{\partial}{\partial t}\theta u_i + \frac{\partial}{\partial x_j}\theta u_i u_j\right\} = \frac{\partial \sigma_{ij}}{\partial x_j} + \frac{\partial \tau_{ij}}{\partial x_j} + \theta\rho^s g_i \tag{3.29}$$

$$\frac{\partial}{\partial t}\left[\rho(1-\theta)\, e + \rho^s \theta e^s\right] + \frac{\partial}{\partial x_j}\left[\rho v_j(1-\theta)e + \rho^s u_j \theta e^s\right]$$

$$= -\frac{\partial}{\partial x_j}\left\{(1-\theta)\, q_i + \theta q_i^s\right\} \tag{3.30}$$

We adjoin to (3.26)-(3.30) constitutive relations for σ_{ij}, τ_{ij}, e, e^s, q_i and q_i^s. Specifically, these equations are

$$\sigma_{ij} = - \delta_{ij} p = - \delta_{ij} (\gamma-1) \rho e \tag{3.31a}$$

$$\tau_{ij} = - \delta_{ij} \left\{ p^s(\theta) + \lambda^s(\theta) \frac{\partial u_k}{\partial x_k} \right\}$$

$$+ \mu^s(\theta) \left\{ \frac{\partial u_i}{\partial x_j} + \frac{\partial u_j}{\partial x_i} - \frac{2}{3} \delta_{ij} \frac{\partial u_k}{\partial x_k} \right\} \tag{3.31b}$$

$$de = c_v \, dT \tag{3.31c}$$

$$de^s = c_v^s \, dT \tag{3.31d}$$

$$(1-\theta) \, q_i + \theta q_i^s = - \kappa(\theta) \frac{\partial T}{\partial x_i} \tag{3.31e}$$

Thus we consider that the average stress in the gas phase is a pressure which is related to the density and energy by the ideal gas law. The solid phase stress is Newtonian in character (c.f., Anderson and Jackson, 1967) and involves both hydrostatic and deviatoric contributions. We take the heat flux to be linearly related to the temperature gradient. The functional forms of $p^s(\theta)$, $\lambda^s(\theta)$, $\mu^s(\theta)$, $\kappa(\theta)$ and of $B(\theta)$ are specified by recourse to laboratory data. These definitions are discussed below.

For the present study we will not consider reactive flows and hence the source terms are neglected in our subsequent numerical calculations. However, when chemistry is introduced, an important aspect will be the definition of interphase mass, momentum and energy exchange associated with reactive flows. There are three considerations of such a coupled model which can be mentioned in the present discussion of the mass exchange functions S, M_i and N. First there is the need to develop kinetic expressions for the chemistry of the salient reactions. Second, we must examine, in some detail, the heterogeneous gas-solid reactions within the context of extraparticle diffusion, interphase mass transport and intraparticle diffusion for a single particle. Third, the influence of such transport phenomena for a single particle must be summed over many particles to provide the necessary source terms (say, S) for our continuum model of the

mixture Equations (3.20)-(3.25). There is an extensive literature (e.g., Ishida and Wen, 1968; Avedesian and Davidson, 1973; Rehmat and Saxena, 1976) relating to heat and mass exchange from single particles where the overall reaction is controlled by the kinetics, the diffusion processes, or some combination of these mechanisms. Such existing theory and data, together with formulations particular to the present model will, in the future, form the basis of this single and multiple particle interphase exchange representation.

A critical aspect of the development of the coupled chemistry and thermohydrodynamic model development will be the relative magnitude of the time scale associated with the gas and solids convective motion as compared to the time scale associated with the overall reaction. Within this context we note that some reactions in, say, coal gasification, such as the combustion reactions associated with char particle burning, involve relatively fast kinetics and that the reaction on a particle level is influenced by convective or diffusive mechanisms (c.f., Avedesian and Davidson, 1973). However, the reactions associated with char gasification involve relatively slow kinetics. A theoretical or numerical formulation for the combined chemistry-thermohydrodynamic model must be developed in such a manner to account for such diverse time scales.

For the study of chemically reactive systems, it is also essential to develop conservation equations for species transport in the solid and fluid phases. A derivation of those equations follows the methodology of Blake and Garg, 1976. Within the context of the assumptions for (3.20)-(3.25) we have, for chemical species α

$$\frac{\partial}{\partial t}(1-\theta)\rho_\alpha + \frac{\partial}{\partial x_i}(1-\theta)\rho_\alpha v_i = (1-\theta)\Omega_\alpha + S_\alpha + \ldots \tag{3.32}$$

$$\frac{\partial}{\partial t}\theta\rho_\alpha^s + \frac{\partial}{\partial x_i}\theta\rho_\alpha^s u_i = \theta\Omega_\alpha^s - S_\alpha + \ldots \tag{3.33}$$

where Ω_α are the volumetric source functions (related to the kinetics) and S_α are the interphase exchange functions for species α. We have neglected diffusional transport in both of these equations.

3.2 MATHEMATICAL STRUCTURE OF EQUATIONS FOR GAS FLUIDIZED BEDS

The balance equations for fluidized beds have previously been developed in Section 3.1. In the following paragraphs, we consider these equations for gas-fluidized beds and we discuss their mathematical character. It is demonstrated that these equations possess only real characteristics, yet they are unstable under small perturbations. Within this context we note that the question of instability must be examined independently of the characteristics of the system. The nature of the characteristics (real or complex), however, determines the posedness of the problem. That is, as discussed by Gidaspow and Solbrig, 1976, a set of linear partial differential equations with complex characteristics cannot be solved as an initial value problem; in that case the problem must be solved as a boundary value problem in the four-dimensional $\underline{x}$ - t space.

Consider the system of mass and momentum balance equations for gas-fluidized beds in Section 3.1 wherein the inertia of the gas phase is neglected. A linear perturbation analysis for this set of differential equations can be presented (c.f., Garg and Pritchett, 1975) and it can be shown that the differential equations in question are unstable to small perturbations. We now analyze the characteristics of this system of differential equations. For this purpose, it will suffice to restrict our attention to time (t) and one space dimension (x). Mass and momentum balance equations can now be written from (3.26) through (3.29) as follows, where we omit the source terms and interphase transport:

Mass:

Solid:

$$\frac{\partial}{\partial t}\left[(1-\phi)\right] + \frac{\partial}{\partial x}\left[(1-\phi)u\right] = 0 \tag{3.34}$$

Gas:

$$\frac{\partial}{\partial t}\left[\rho\ \phi\right] + \frac{\partial}{\partial x}\left[\rho\ \phi\ v\right] = 0 \tag{3.35}$$

Momentum:

Solid:

$$\rho^s(1-\phi)\left[\frac{\partial u}{\partial t} + u\ \frac{\partial u}{\partial x}\right] = -\ \frac{\partial p}{\partial x} - G(\phi)\ \frac{\partial \phi}{\partial x} + \frac{\partial}{\partial x}\left[\nu\ \frac{\partial u}{\partial x}\right] + (1-\phi)\ \rho^s g \tag{3.36}$$

Gas:

$$B(\phi)\ (v-u) = -\phi\ \frac{\partial p}{\partial x} \tag{3.37}$$

where we write $\phi = 1 - \theta$.

We need to adjoin Equations (3.34)-(3.37) with an equation of state for the gas phase. We will consider two cases:

Case I

Fluid obeys the ideal gas equation of state, and the flow is isothermal. Thus

$$p = (\gamma-1)\, C_v\, T_0\, \rho = \bar{R}\, \rho \tag{3.38}$$

where γ is the ratio of specific heats for gas, C_v is the gas heat capacity at constant volume, and T_0 is the constant bed temperature.

Case II

Fluid is incompressible.

$$\rho = \text{constant} \tag{3.39}$$

3.2.1 Ideal (Isothermal) Equation of State

Introducing

$$w = \partial u/\partial x\ , \tag{3.40}$$

and substituting for p from Eq. (3.38) into Eqs. (3.36) - (3.37), we obtain a set of five equations for five unknowns (ϕ, v, ρ, u and w). The characteristic determinant is given by:

$$D \equiv \begin{vmatrix}
1 & u & 0 & 0 & 0 & 0 & 0 & 0 & 0 & 0 \\
\rho & \rho v & 0 & 0 & \phi & \phi u & 0 & \rho\phi & 0 & 0 \\
0 & (\nu' w - G) & -\rho^s(1-\phi) & 0 & 0 & -\bar{R} & 0 & 0 & 0 & \nu \\
0 & 0 & 0 & -\phi\bar{R} & 0 & 0 & 0 & 0 & 0 & 0 \\
0 & 0 & 0 & 0 & 0 & 1 & 0 & 0 & 0 & 0 \\
dt & dx & 0 & 0 & 0 & 0 & 0 & 0 & 0 & 0 \\
0 & 0 & dt & 0 & 0 & 0 & 0 & 0 & 0 & 0 \\
0 & 0 & 0 & 0 & dt & dx & 0 & 0 & 0 & 0 \\
0 & 0 & 0 & 0 & 0 & 0 & dt & dx & 0 & 0 \\
0 & 0 & 0 & 0 & 0 & 0 & 0 & 0 & dt & dx
\end{vmatrix} = 0$$

Expansion of the determinant yields 4 zero (dt = 0) and 1 non-zero (dx/dt = u) characteristic. Therefore, the system of equations is of the parabolic-hyperbolic type. The latter conclusion remains unchanged even when one assumes that the viscosity of the particle assemblage ν is zero. It is straightforward to verify that when $\nu = 0$, we have 3 zero (dt = 0) and 1 non-zero (dx/dt = u) characteristic. Furthermore, the presence or absence of the $-G\,\partial\phi/\partial x$ term in Eq. (3.36) has no influence on the nature of the characteristics; this is particularly interesting in view of the fact that the stability of the present system of equations depends strongly on the $-G\,\partial\phi/\partial x$ term (see Garg and Pritchett, 1975).

3.2.2 Incompressible Gas

We shall now consider the case when the gas may be regarded as incompressible (Eq. (3.39)). To simplify our considerations, we shall also assume that $G(\phi) = \nu(\phi) = 0$. Substituting from Eq. (3.39) into Eq. (3.35), we obtain a set of four linear partial differential equations for four unknowns (ϕ, v, u, p). The characteristic determinant is now given by:

$$D \equiv \begin{bmatrix} 1 & u & 0 & -(1-\phi) & 0 & 0 & 0 & 0 \\ 1 & u & 0 & 0 & 0 & \phi & 0 & 0 \\ 0 & 0 & \rho^s(1-\phi) & \rho^s(1-\phi)u & 0 & 0 & 0 & 1 \\ 0 & 0 & 0 & 0 & 0 & 0 & 0 & -\phi \\ dt & dx & 0 & 0 & 0 & 0 & 0 & 0 \\ 0 & 0 & dt & dx & 0 & 0 & 0 & 0 \\ 0 & 0 & 0 & 0 & dt & dx & 0 & 0 \\ 0 & 0 & 0 & 0 & 0 & 0 & dt & dx \end{bmatrix} = 0$$

Solution of the determinant yields two zero (dt = 0) and two non-zero (dt/dx = u) characteristics. Thus the system of differential equations possesses a parabolic-hyperbolic character.

We have demonstrated in this and in the previous section that the governing equations for gas-fluidized beds as formulated possess real characteristics even when one neglects fluid compressibility, and particle assemblage viscosity and compressibility. The system of equations is, however, unstable to small perturbations (see Garg and Pritchett, 1975).

3.2.3 Generalized Equations for Fluidized Beds

In this section, we shall consider the more general differential equations for fluidized beds which include inertia in the gas phase and which have also been examined by Garg and Pritchett [1975]. To simplify our considerations, we shall assume the fluid to be incompressible (ρ = const). Mass and momentum balance equations (in one space dimension and time) are:

Mass:

Solid:

$$\frac{\partial \phi}{\partial t} + u \frac{\partial \phi}{\partial x} - (1-\phi) \frac{\partial u}{\partial x} = 0 \tag{3.41}$$

Fluid:

$$\frac{\partial \phi}{\partial t} + v \frac{\partial \phi}{\partial x} + \phi \frac{\partial v}{\partial x} = 0 \tag{3.42}$$

Momentum:

Solid:

$$\rho^s \left[\frac{\partial u}{\partial t} + u \frac{\partial u}{\partial x}\right] = - \frac{\partial p}{\partial x} - \frac{G(\phi)}{1-\phi} \frac{\partial \phi}{\partial x} + \frac{1}{1-\phi} \frac{\partial}{\partial x} \left(\nu \frac{\partial u}{\partial x}\right) + \rho^s g + \frac{(F_1 + F_2)}{1-\phi} \tag{3.43}$$

Fluid:

$$\rho_f \left[\frac{\partial v}{\partial t} + v \frac{\partial v}{\partial x}\right] = - \frac{\partial p}{\partial x} - \frac{(F_1 + F_2)}{\phi} \tag{3.44}$$

where

$$F_1 = B(\phi) \ (v-u) \ ,$$

$$F_2 = (1-\phi) \ c(\phi) \ \rho_f \frac{d}{dt} \ (v-u) .$$

Note that F_2 where $C(\phi)$ is the virtual mass coefficient, is proportional to the relative acceleration of the two phases and to the mass of fluid displaced by the particles. There is some question as to what the relative acceleration term d/dt (v-u) means (see e.g., Jackson [1971]). Fortunately, for our present purposes, we do not need to consider the explicit presence of F_2 in Equations (3.42) and (3.43).

Gidaspow and Solbrig [1976] suggest that particle assemblage elasticity and viscosity, and induced mass are higher order effects. If we put $\nu = G = F_2 = 0$ in Eqs. (3.42) and (3.43), we obtain a system of equations equivalent to Eqs. (4-29) - (4-32) of Gidaspow and Solbrig [1976]. This system of equations has two real (dt = 0) and two complex characteristics; and is thus of the parabolical-elliptical type. As correctly pointed out by Gidaspow and Solbrig, such a system of equations cannot be solved as an initial value problem; it must be solved as a boundary value problem in the x - t space.

We maintain, however, that the particle assemblage viscosity and elasticity are first order effects, and must be included in any realistic description of fluidized beds. Viscosity of fluidized beds has been measured by Schugerl and his co-workers (see, e.g., Schugerl [1971]); in general, viscosity of fluidized beds is much greater than that of the fluid in isolation. Elasticity of fluidized beds has been the subject of several papers by Rietema and his co-workers. There is considerable evidence that the solid particles in a fludized bed are in permanent contact. Rietema and Mutsers [1975] state that:

> *"At present the experimental proofs of this permanent contact are so overwhelming that they can no longer be denied. Furthermore, the stability of homogeneously expanded gas-fluidized beds can only be understood by assuming a permanent structure of the dense phase which must have a certain elasticity. The experimental proofs which is referred to above are: ... c) exact measurements of the pressure drop over a fluidized bed indicate that it is smaller than the weight of the particles divided by the cross-sectional area of the bed. This is only possible if the difference is carried by the wall, which is only possible if there is momentum transport through the dense phase."*

The experimental data thus clearly demonstrate the need to include the particle assemblage viscosity and elasticity in the momentum balance laws (3.43) and (3.44). In the remainder of this section, we will investigate the effects of non-zero G and ν on the mathematical structure of Eqs. (3.41) through (3.44). We shall first consider the case when $G \neq 0$, but $\nu = F_2 = 0$. In this case, we obtain a set of four linear partial differential equations for four unknowns (ϕ, v, u, p). The characteristic determinant is:

$$D = \begin{bmatrix} 1 & u & 0 & -(1-\phi) & 0 & 0 & 0 & 0 \\ 1 & v & 0 & 0 & 0 & \phi & 0 & 0 \\ 0 & G_1 & \rho^s & \rho^s v & 0 & 0 & 0 & 1 \\ 0 & 0 & 0 & 0 & \rho & \rho v & 0 & 1 \\ dt & dx & 0 & 0 & 0 & 0 & 0 & 0 \\ 0 & 0 & dt & dx & 0 & 0 & 0 & 0 \\ 0 & 0 & 0 & 0 & dt & dx & 0 & 0 \\ 0 & 0 & 0 & 0 & 0 & 0 & dt & dx \end{bmatrix} = 0$$

where $G_1 = G/(1-\phi)$.

Expansion of the determinant yields two zero characteristics ($dt = 0$); the other two characteristics are given by the quadratic equation:

$$\left(\frac{dx}{dt}\right)^2 \left[\rho\ (1-\phi) + \phi\rho^s\right] - 2\left(\frac{dx}{dt}\right)\left[u\phi\ \rho^s + (1-\phi)\ v\ \rho\right] + \left[\rho^s\ u^2\phi + \rho\ v^2\ (1-\phi) + \phi(1-\phi)\ G_1\right] = 0 \tag{3.45}$$

Equation (3.45) has real roots for

$$-G_1\ \frac{[(1-\phi)\ \rho + \phi\rho^s]}{\rho^s\ \rho} > (u-v)^2 \tag{3.46}$$

From the measurements of Rietema and Mutsers on gas-fluidized beds, we have

$$-G \sim (10^5 \text{ dynes/cm}^2)$$

This implies that inequality (3.46) is satisfied for at least $(u-V) \sim$ of the order of 10^2 cm/sec. Thus, while the inclusion of bed elasticity in Eqs. (3.42)-(3.44) does not totally eliminate the possibility of complex characteristics, it does certainly imply that in many practical cases the system of equations possesses real characteristics.

We shall next investigate the effects of including both the particle assemblage viscosity and elasticity terms in Eqs. (3.43) and (3.44). For the sake of simplicity, we shall assume that $F_2 = 0$. Putting

$$w = \frac{\partial u}{\partial x} \tag{3.47}$$

in Eqs. (3.41) - (3.44), we obtain a set of five linear partial differential equations for five unknowns (ϕ, p, u, v, w). The characteristic determinant is given by:

$$D \equiv \begin{bmatrix}
0 & 0 & 0 & 0 & 0 & 0 & 0 & 1 & 0 & 0 \\
1 & u & 0 & 0 & 0 & 0 & 0 & 0 & 0 & 0 \\
1 & v & 0 & 0 & 0 & 0 & 0 & 0 & 0 & 0 \\
0 & (-\bar{\nu}'w+G_1) & 0 & 1 & 0 & 0 & \rho^s & 0 & 0 & -\bar{\nu} \\
0 & 0 & 0 & 1 & \rho & \rho v & 0 & 0 & 0 & 0 \\
dt & dx & 0 & 0 & 0 & 0 & 0 & 0 & 0 & 0 \\
0 & 0 & dt & dx & 0 & 0 & 0 & 0 & 0 & 0 \\
0 & 0 & 0 & 0 & dt & dx & 0 & 0 & 0 & 0 \\
0 & 0 & 0 & 0 & 0 & 0 & dt & 0 & 0 & 0 \\
0 & 0 & 0 & 0 & 0 & 0 & 0 & 0 & dt & dx
\end{bmatrix} = 0$$

where $\bar{\nu} = \nu/(1-\phi)$, and $\bar{\nu}' = \frac{1}{1-\phi}\, d\nu/d\phi$.

Expansion of the determinant yields four zero ($dt = 0$) and one non-zero ($dx/dt = u$) real characteristic. Thus the system of generalized differential equations for fluidized beds is of the parabolic-hyperbolic type, and may be properly solved as an initial value problem.

3.2.4 Conclusions on Mathematical Character of Differential Equations

On the basis of the preceding discussion, we can state the following conclusions:

Partial differential equations for gas-fluidized beds as used in the present model are of the hyperbolic-parabolic type, and may be properly solved as an initial value problem. Although the characteristics are real, the system of differential equations is unstable (under small perturbations); this implies that the question of stability should be considered apart from the nature (i.e., real or complex) of characteristics of a system of linear partial differential equations.

Generalized partial differential equations for fluidized beds (like the partial differential equations for gas-fluidized beds) are also of the parabolic-hyperbolic type. The conclusion by Gidaspow and Solbrig that the generalized partial differential equations possess complex characteristics is based on the erroneous assumption that the particle assemblage viscosity and compressibility are higher order effects. We maintain that the latter effects must be included in any realistic description of fluidized beds.

3.3 CONSTITUTIVE RELATIONS

Momentum and energy balance relations described in Section 3.1 involve five functions, $P^s(\phi)$ - normal component of particle-particle interactions, λ^s - bulk viscosity of particle assemblage, μ^s - shear viscosity of particle assemblage, $B(\phi)$ - local mean drag coefficient, and $\kappa(\phi)$ - mixture (solid/fluid) heat conduction coefficient, which must be determined empirically. During the last year, considerable effort was spent in reviewing the existing literature on fluidized beds to locate appropriate data for use in developing suitable functional forms for B, λ^s, μ^s, f and κ. Our main findings are summarized in the following subsections.

3.3.1 Local Mean Drag Coeffieient $B(\phi)$

The local mean drag coefficient $B(\phi)$, in the particulate fluidization regime (no bubbles), can be found in a straightforward manner from bed expansion measurements. One of the earliest correlations for $B(\phi)$ is due to Ergun [1952]. Ergun's correlation — valid for only packed beds — shows that B depends upon particle diameter d, fluid viscosity μ, and Reynolds number R (based upon particle diameter) in addition to voidage ϕ. More recently, Richardson [1971] has analyzed data for both packed (or fixed) and fluidized beds. Figure 3.1, taken from Richardson [1971], compares the friction factor ψ — Reynolds number R relation for fluidized and sedimentary systems with that for fixed beds. Here ψ and R are defined by

$$\psi = \frac{\phi\ \rho^s\ g}{\tilde{A}\ \rho\ (|\underline{u}-\underline{v}|)^2} \tag{3.48}$$

$$R = \frac{\phi(|\underline{u}-\underline{v}|)\ \rho}{\tilde{A}\ \mu\ (1-\phi)} \tag{3.49}$$

where $\tilde{A}$ denotes the specific surface of solid and equals $6/d$ for spherical particles.

Multiplying Eqs. (3.48) and (3.49), putting $-\nabla p = (1-\phi)\ \rho^s g$ (uniform fluidization, see Garg and Pritchett [1975]), and utilizing the momentum balance law for the gas $B(\phi)\ (\underline{u}-\underline{v}) = -\phi\ \nabla p$, we obtain:

$$B = \frac{(1-\phi)^2}{\phi}\ \tilde{A}^2\ \mu\ (\psi R) \tag{3.50}$$

For small values of R, ψR is approximately constant; for $R > 1$, ψR is a highly nonlinear function of R. Thus in general, ψR exhibits a dependence on R.

In analogy with flow through fixed beds, we can put

$$B = \frac{\phi^2\ \mu}{k} \tag{3.51}$$

where k is the permeability of the fluidized bed. Combining

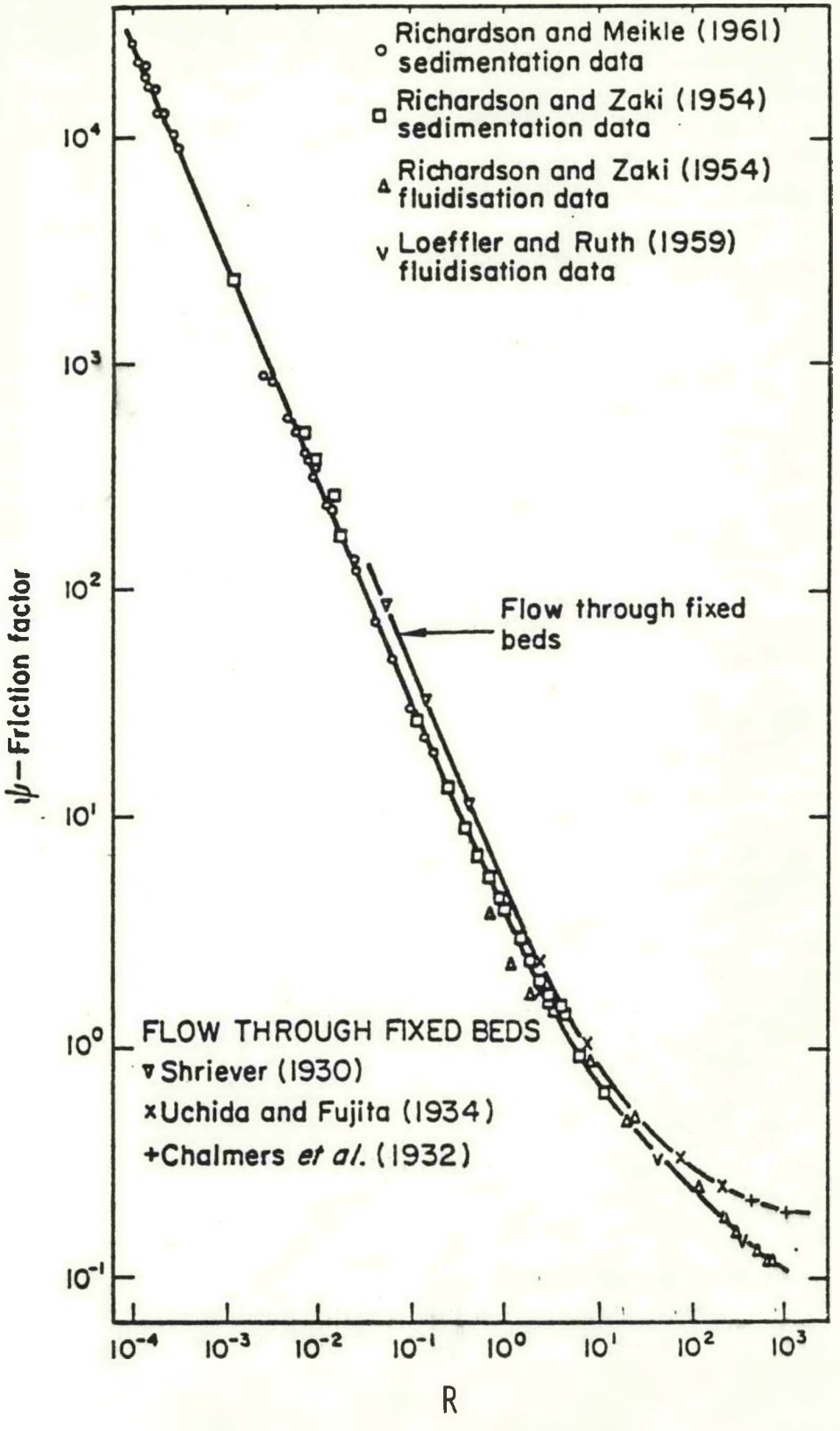

Figure 3.1. Friction factor - Reynolds number relation of fluidized and sedimentary systems compared with fixed beds (from Richardson [1971]).

Eqs. (3.50) and (3.51), we have

$$k = \frac{\phi^3}{(1-\phi)^2} \frac{1}{\tilde{A}^2 (\psi R)} \tag{3.52}$$

Equation (3.52) suggests that k may be written as follows:

$$k = \frac{144}{\tilde{A}^2} F_1(\phi)\ F_2(N) \tag{3.53}$$

where N is a local Reynolds number ($N \neq R$) associated with the relative velocity between particles and gas:

$$N \equiv \phi\ \rho \frac{12}{\tilde{A}} \frac{|\underline{u}-\underline{v}|}{\mu} \tag{3.54}$$

This choice for Reynolds number is especially convenient insofar as it brings the drag data for free-falling spheres [see, e.g., Vennard, 1946], into line with the drag data for fluidized beds.

At small Reynolds number ($N << 1$), F_2 may be taken as unity. Under these conditions, for low values of ϕ, it is well-known that the permeability obeys the Karman-Kozeny law. On the other hand, as ϕ approaches unity, the drag rule should approach Stokes law. These considerations suggest the following formulation for $F_1(\phi)$:

$$F_1 = A\ \phi^a\ (1-\phi)^b \tag{3.55}$$

where the constants A, a and b take on the values:

Range of ϕ	A	a	b
$1 \geq \phi > 0.854102$	2/9	+1	-1
$0.854102 \geq \phi \geq 0$	2/45	3	-2

(3.56)

Now, as the Reynolds number increases, the resistance to gas flow also increases. Three regions can be identified,

as Reynolds number increases. These regions may be fit with the following formula:

$$F_2(N) = [1 + B\, N^C]^{-1} \tag{3.57}$$

where B and c take on values:

Range of N	B	c
$0 \leq N < 3$	0.40815	1/3
$3 \leq N < 1000$	0.283	2/3
$1000 \leq N < \infty$	0.0283	1

Comparison of this fit with experimental data for both free-falling spheres [Vennard, 1946] and for fluidized beds of spherical particles compiled by Richardson [1971] is illustrated in Figure 3.2. The fit is everywhere within 12 percent of the data and is in general much better. Therefore, the final relation for permeability (k) is as follows:

$$k = A\, \phi^a\, (1-\phi)^b \left[1 + B \left(\frac{\phi\, \rho(12)\, |\bar{u}-\bar{v}|}{\tilde{A}\, \mu} \right)^C \right]^{-1} \frac{144}{\tilde{A}^2} \tag{3.58}$$

We note that the particle surface roughness does not explicitly appear in the correlation for k, Eq. (3.58). Although presently available data are insufficient to evaluate the effects of surface roughness, it can be hypothesized that it would affect this relationship, likely in a manner similar to A.

Particle density ρ^s enters into the correlation for k implicitly through ψ (see Eq. (3.48)). For vesicular materials (e.g., coal) the appropriate ρ^s for use in Eq. (3.48) is not necessarily the same as the granular density; in general, ρ^s will need to be evaluated from fluidization experiments (c.f., Leva [1959]).

In industrial processes, the fluidized particles are usually not of a uniform size. The correlation for k may be extended to these cases by introducing an equivalent particle diameter $\bar{d}$:

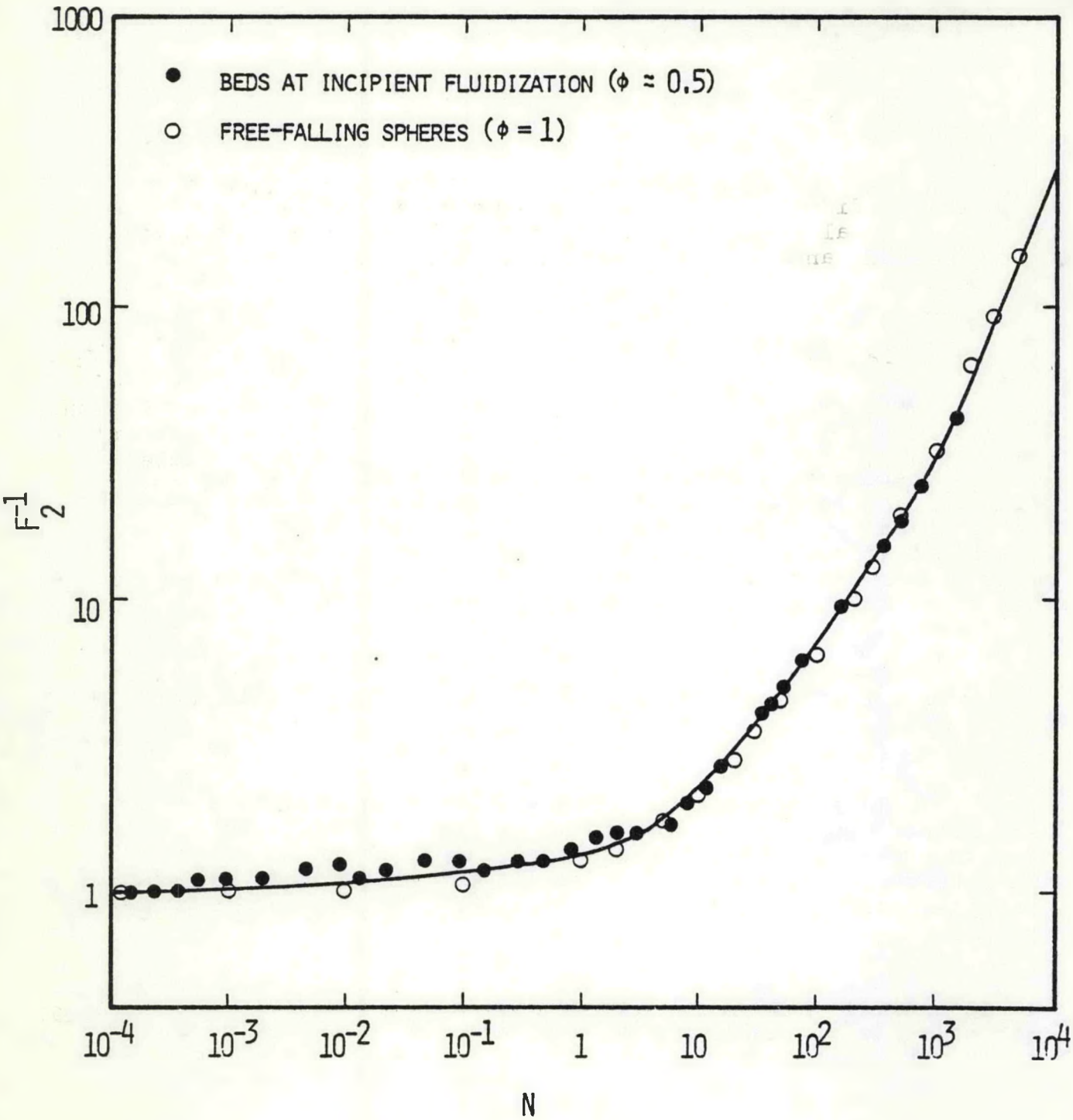

Figure 3.2. Influence of Reynolds number (N) upon bed permeability.

$$\bar{d} = \frac{1}{\sum \frac{x_i}{d_i}} \tag{3.59}$$

where x_i is the fraction of particles with diameter d_i.

The correlation for k may be directly applied to coal gasification processes by supplying appropriate ρ^s and $\bar{d}$. Chemical reactions will undoubtedly alter vesicularity (hence ρ^s) and particle size (i.e., $\bar{d}$). Thus, one will, in general, also need to prescribe relationships for ρ^s and $\bar{d}$ in terms of the time history of chemical reaction.

3.3.2 Particle Assemblage Elastic (Bulk) Modulus $-G(\phi)$

It is often convenient, both in theoretical formulations and in the correlation of empirical data to employ the particle assemblage elastic modulus $-G(\phi)$, instead of the particle-particle interaction function $p^s(\phi)$. These functions are related by the definition

$$-G(\phi) \equiv \frac{d}{d\phi} [p^s(\phi)]. \tag{3.60}$$

The elastic modulus $-G(\phi)$ has important consequences for bed stability. Thus, for example, Garg and Pritchett [1975] give the following conditions for the stability of a uniformly fluidized bed:

$$-G(\phi) \geq \rho^s (1-\phi)^2 v^2 \left(2 - \frac{\phi}{1-\phi} - \frac{B'(\phi)}{B(\phi)} \phi\right)^2 \tag{3.61}$$

where v denotes the fluidization velocity (not necessarily minimum), ϕ is uniform bed porosity and

$$B'(\phi) \equiv \frac{dB(\phi)}{d\phi} \tag{3.62}$$

We note in passing that the stability condition of Rietema and Mutsers [1975] can be derived from Eq. (3.61) by utilizing the correlation of Ergun [1952] for $B(\phi)$. Equation (3.61) also suggests a way for measuring $-G(\phi)$. Given ϕ (say ϕ^*) at which bubbles first start appearing, we can determine $-G(\phi^*)$ from (3.61) by taking $-G(\phi^*)$ equal to the right hand side of

(3.61). We also know that $-G(\phi)$ monotonically decreases with increasing ϕ. We have, therefore,

1. For $\phi < \phi^*$: $-G(\phi) > -G(\phi^*)$

$$\lim_{\phi \to 0} -G(\phi) \to \infty \tag{3.63a}$$

2. For $\phi > \phi^*$: $-G(\phi) < -G(\phi^*)$

$$\lim_{\phi \to 1} -G(\phi) \to 0 \tag{3.63b}$$

Rietema and Mutsers [1975] report some preliminary measurements for $-G(\phi)$. (As far as we know, these are the only presently available measurements for $-G(\phi)$.) These data were taken in experiments involving incipient bubbling in homogeneously fluidized beds, and in separate experiments measuring the interaction of such a bed with a vibrating body made of wire netting immersed in it. The observed responses of the vibrating body are attributed by Rietema and Mutsers [1975] to a mechanical resistance resulting from interparticle forces which manifest themselves as an elastic property of the bed related to our $-G(\phi)$.

In order to apply (3.61) to experimental data and thereby determine $G(\phi)$ it is necessary to first establish the nature of $B(\phi)$. We have assumed that $B(\phi)$ is known from other bed measurements. Rietema and Mutsers assume that $B(\phi)$ is given by the following empirical relation due to Ergun:

$$B(\phi) = 150 \frac{(1-\phi)^2}{\phi} \frac{\mu}{d^2} \tag{3.64}$$

Substituting from (3.64) into (3.61), we have

$$-G(\phi)\Big|_{\phi=\phi^*} = \frac{(\rho^s)^3 g^2 d^4}{\mu^2} \left[\frac{\phi^2 (3-2\phi)}{150 (1-\phi)}\right]^2_{\phi=\phi^*} \tag{3.65}$$

Equation (3.64) was originally derived by Ergun for fixed beds, and is really inapplicable to fluidized beds. In the preceding section, Eqs. (3.51) - (3.58), we presented an empirical relation for $B(\phi)$ based on the available measurements

for fluidized beds; in the appropriate range (i.e., appropriate to Rietema and Mutsers' experiments), this relationship is:

$$B(\phi) \sim 90 \frac{(1-\phi)^2}{\phi} \frac{\mu}{d^2} \tag{3.66}$$

Comparison of (3.64) and (3.66) shows that Ergun's equation overestimates the mean particle drag, and underestimates $-G(\phi^*)$. Thus, we have:

$$\frac{-G(\phi^*)\Big|_{\text{Present Report}}}{-G(\phi^*)\Big|_{\text{RM}}} \sim \left(\frac{150}{90}\right)^2 \sim 3 \tag{3.67}$$

Equation (3.67) implies that $-G(\phi^*)$ values of Rietema and Mutsers (inferred from incipient bubbling experiments) need to be multiplied by a factor of three. This fact is especially interesting since it can be shown that it brings the measurements from the two separate experiments (i.e., from bubbling experiments, and from vibrating body experiments) into close agreement.

Let us now examine the functional form for $-G(\phi^*)$. Figure 3.3 shows the experimental results (uncorrected for $B(\phi)$) of Rietema and Mutsers for cracking catalyst particles (of several size distributions) fluidized with several different gases. These data can be approximated by the following relation:

$$\frac{-G(\phi^*)}{N/m^2} = \text{Antilog}_{10}\left[m\,(\phi^* - \phi_0) + a + b\,\frac{\sigma}{\bar{d}}\right] \tag{3.68}$$

where

ϕ_0 = minimum bed porosity = 0.4

m = -8.87

a = 0.209

b = 2.30

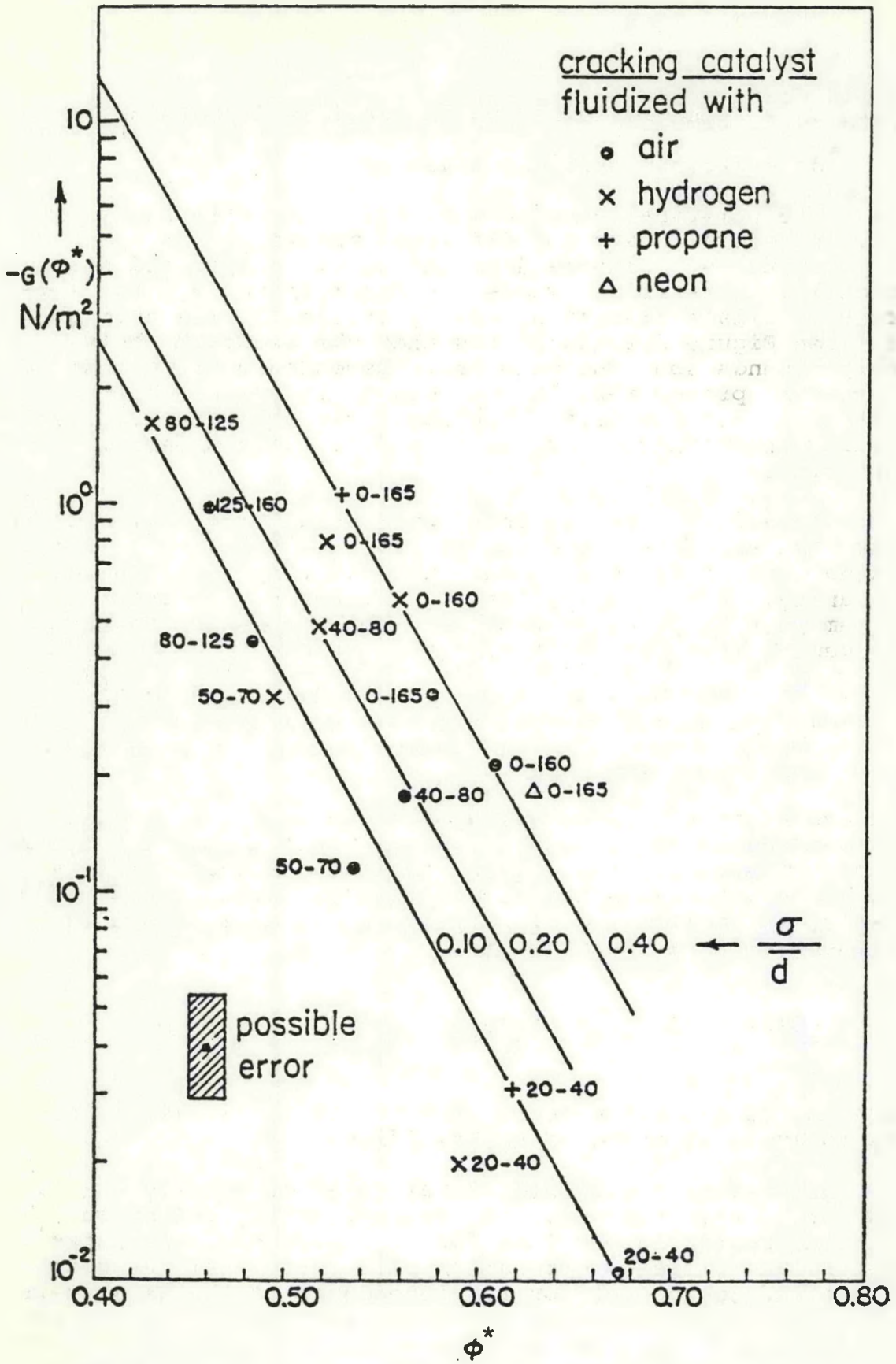

Figure 3.3. Measurements of $-G(\phi^*)$ for cracking catalyst (incipient bubbling experiments).

σ = standard deviation in particle diameters

$\bar{d}$ = average particle diameter

The numerical constants m, ϕ_0, a and b in Eq. (3.68) will, in general, vary for different materials. Minimum bed porosity ϕ_0 depends upon the particle size and shape. Basically, there is no problem in determining ϕ_0 for different materials (including coal particles). The available data (see Figure 3.4) indicates that the slope m only weakly depends upon the material. Dependence of a and b on material properties, if any, cannot be evaluated from the presently available data. Clearly, more data are required to study the variation of m, a and b with material properties.

Equation (3.68) is only applicable for $\phi > \phi_0$. It is clear that an upper bound exists upon the solidity θ ($\theta = 1-\phi$) attainable in a fluidized bed, and that this limit is less than unity. For example, for rigid spheres, the theoretical maximum packing function with optimum (i.e., hexagonal) arrangement is equal to $2\pi/9$, or

$$\theta_{max} = 0.6981, \quad \phi_{min} = 1-\theta_{max} = 0.3019 \tag{3.69}$$

In a bed at rest, therefore, some value of θ ($=\theta_0 \leq \theta_{max}$) will correspond to the bed solidity in the absence of fluidization. Therefore, any attempt to increase that solidity will be met with substantial resistance, owing to the assumed rigidity of the individual particles. We have chosen to represent this resistance as:

$$-G(\phi) = -G(\phi_0) + A^2 \ (\phi_0-\phi) \ , \ \phi < \phi_0 \tag{3.70}$$

where A is a large number. The use of Eq. (3.70) is necessary to avoid slumping of non-fluidized beds.

Equations (3.68) and (3.70) together specify $-G(\phi)$. This correlation for $-G(\phi)$ may be applied to coal by substituting appropriate values for ϕ_0 and $\sigma/\bar{d}$. As noted earlier, the present correlation will most likely need to be modified to account for the dependence of the parameters m, a and b in the material properties. However, we remark that while $G(\phi)$ is quite important in the evaluation of bed stability, its influence diminishes rapidly as ϕ becomes

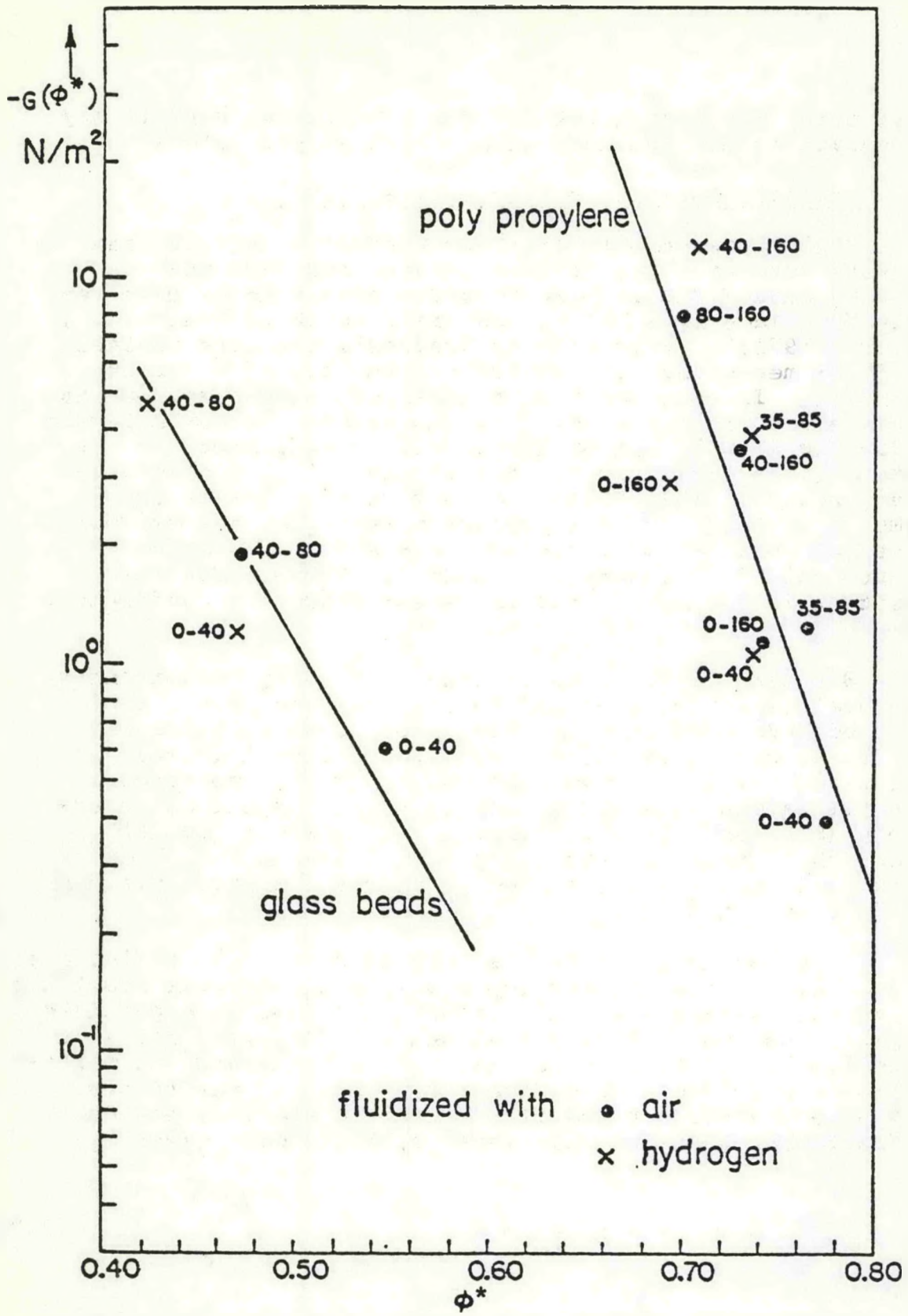

Figure 3.4. Measurements of -G(ϕ*) for glass beads and poly propylene.

larger than ϕ_0; consequently, from a practical view it may be adequate to use approximations to these parameters.

3.3.3 Particle Assemblage Viscosities λ^s, μ^s

Early measurements of shear viscosity in fluidized beds were more of a qualitative nature, and have been reviewed by Leva [1959]. More accurate measurements have recently been made by Schügerl and his co-workers (see, e.g., Schügerl [1971]). According to Schügerl, the most reliable method for measuring μ^s is through the use of a Couette viscometer. In this section we will use these measurements to derive a correlation for μ^s. As pointed out by Anderson and Jackson [1967], the bulk viscosity coefficient λ^s is, at present, inaccessible to measurement. It has been suggested, however, that it may be considerably larger than μ^s [Murray, 1965]. We are presently reviewing the existing analytical work and will attempt in the second year to evaluate λ^s from theoretical considerations. For the present it is estimated from the shear viscosity coefficient μ^s.

Schügerl [1971] reports shear viscosity measurements on several semi-fluidized and fully-fluidized beds. Semi-fluidized beds exhibit a complex rheological behavior and will not be considered here. Even for fully-fluidized, a shear viscosity in the Newtonian sense is only meaningful for small values of shear stress ($\tau \to 0$). Empirical observations (Schügerl [1971]; Gelperin and Einstein [1971b]) suggest that the shear viscosity μ^s decreases with bed expansion (i.e., $1-\phi/\phi-\phi_0$), and increases with particle density (ρ^s) and size (d).

In order to quantify the dependence of μ^s on $1-\phi/\phi-\phi_0$, ρ^s and d, we will now develop a simple theoretical model for μ^s. We will assume that μ^s primarily arises from particle slippage. Let us consider an element of fluidized bed (see Figure 3.5a). It is assumed that both the gas and the particle flow are in the upward direction. Let τ denote the shear stress acting on the face normal to the x-direction. The frictional force on this face is, therefore, given by:

$$F = \tau \times m \times \ell = \mu^s \frac{\partial u}{\partial x} m \ell \qquad (3.71)$$

We now consider a slice of width $\Delta\xi (= 2d)$. The frictional force due to frictional sliding between the particles in $\Delta\xi$ (see Figure 5b) is given by:

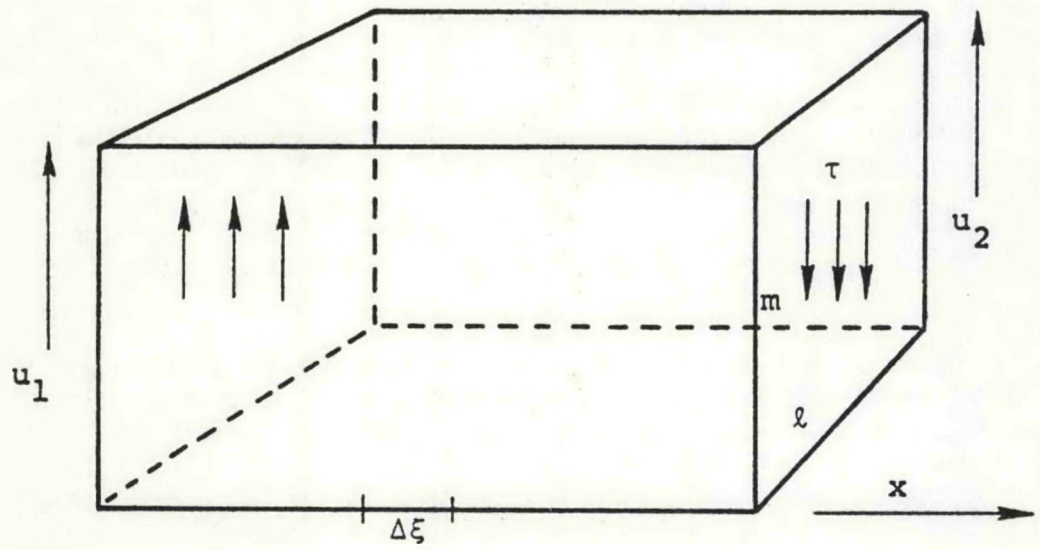

Figure 3.5a. Element of fluidized bed.

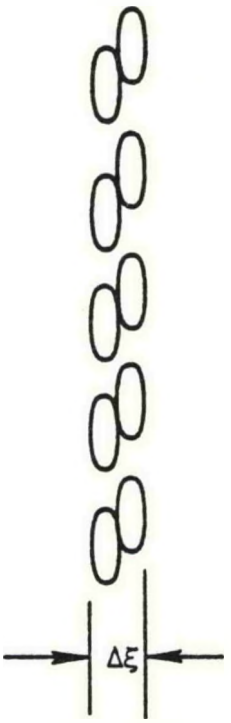

Figure 3.5b. Frictional sliding between the particles.

$$F_\xi = A\,\Delta u\,c_f\,\rho^s = A\,\frac{\partial u}{\partial x}\,d\,c_f\,\rho^s \tag{3.72}$$

where

A = contact area between particles

c_f = coefficient of friction

Δu = slip velocity between particles.

Equilibrium considerations require that $F = F_\xi$. This yields:

$$\mu^s = c_f\,\frac{A\,d\,\rho^s}{\ell \times m} \tag{3.73}$$

The particle contact area A can be written as:

$$A = \frac{\text{particle surface area}}{F(\phi-\phi_0)} = \frac{(1-\phi)(\ell m)}{F(\phi-\phi_0)} \tag{3.74}$$

where ϕ_0 is the bed porosity at minimum fluidization, and $F(\phi-\phi_0)$ is a monotonically increasing function of $(\phi-\phi_0)$. Equation (3.74) implies that A is maximum for $\phi = \phi_0$ and decreases with increasing $\phi-\phi_0$. Combining Eqs. (3.73) and (3.74), we finally obtain:

$$\mu^s = c_f\,d\,\rho^s\,\frac{(1-\phi)}{F(\phi-\phi_0)} \tag{3.75}$$

Equation (3.75) shows that μ^s increases linearly with d and ρ^s, and decreases with $1-\phi/F(\phi-\phi_0)$. Roughness and particle shape do not appear to affect μ^s except through c_f and ϕ_0. As a matter of fact, experimental data of Schügerl show that roughness does not appreciably affect μ^s.

We will now use the experimental data of Schügerl to develop a correlation for μ^s. Figure 3.6 shows a plot of $\bar{\mu}^s$ [$\bar{\mu}^s = \mu^s\,(10^{-2}\,d^{-2})\,(2.65\,\rho_s^{-1})$; d and ρ^s are in CGS units] versus $1-\phi/\phi-\phi_0$. It can be seen from Figure 3.6 that $\bar{\mu}^s$ exhibits a linear dependence on $1-\phi/\phi-\phi_0$.

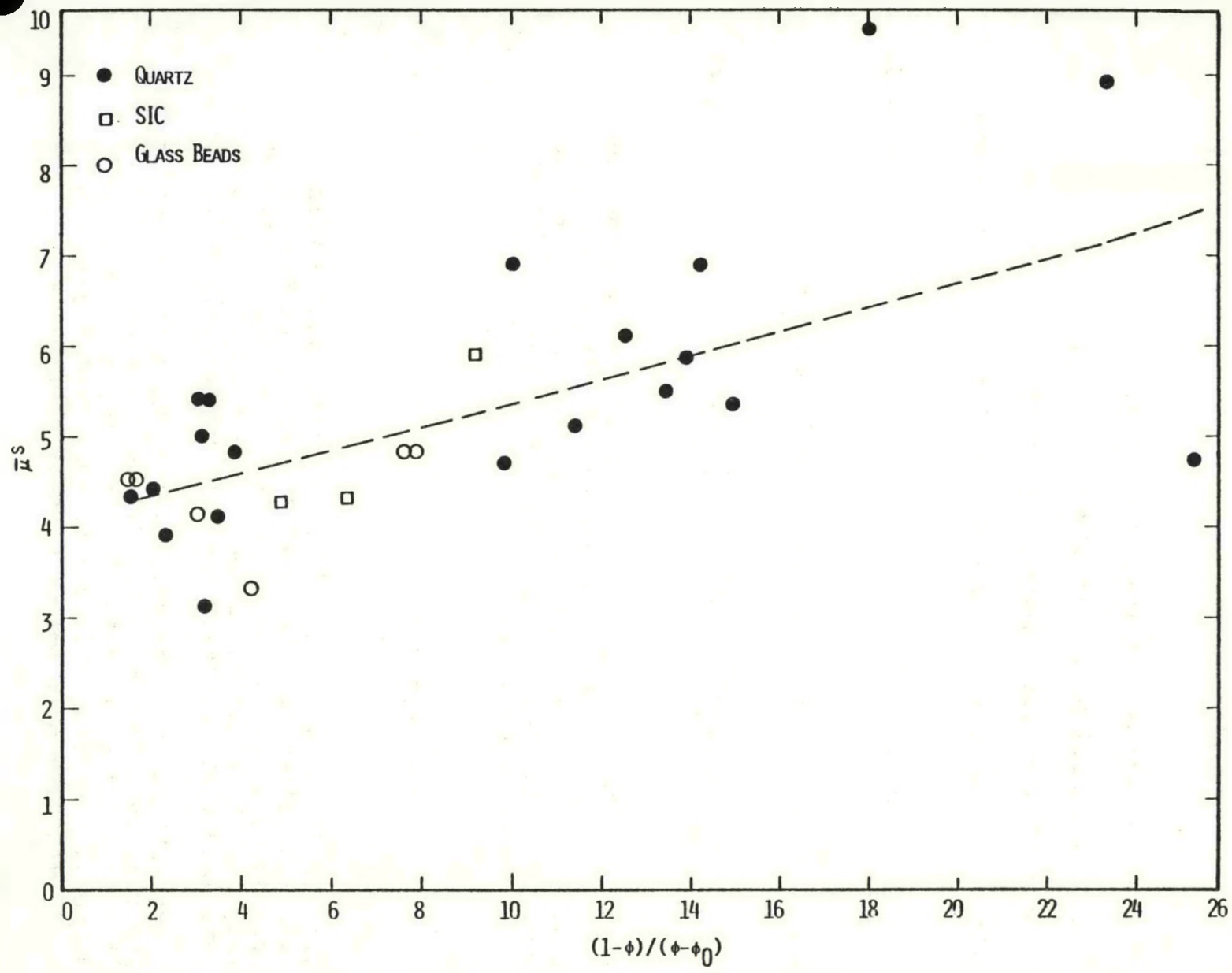

Figure 3.6. Shear viscosity measurements.

$$\bar{\mu}^s = \left[4.35 + 0.13\left(\frac{1-\phi}{\phi-\phi_0}\right)\right] \text{ poise} \qquad (3.76)$$

It should be mentioned here that data for light particles (e.g., polystyrene) cannot be described by Eq. (3.76). The reasons for the latter are at present only poorly understood (see Schügerl [1971]). Experimental data (and hence Eq. (3.76)) of Figure 3.6 cover only moderate bed expansions ($2 \leq 1-\phi/\phi-\phi_0 \leq 25$). For very small bed expansions ($1-\phi/\phi-\phi_0 \geq 100$), the fluidized beds exhibit non-Newtonian behavior. For want of better data in this regime (and also for practical reasons insofar as we are primarily interested in fully fluidized beds), it is suggested that Eq. (3.76) be used in the range $2 \leq 1-\phi/\phi-\phi_0 \leq 100$; and for $1-\phi/\phi-\phi_0 > 100$, $\bar{\mu}^s$ be taken equal to its value at $1-\phi/\phi-\phi_0 = 100$.

$$\bar{\mu}^s\left(\frac{1-\phi}{\phi-\phi_0} > 100\right) = \bar{\mu}^s\left(\frac{1-\phi}{\phi-\phi_0} = 100\right) . \qquad (3.77)$$

Little or no experimental data are available for large bed expansions ($1-\phi/\phi-\phi_0 < 2$). The particle assemblage viscosity μ^s will presumably approach zero as ϕ approaches unity ($1-\phi/\phi-\phi_0 \to 0$). For very dilute ($\phi \sim 1$) systems, the theoretical model described above will most probably break down; here, the principal mechanism for transmitting shear forces may be the viscous flow around the particles [Murray, 1965]. Pending availability of better experimental data and more accurate theoretical models, we suggest using the following relation for $\bar{\mu}^s$ in the range $0 \leq 1-\phi/\phi-\phi_0 \leq 2$:

$$\bar{\mu}^s = 0.5\ \bar{\mu}^s\left(\frac{1-\phi}{1-\phi_0} = 2\right) \times \left(\frac{1-\phi}{\phi-\phi_0}\right) \qquad (3.78)$$

where $\bar{\mu}^s\left(\frac{1-\phi}{\phi-\phi_0} = 2\right)$ is determined by using Eq. (3.76).

Equations (3.76) - (3.78) together specify $\bar{\mu}^s$ (and hence μ^s). These equations will be directly applied to characterize the shear viscosity of fluidized beds containing coal particles. That is, we assume that the model assumptions (3.72) - (3.75) together with the correlation of empirical data leading to (3.76) includes an adequate description for coal particles.

3.3.4 Heat Conduction Coefficient $\kappa(\phi)$

Fluidized beds used in coal gasification operate more or less under isothermal conditions (except near heat transfer surfaces). Therefore, an adequate specification of κ should only require the definition of an "effective thermal conductivity" for the mixture. The so-called "effective thermal conductivity" includes conductive, convective and radiative components. In our theoretical model for fluidized beds, convective and radiative components are accounted for separately. We, therefore, need to find an expression for the conductive component alone. Most likely, in fluidized beds, radiative (at high temperatures) and convective (associated with solid particle motion) components dominate the heat transfer; purely conductive component is relatively small. Overall heat transfer measurements, on fluidized beds are, therefore, likely to obscure the conductive component.

Therefore, to evaluate the conductive component, it is useful to consider heat transfer data on fixed beds. Fixed beds have, by their very nature, no solid motion. Assuming that the convective component due to gas flow is small, the heat transfer data for fixed beds may be used to approximately evaluate κ. Gelperin and Einstein [1971a] recommend that the graph in Figure 3.7 be used to evaluate κ. In the range $\kappa^s/k^f \leq 5000$, κ can be approximated by the relation:

$$\frac{\kappa(\phi)}{\kappa^f} = 1 + \frac{(1-\phi)(1-\kappa^f/\kappa^s)}{\frac{\kappa^f}{\kappa^s} + 0.28\ \phi^{0.63(\kappa^s/\kappa^f)^{0.18}}} \qquad (3.79)$$

Note that neglecting the second term in the denominator yields the classical "law of mixtures" rule for $\kappa(\phi)$. Eq. (3.79) shows that $\kappa(\phi)$ does not depend upon particle shape, or particle size, or particle density; it is a unique function of ϕ and particle and gas thermal conductivities.

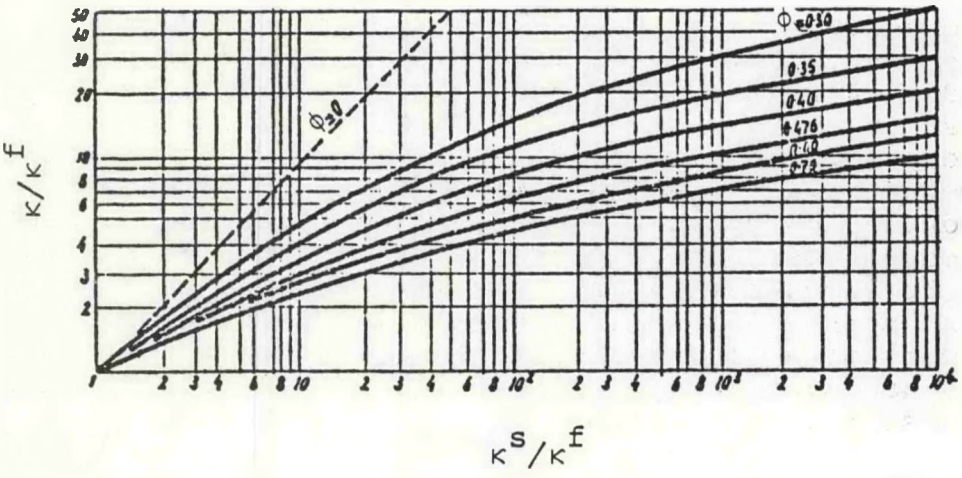

Figure 3.7. Diagram for determination of the effective conductivity of a fixed bed.

SECTION 4

IMPLICIT FINITE DIFFERENCE FORMULATION OF THERMOHYDRODYNAMIC MODEL

In this section we discuss the numerical model for non-reactive flows in gas fluidized beds. This model is based upon the theoretical formulation presented in Section 3 and includes major portions of the research effort in Tasks 01 and 02 as summarized in Section 2.

The differential equations for gas fluidized beds (Eqs. (3.26) - (3.30)), together with appropriate initial and boundary conditions, define a complicated initial value problem which, in general, must be solved with numerical methods. A finite difference computer model has been developed to provide such a solution. The mathematical character of the system of equations is of the mixed hyperbolic-parabolic type, and consequently we have used a methodology based upon an iterative, implicit, finite difference scheme. While there is an extensive literature related to such techniques and further documentation exists in text books (e.g., Richtmeyer and Morton, 1967) the development of an iterative, implicit method for the coupled solids-gas system of equations (3.26) - (3.30) is unique to the present investigation.

In the following paragraphs we discuss this numerical model within the context of two-dimensional Cartesian geometry. The extension of this code to axisymmetric geometry will be undertaken in the second year of the contract.

4.1 DIFFERENTIAL EQUATIONS

The equations for mass, momentum and energy conservation in two-dimensional Cartesian geometry are obtained from the general tensorial Eqs. (3.26) - (3.30). The conservation of mass for the solid and gas phases is respectively given by

$$\frac{\partial \theta}{\partial t} + \frac{\partial}{\partial x}\left[\theta u_x\right] + \frac{\partial}{\partial y}\left[\theta u_y\right] = 0 \tag{4.1}$$

$$\frac{\partial}{\partial t}\left[(1-\theta)\rho\right] + \frac{\partial}{\partial x}\left[(1-\theta)\rho v_x\right] + \frac{\partial}{\partial y}\left[(1-\theta)\rho v_y\right] = 0 \tag{4.2}$$

There are two equations of momentum conservation for each phase; in the case of the solid we have

$$\rho^s\left\{\frac{\partial}{\partial t}\left[\theta u_x\right]+\frac{\partial}{\partial x}\left[\theta u_x u_x\right]+\frac{\partial}{\partial y}\left[\theta u_x u_y\right]\right\}=\rho^s\theta g_x-\frac{d}{d\theta}\left(P^s\right)\frac{\partial\theta}{\partial x}$$
$$+\frac{\partial}{\partial x}\left[\left(\lambda^s+\frac{4}{3}\mu^s\right)\frac{\partial u_x}{\partial x}+\left(\lambda^s-\frac{2}{3}\mu^s\right)\frac{\partial u_y}{\partial y}-P\right]$$
$$+\frac{\partial}{\partial y}\left[\mu^s\left(\frac{\partial u_x}{\partial y}+\frac{\partial u_y}{\partial x}\right)\right] \qquad (4.3)$$

$$\rho^s\left\{\frac{\partial}{\partial t}\left[\theta u_y\right]+\frac{\partial}{\partial x}\left[\theta u_y u_x\right]+\frac{\partial}{\partial y}\left[\theta u_y u_y\right]\right\}=\rho^s\theta g_y-\frac{d(P^s)}{d\theta}\frac{\partial\theta}{\partial y}$$
$$+\frac{\partial}{\partial y}\left[\left(\lambda^s+\frac{4}{3}\mu^s\right)\frac{\partial u_y}{\partial y}+\left(\lambda^s-\frac{2}{3}\mu^s\right)\frac{\partial u_x}{\partial x}-P\right]$$
$$+\frac{\partial}{\partial x}\left[\mu^s\left(\frac{\partial u_y}{\partial x}+\frac{\partial u_x}{\partial y}\right)\right] \qquad (4.4)$$

while the conservation of gas momentum is expressed by

$$v_x=u_x-\frac{k(\theta)}{(1-\theta)\mu}\frac{\partial p}{\partial x} \qquad (4.5)$$

$$v_y=u_y=\frac{k(\theta)}{(1-\theta)\mu}\frac{\partial p}{\partial y} \qquad (4.6)$$

The energy equation for the two phases, again based upon the assumption of local thermodynamic equilibrium, is

$$\frac{\partial}{\partial t}\left\{\left[\theta+(1-\theta)\left(\frac{\rho\, c_v}{\rho^s\, c_v^s}\right)\right]T\right\}$$
$$+\frac{\partial}{\partial x}\left\{\left[\theta u_x+(1-\theta)\left(\frac{\rho\, c_v}{\rho^s\, c_v^s}\right)v_x\right]T\right\}$$
$$+\frac{\partial}{\partial y}\left\{\left[\theta u_y+(1-\theta)\left(\frac{\rho\, c_v}{\rho^s\, c_v^s}\right)v_y\right]T\right\}$$
$$=\frac{\partial}{\partial x}\left(\alpha\frac{\partial T}{\partial x}\right)+\frac{\partial}{\partial y}\left(\alpha\frac{\partial T}{\partial y}\right) \qquad (4.7)$$

We have already noted (Section 3) the use of the ideal gas relationship which we write as

$$p = \frac{R}{m}\,\rho T \tag{4.8}$$

It is also assumed that the viscosity is a function of temperature

$$\mu = \mu_0 (T/T_0) \tag{4.9}$$

and that (ρ^s, c_v^s, c_v) are constants. The constitutive relationships for $dp^s/d\theta$, λ^s, μ^s, $k(\theta)$, $\kappa(\theta)$ have been discussed in Section 3.3. It is convenient to eliminate the gas velocity components v_x, v_y from this system of equations. This can be accomplished by combining the momentum equations for the gas phase, (4.5) and (4.6), with the mass equation for the gas phase (4.2) and the mixture energy equation (4.7). We obtain the transformed gas mass and mixture energy equations

$$\frac{\partial}{\partial t}\left[(1-\theta)\rho\right] + \frac{\partial}{\partial x}\left[(1-\theta)\rho u_x\right] + \frac{\partial}{\partial y}\left[(1-\theta)\rho u_y\right] = \frac{\partial}{\partial x}\left[\frac{\rho k}{\mu}\frac{\partial p}{\partial x}\right] + \frac{\partial}{\partial y}\left[\frac{\rho k}{\mu}\frac{\partial p}{\partial y}\right] \tag{4.10}$$

$$\begin{aligned}
&\frac{\partial}{\partial t}\left\{\left[\theta + (1-\theta)\frac{\rho c_v}{\rho^s c_v^s}\right] T\right\} \\
&\quad + \frac{\partial}{\partial x}\left\{\left[\theta + (1-\theta)\frac{\rho c_v}{\rho^s c_v^s}\right] u_x T\right\} \\
&\quad + \frac{\partial}{\partial y}\left\{\left[\theta + (1-\theta)\frac{\rho c_v}{\rho^s c_v^s}\right] u_y T\right\} \\
&\quad = \frac{\partial}{\partial x}\left(\alpha \frac{\partial T}{\partial x}\right) + \frac{\partial}{\partial y}\left(\alpha \frac{\partial T}{\partial y}\right) \\
&\quad + \frac{\partial}{\partial x}\left\{\left(\frac{\rho c_v}{\rho^s c_v^s}\right)\frac{Tk}{\mu}\frac{\partial p}{\partial x}\right\} + \frac{\partial}{\partial y}\left\{\left(\frac{\rho c_v}{\rho^s c_v^s}\right)\frac{Tk}{\mu}\frac{\partial p}{\partial y}\right\}
\end{aligned} \tag{4.11}$$

Thereby with (4.1), (4.3), (4.4), (4.8), and (4.9) and these transformed equations (4.10), (4.11) we obtain a system of

equations for the solution of θ, ρ, T, u_x u_y. In general, numerical techniques are required to obtain solutions for such a complex system of equations; the present numerical model is introduced in the following paragraphs.

4.2 SUMMARY OF NUMERICAL METHOD

The numerical model involves a combined Eulerian-Lagrangian formulation which permits a calculation of both the large displacements associated with the gas motion as well as the histories of the solid particle locations. This character of the model leads to the use of two finite difference grids and is illustrated by the finite difference zones shown in Figure 4.1. The (x, y) space is divided into zones Δx, Δy by a conventional Eulerian grid which is fixed in space. Superimposed upon this grid is a large collection of Lagrangian particles which provide a grid for the solid phase. The representative solid particles move through the Eulerian grid as the calculation proceeds. These particles, which describe the average behavior of a large number of actual physical particles, carry the mass, momentum and energy of the solid phase. For the case of non-reactive flows, as in our present discussion, the mass associated with each particle does not change with time, but both momentum components and the particle solid temperature may change in accordance with the convective and diffusive terms of the relevant governing equations. The motion of these representative particles thus takes into account all solid advection effects.

For a particular time step, the positions of the solid particles are first changed by an amount $(\vec{u} \cdot \Delta t)$, and the field variables assigned to the Eulerian grid are altered to reflect the new particle distribution. Then, the additional terms in the field equations for mass, momentum and energy conservation (viscous stresses, pressure forces, heat conduction, etc.) are taken into account using the Eulerian grid. Finally, the field variable quantities assigned to the representative particles are changed to reflect the effect of these latter terms. This general procedure (or "time cycle") may be repeated as many times as desired, with each such repetition advancing the solution further in time. The use of a superposed Lagrangian grid of representative particles to treat advective effects avoids the computational "smearing" of field variables which occurs in purely Eulerian computational procedures.

The nature of the calculational cycle is indicated in the schematic diagram of Figure 4.2. The calculation occurs in three phases; the first of these involves the updating of the solidity θ through the solution of the finite difference

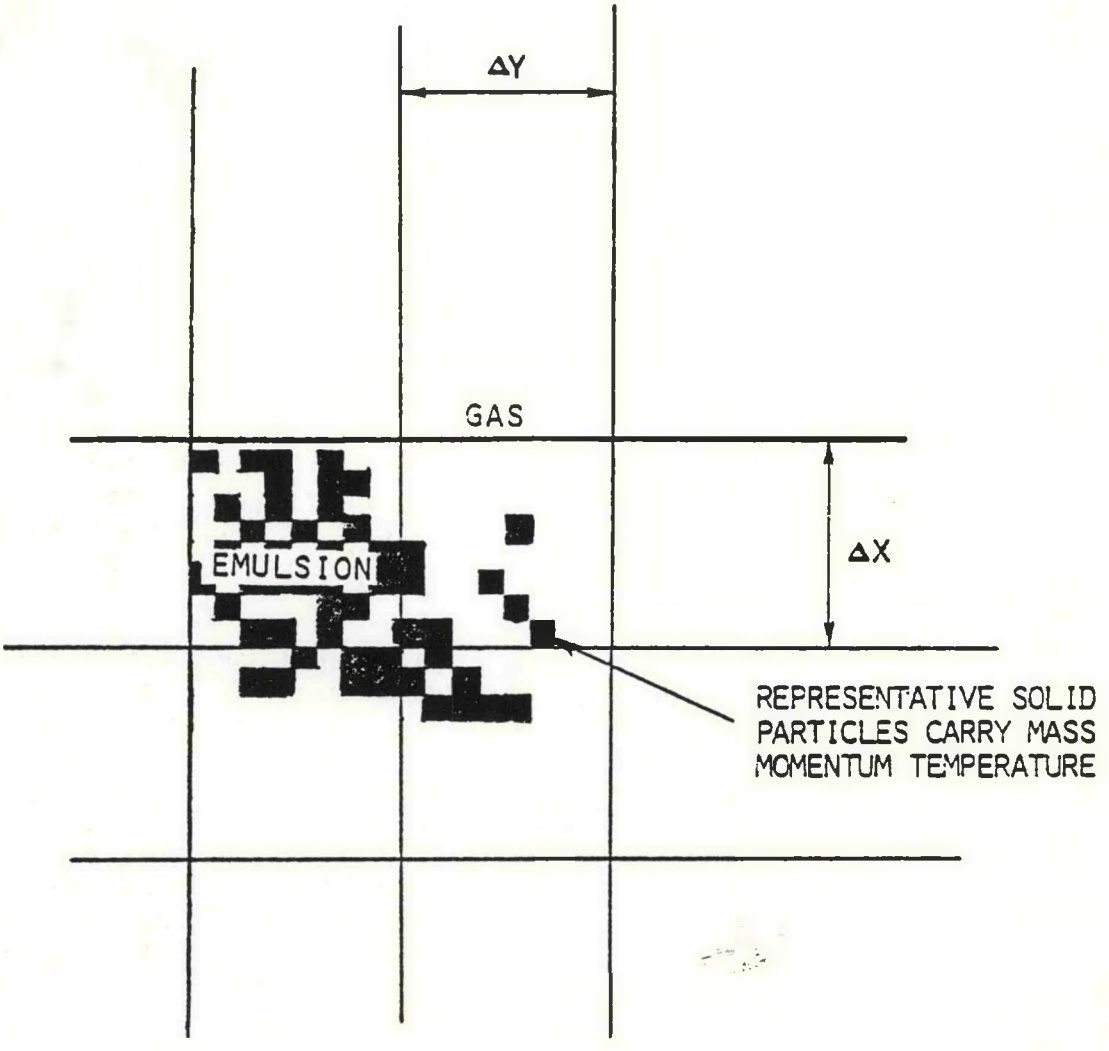

Figure 4.1. Eulerian/Lagrangian formulation of solid-gas motion with chemical reaction.

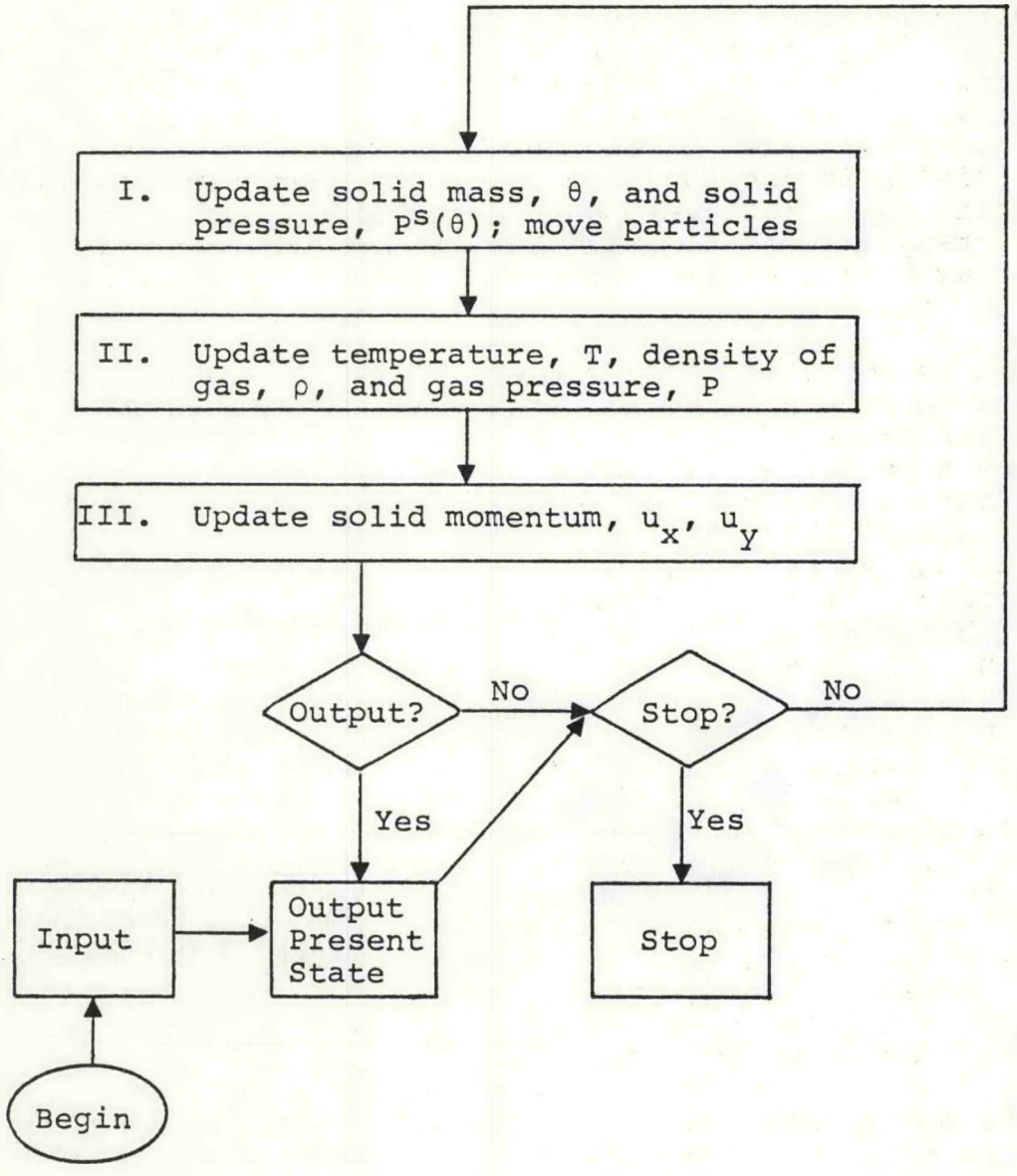

Figure 4.2. Schematic of computational cycle for thermo-hydrodynamic code.

form of (4.1). This provides, as well, a definition of both the new solid pressure $P^s(\theta)$ and the new particle positions. Then the new gas density, ρ, and temperature, T, are determined by simultaneous solution of Eqs. (4.8) through (4.11) in phase II. The gas pressure is obtained from the density and temperature. Finally, the solid momentum equations (4.3) and (4.4) are solved to determine the solid velocities u_x and u_y in phase III. Given these new temperature and solid velocity fields in the Eulerian grid, the energy and momentum of the solid particles are updated according to the location of the Lagrangian particles in that grid. The local gas velocity may be calculated from the finite difference equivalent of the gas momentum equations (4.5) and (4.6).

Let us consider, in some detail, the nature of the solid mass update in Stage I. This will provide an insight into the structure of the numerical procedure and will also illustrate some of the conceptual aspects of this model. Each Lagrangian particle is, again, representative of a large number of actual physical particles which comprise the solid phase. Within this context we note the usual finite difference approximation. That is, in the limit, as the finite difference zone (in this case the Lagrangian particle size) becomes smaller the finite difference approximation becomes a more accurate representation of the particle dynamics. These Lagrangian particles have, for Cartesian geometry, a rectangular shape and an "area". This "area", associated with each particle, is such, that at the initial solidity $\theta = \theta_0$, the sum of the particle "areas" will exactly fill the area of the Eulerian grid zone in question. The rectilinear shape and area of these Lagrangian particles does not, of course, affect the physical representation of particle size distribution and shape which is inherent in the constitutive equations for the solid phase. These geometric aspects of the representative particles are merely artifices which are part of the finite difference accounting procedures.

The solid mass update, or calculation of θ, at $t^{n+1} = t^n + \Delta t$, is based upon two prerequisites. First we calculate θ based upon the solid velocity field u_x^n, u_y^n at t^n. Second, we implicitize the effects of solid compaction waves occurring because of the presence of the solid pressure term $d/d\theta\,[\theta f(\theta)]\,\partial\theta/\partial x$ in the conservation of solid momentum (c.f., Eqs. (4.3) and (4.4). Consequently, we write the conservation of solid mass (4.1) as

$$\frac{\theta^{n+1} - \theta^n}{\Delta t} = - \frac{\partial}{\partial x} [\widetilde{\theta u}_x]^{n+1} - \frac{\partial}{\partial y} [\widetilde{\theta u}_y]^{n+1} \qquad (4.12)$$

where, for example, we define the x direction mass flux contribution as

$$[\widetilde{\theta u_x}]^{n+1} = [\theta u_x]^n + \Delta t \left[\frac{\partial}{\partial t} \widetilde{\theta u_x}\right]^{n+1} \tag{4.13}$$

The last term in this equation (4.13) can be evaluated, within the finite difference approximation, through recourse to the momentum equation for the solid phase (4.3). Specifically, we retain the solid pressure term to provide the implicitization and also include gas pressure and gravitational effects for completeness. This yields the definition

$$\left[\frac{\partial}{\partial t} \widetilde{\theta u_x}\right]^{n+1} = \frac{1}{\rho^s}\left\{\left[-\frac{\partial P}{\partial X} + \rho^s \theta g_x\right]^n - \left[P^s(\theta)\right]^{n+1}\right\} \tag{4.14}$$

With these relationships (4.13) and (4.14), and corresponding equations for the y-direction mass flux contribution, are used in (4.12) we have

$$\begin{aligned}\frac{\theta^{n+1} - \theta^n}{\Delta t} = &- \frac{\partial}{\partial x}\left[\theta u_x\right]^n - \frac{\partial}{\partial y}\left[\theta u_y\right]^n \\ &+ \frac{\Delta t}{\rho_s}\frac{\partial}{\partial x}\left[\frac{\partial P}{\partial x} - \rho^s \theta g_x\right]^n + \frac{\Delta t}{\rho_s}\frac{\partial}{\partial y}\left[\frac{\partial P}{\partial Y} - \rho^s \theta g_y\right]^n \\ &+ \frac{\Delta t}{\rho_s}\frac{\partial^2}{\partial x^2}\left[P^s(\theta)\right]^{n+1} + \frac{\Delta t}{\rho_s}\frac{\partial^2}{\partial y^2}\left[P^s(\theta)\right]^{n+1}\end{aligned} \tag{4.15}$$

The θ distribution is updated in two steps. First, the convective influence, based upon the particle velocities at t^n, represented by the first two terms on the right hand side of (4.15), is calculated. This provides a first approximation to the value of θ^{n+1}. During the particle motion the total mass flux across each zone interface, due to displacement, is recorded. Once all particles are moved, the fluxes for each zone interface are known and, if necessary, various flux corrections are imposed. Then the influence of the remaining terms in (4.15) are accounted for, using the donor cell technique. The resulting system of equations is reduced to a sequence of one-dimensional problems by the iterative Alternating-Direction-Implicit (ADI) method. The individual one-dimensional passes are nonlinear because of the nature

of (4.15) and consequently they are solved by an inner "module" which, itself, has an iterative character. This process yields new values for the "solid pressures" (P^s) in each Eulerian zone. With the completion of this step, the particle positions are corrected to account for the fluxes associated with mass redistribution in this second step of the θ calculation. A final "census" of the particles at these corrected locations, together with values of θ appropriate to the "area" of the particles completes the update of θ and solid mass.

The Stage II update of temperature and gas density and the Stage III update of solid momentum require the solution of equations containing diffusional terms which reflect the influence of the Darcian flow of gas, the conductive flux of heat, and the viscous shear stresses in the solid phase. This is evident in the simultaneous solution of (4.10) and (4.11) in Stage II and in the simultaneous solution of (4.3) and (4.4) in Stage III. The solution of these equations is also accomplished in multiple steps analogous to the Stage I update of solid mass. That is, we explicitly account for the convection of energy and momentum of the solid phase through the motion of the Lagrangian particles and we utilize iterative implicit methodology to treat the influence of the diffusive mechanisms.

The numerical code includes a very general capability to treat a variety of boundary conditions which are appropriate to gasifiers. For example, this capability can be used to represent solid walls, distributor plates, open ducts and screens; this is possible through boundary conditions imposed upon the variables θ, ρ, T, u_x and u_y. Since any face of any Eulerian zone may be designated as a boundary of any of these types, considerable generality as to problem geometry is available. In the following section we will illustrate, through sample calculations, some aspects of the numerical modeling of fluidized bed phenomena.

4.3 NUMERICAL CALCULATIONS AND VERIFICATION OF CONSTITUTIVE EQUATIONS

The numerical formulation described in Section 4.2 has been used to develop two codes for fluidized beds. These codes represent, respectively, flows in one and two spatial dimensions. The former code has been designated primarily as a "testbed" to examine numerical methodology and to also model simple fluidized bed experiments. For example, experimental flows up to the regime of incipient fluidization are approximately one-dimensional in character. In the following paragraphs we discuss some sample calculations obtained from

the one- and two-dimensional codes and we also present a brief comparison of the code calculations with measurements.

A schematic of a typical one-dimensional calculation is shown in Figure 4.3. In general, we wish to examine the relationship between flow rate, pressure drop and bed expansion for such a case. Of course, it is not possible to model the multidimensional effects associated with bubble formation and the subsequent interactions of bubbles with the one-dimensional code; however, most aspects of the flow field prior to bubble growth can be represented in such a calculation.

For example, we have used this one-dimensional code to model the anthracite fluidization experiments of Leva, et al., 1951. In those experiments air was used to fluidize beds of anthracite particles, with different weight-size distributions, for a range of air flow rates. The data are particularly interesting from a modeling viewpoint because the calculation must include the definition and utilization of shape factors and mean particle diameters. The weight size distributions for two of Leva's experiments are shown in the upper half of Figure 4.4. We use a mean particle diameter defined as

$$\bar{d} = \frac{1}{\sum \frac{X_i}{d_i}}$$

where X_i is the mass fraction of particles of diameter d_i. This particle diameter together with a shape factor* based upon the measurements of Leva, was used in the constitutive equations (c.f., Section 3.3) for the present model.

A comparison between the calculated and experimental pressure drop-Reynolds number relationship is shown in the lower half of Figure 4.4; the Reynolds number is based upon a particle diameter obtained from the sieve ratings D_p (c.f., Leva, et al., 1951) and the superficial gas velocity, V. These curves have an initial slope of approximately unity and, then, at fluidization, when the pressure drop balances the gravitational effects, the slope is approximately zero. The agreement between the calculation and the measurement is rather good, providing a verification of the drag

*We use the definition of the shape factor as the ratio of the area of a sphere equivalent to the volume of the particle divided by the actual surface area of the particle.

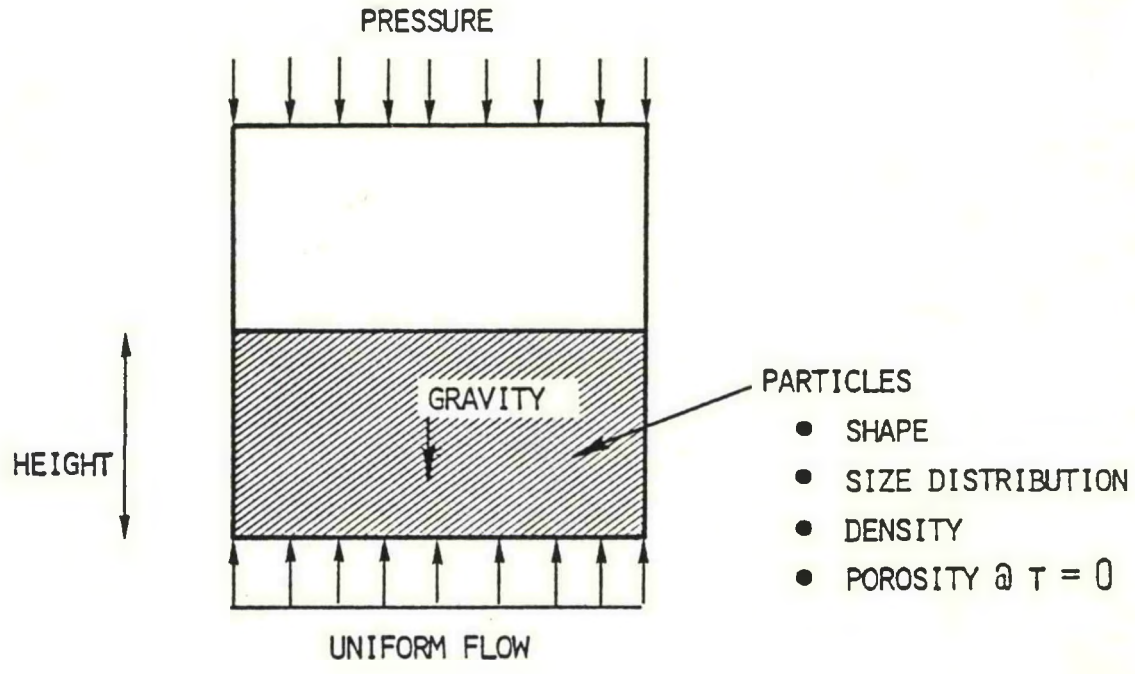

Figure 4.3. Schematic of one-dimensional calculation/experiment.

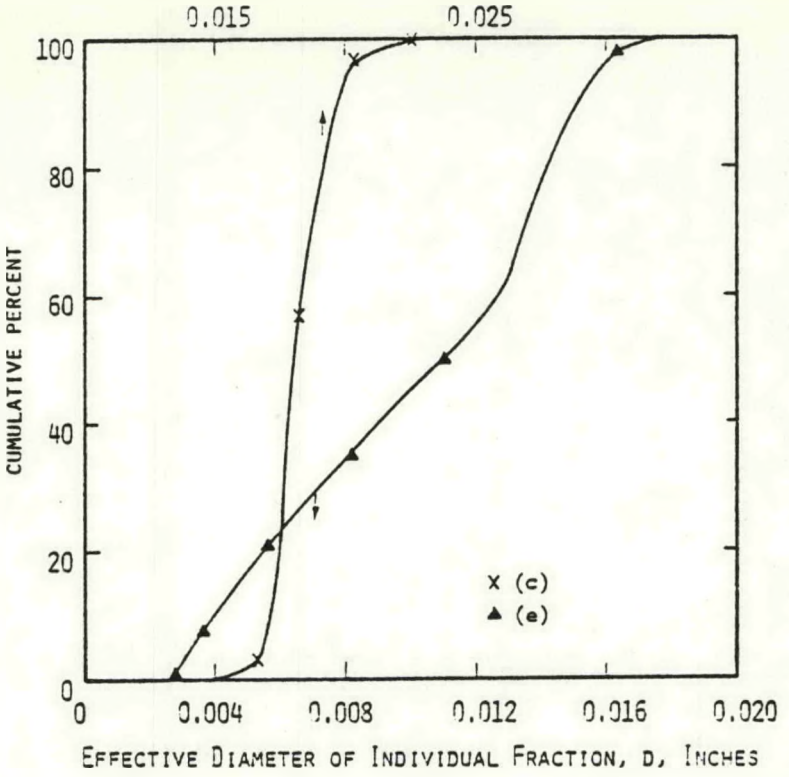

WEIGHT-SIZE DISTRIBUTION OF BEDS INVESTIGATED

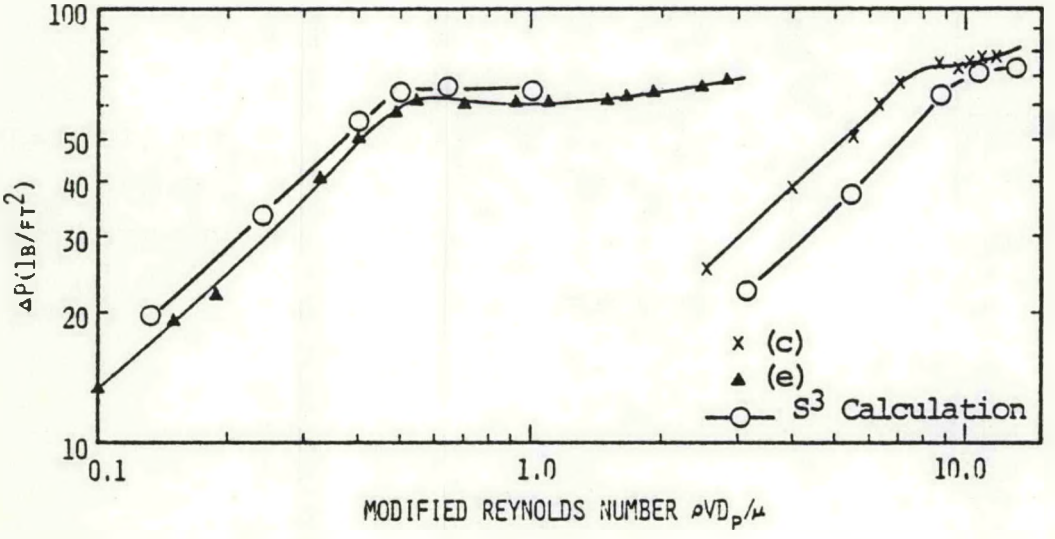

PRESSURE DROP-REYNOLDS NUMBER CALCULATIONS COMPARED TO ANTHRACITE-FLUIDIZATION DATA

Run	D_p (inches)	$\bar{D}$ (inches)	Γ	Φ
(c)	0.0232	0.0220	0.794	0.50
(e)	0.0121	0.0098	0.588	0.44

Figure 4.4. One-dimensional calculation of Leva, et al. [1951] experiments on fluidization of anthracite beds.

coefficient, $B(\phi)$, (or permeability relationship, $K(\phi)$) and also a partial verification of the elastic modulus $G(\phi)$ (c.f., Section 3.3). For example, if the elastic modulus in the model was not "stiff" enough, there would be a slumping of the bed which would give a different slope to the calculated curves.

A further evaluation of the constitutive equations being used in the model is illustrated in Figure 4.5, where one-dimensional code calculations are compared with experimental measurements. The curve presents a correlation between Reynolds and Galileo numbers for the prediction of minimum fluidization velocity; this correlation was developed by IGT. Numerical calculations, indicated by the large asterisks, are in good agreement with that correlation. Again this agreement tends to verify the drag coefficient formulation $B(\phi)$ in the model.

A more extreme flow condition is that associated with the porosity measurements of Bakker and Heertjes, 1960, where time averaged porosity distributions in air-fluidized beds of glass beads were measured and related to gas flow rates. These data were for regimes which included bubbling beds. While such regimes are not really one-dimensional, it is of interest to determine if global aspects of fluidized bed behavior, such as bed height changes, can be inferred from the one-dimensional calculations. To that end we modeled one of the experiments of Bakker and Heertjes in the manner indicated earlier in Figure 4.3. A computer plot of time-averaged porosity distribution in the bed at 2.1 secs after the start of the calculation is shown in Figure 4.6. Such a time average does not, of course, show the instantaneous porosity distribution in the calculation, but instead represents the averaged expansion of the bed due to bubbling phenomena. That time-average porosity is seen to be rather uniform for some distance in the bed and then it rapidly increases to unity (no solids). In a physical sense, the flat portion of this curve indicates the main region of the expanded bed while the rise to unit porosity indicates a region where particles are lofted in an underdense region above the bed. The instantaneous state of the bed is, of course, more chaotic, as can be understood from the gas pressure distribution at 2.1 secs shown in Figure 4.7, where the high pressure is at the distributor plate to the left and the low pressure is at the exit plane to the right of the figure. In that figure the regions with no pressure drop indicate bubbles which are propagating through the bed. There is a linear pressure drop in the dense or emulsion region of the flow field. From the calculation of mean porosity in Figure 4.6 we can define bounds on the expanded bed height; the lower bound is the knee of the porosity distribution while the upper bound is the height at which this

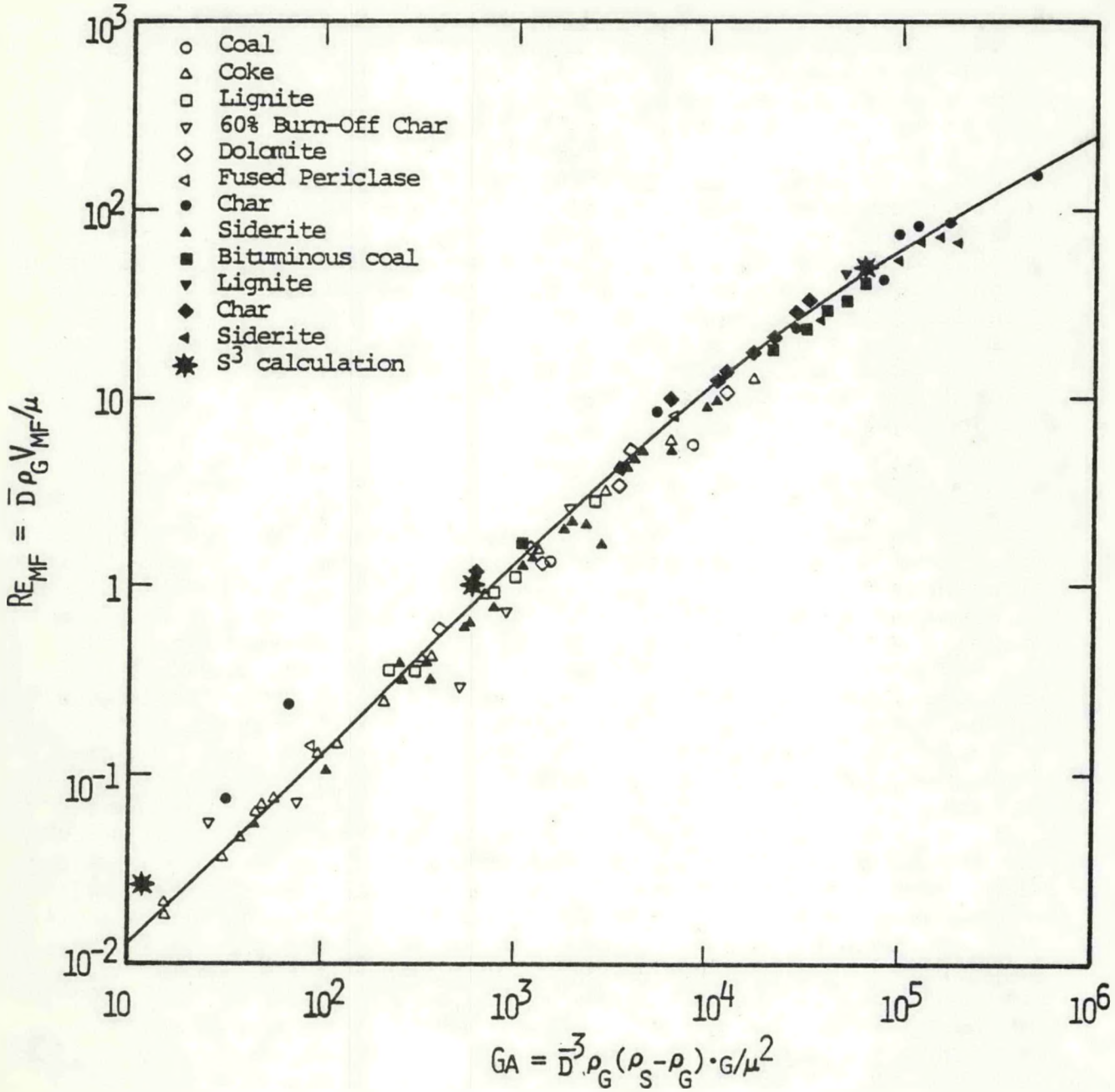

Figure 4.5. Comparison of S^3 calculation with IGT correlation for the prediction of minimum fluidization velocity.

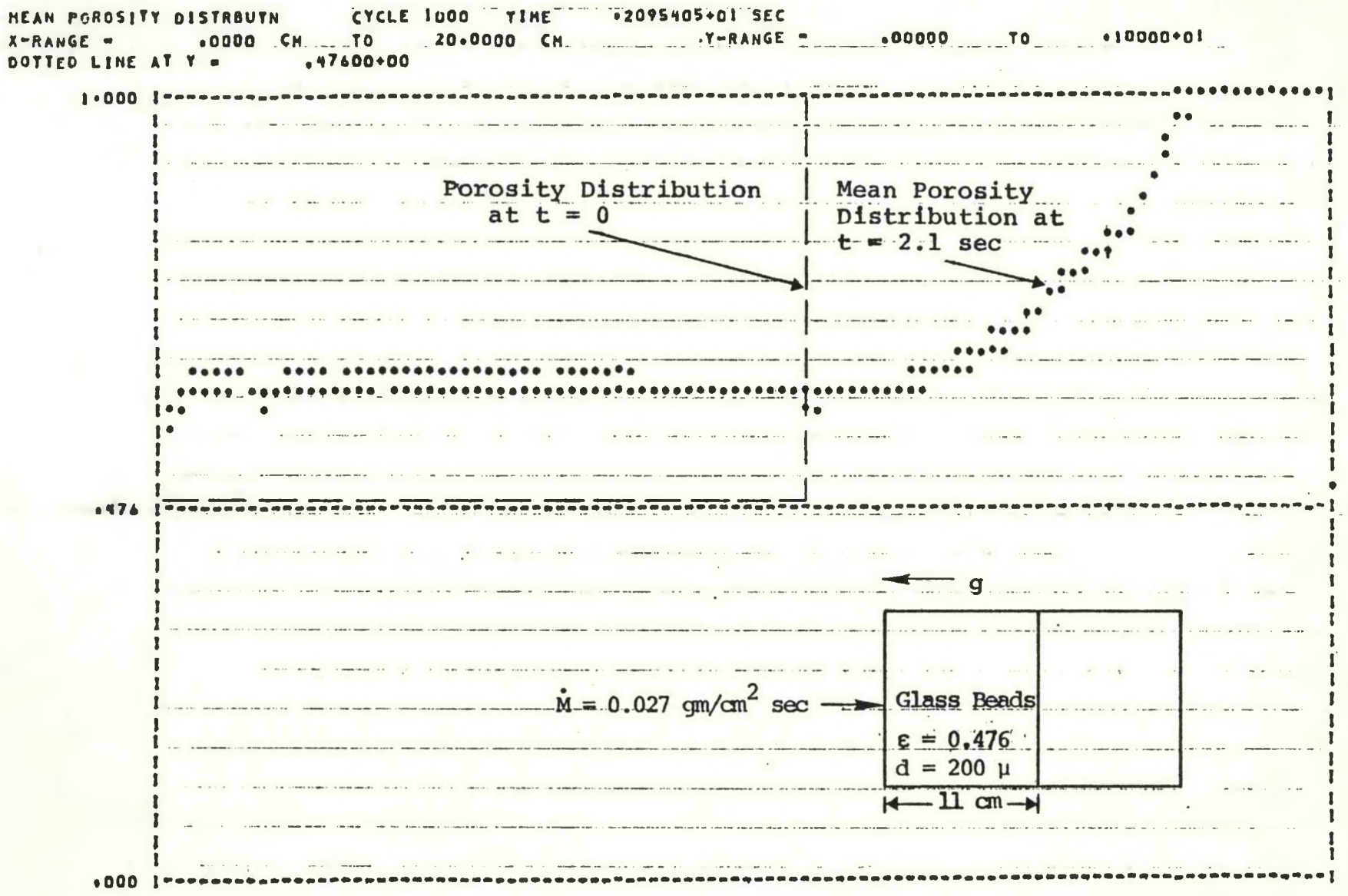

Figure 4.6. One-dimensional calculation of Bakker and Heertjes [1960] experiment - time average of porosity distribution.

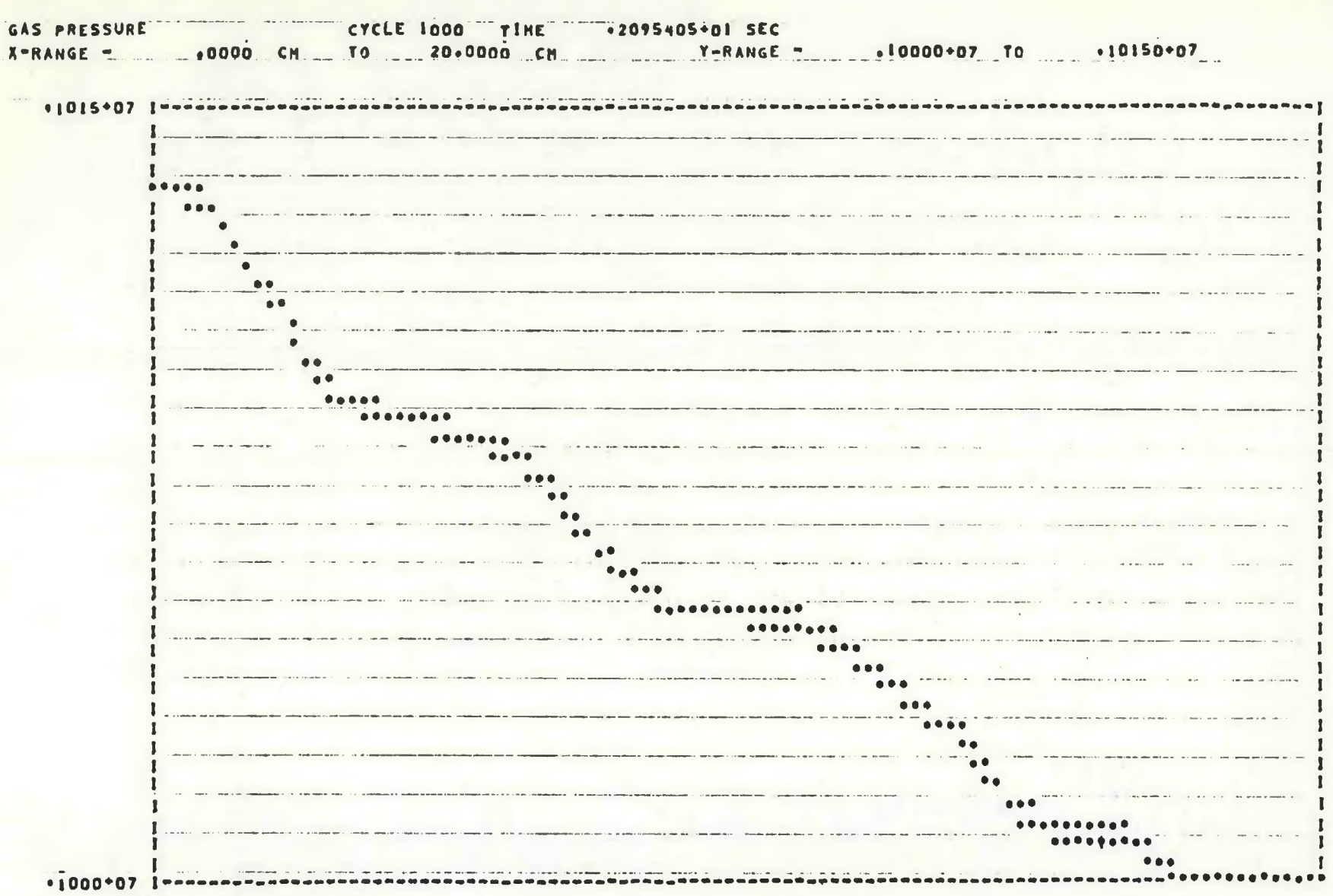

Figure 4.7. One-dimensional calculation - instantaneous pressure distribution.

distribution goes to unity. A comparison of this calculation with experimental data is shown in Figure 4.8; the specific measurements of Bakker and Heertjes [1960] for bed height are shown in the upper half of the figure as a function of flow rate. The calculation, indicated by the bracket, is in good agreement with that data. We have also compared the same calculation with a correlation of bed expansion from Matsen, et al. [1969], for slugging beds shown in the lower half of the figure. That correlation relates the ratio (bed height/bed height at minimum fluidization) to a parameter which involves the superficial velocity V, the superficial velocity at minimum fluidization, V_{MF}, and bubble velocity $V_B \sim 0.35\ (g\ D_{BED})^{\frac{1}{2}}$. Since the one-dimensional calculation in the bubbling regime is like a slugging bed, it is of interest to note the agreement between the calculation and the correlation. A comparison of the code results with data such as shown in Figure 4.8 provides a partial verification of $B(\phi)$, $G(\phi)$, $\lambda^s(\phi)$, and $\mu^s(\phi)$ (c.f., Section 3.3).

4.4 PARAMETRIC TWO-DIMENSIONAL NUMERICAL CALCULATIONS

Fluidized bed processes are dominated by multidimensional phenomena such as bubble motion, solids recirculation and surface waves. Several preliminary parametric calculations have been performed, with the two-dimensional numerical code, to study bubble formation and evolution in a shallow bed. The geometry of these problems is shown in Figure 4.9; we consider a planar bed, infinite in the lateral dimension, which is 32 cm in height. This bed consists of spherical glass particles, 860 microns in diameter. The air flows, at a prescribed and constant rate, through orifices in the distributor plate which are separated by 32 cm. Above the initial bed height is a free-board region of 24 cm topped by a screen, impermeable to the solid particles. Atmospheric pressure acts on the gas flowing through this screen. We assume that the initial state of the glass particles is at rest with a porosity of 0.50; at time t = 0, the gas flow is initiated.

Because of the symmetries of this boundary initial value problem it is only necessary to consider the flow field between two vertical planes perpendicular to the plane of the figure. One plane bisects an individual orifice; the second plane bisects the lateral distance between two of the orifices. For the sake of illustration this quadrant of flow can be unfolded to encompass the region shown in Figure 4.9, which includes one and one-half orifices. It is that region which will be examined in the subsequent discussion and related figures.

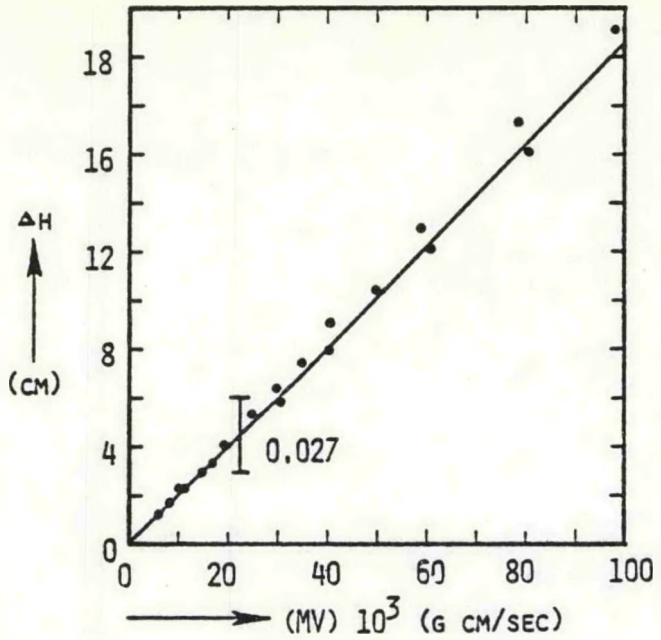

ΔH AS A FUNCTION OF BED WEIGHT × FLUIDIZATION VELOCITY, BAKKER AND HEERTJES (1960).

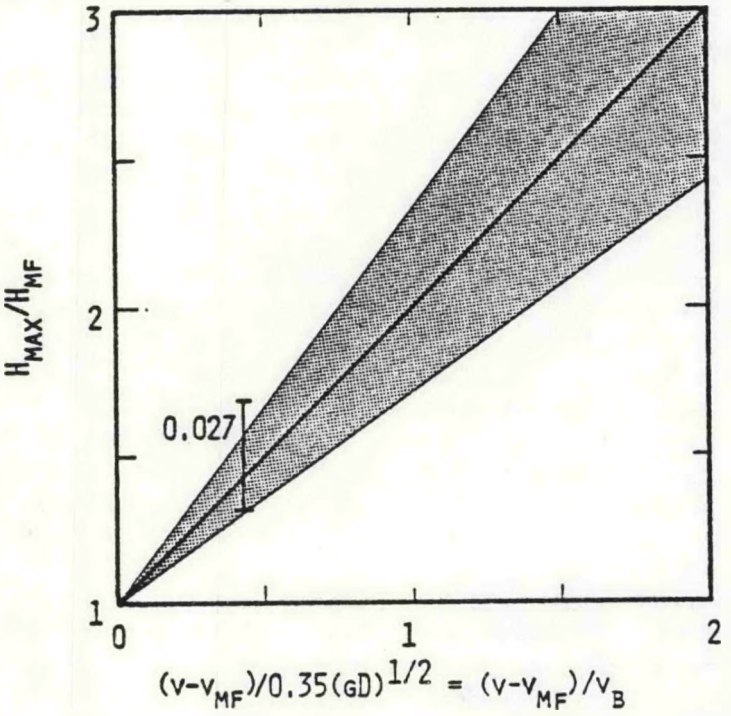

BED HEIGHT FOR SLUGGING FLUIDIZED BED, AS A FUNCTION OF SUPERFICIAL VELOCITY V, AND BUBBLE VELOCITY V_B, MATSEN, ET AL. (1969).

Figure 4.8. Calculated bed height, based upon mean porosity distribution compared with data.

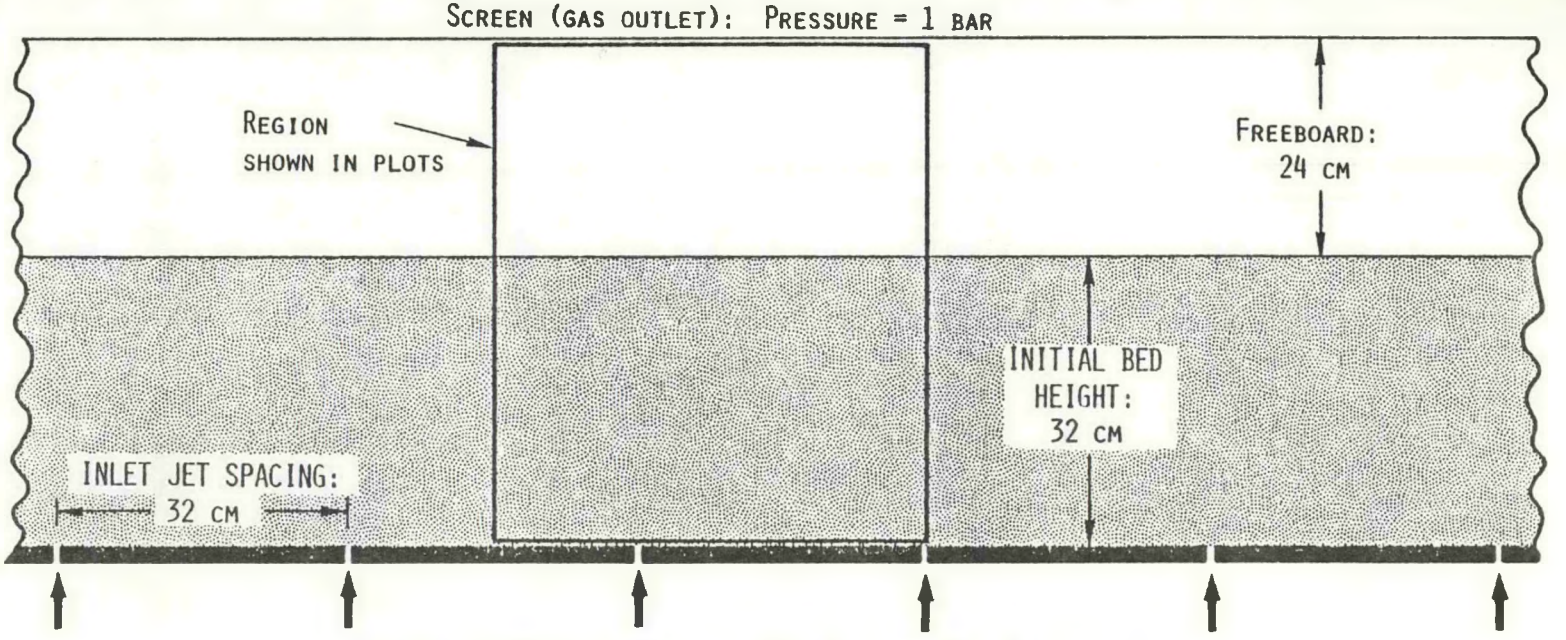

INITIAL CONDITIONS:

System at rest
Interior gas pressure = 1 bar
Interior temperature = 0°C

GAS PROPERTIES:

Type -- Air
Molec. Wt. = 29
Specific heat = 0.167 cal/g-°C
Conductivity = 573 cal/cm-°C
Viscosity = 170.8 micropoise

BOUNDARY CONDITIONS:

Upper boundary:
  Gas pressure = 1 bar
  No solid transfer
Lower boundary:
  Impermeable (except at inlets)
  No solid transfer
Inlet flow turned on at t = 0
  with T = 0°C gas at various flowrates

SOLID PROPERTIES:

Type -- Spherical glass beads
Particle diameter = 860 microns
Density = 3 grams/cm^3
Ambient packing porosity = 50%
Specific heat = 0.167 cal/g-°C
Conductivity = 2×10^{-3} cal/g-°C
Effective shear (bulk) "viscosity" = 10(20) poise

INLET FLOWRATES:

Problem	Mass Rate	Average Gas Velocity
A	12.2 g/sec-cm	295 cm/sec
B	13.6 g/sec-cm	328 cm/sec
C	15.0 g/sec-cm	361 cm/sec

Figure 4.9. Boundary value problem for two-dimensional calculation of shallow fluidized bed.

Let us consider the flow rate for the problem designated by B in Figure 4.9. This flow rate is sufficient to produce a sequence of bubbles at the orifice leading to classical patterns of solid recirculation in the bed. This history of bubble evolution is shown in Figure 4.10, beginning with the quiescent state at t = 0 in Figure 4.10a. The black symbols in the figure indicate the location of the Lagrangian particles which represent the solid phase in the gas-solid mixture. A large bubble forms at the orifice and rises from that orifice approximately 0.6 sec (Figures 4.10b - 4.10g) after the gas flow is initiated. Simultaneously, gas diffuses through the dense emulsion region from the bubble. As the bubble grows and rises from the orifice it produces a significant wave pattern at the free surface of the bed of particles. This is shown by the solid particle displacements at the surface. As the bubble approaches the surface in Figures 4.10h - 4.10k, the interaction culminates in a complete collapse of both the bubble and the free surface with gas in the bubble completely diffusing through the bed and passing through the free-board region. A second bubble develops at the orifice at t = 1.1 secs in Figure 4.10l and rises to the surface of the bed in Figures 4.10l to 4.10p; we note the development of a third bubble at t = 1.5 secs, shown in that latter figure. The pattern of solid particle convection and recirculation in this boundary value problem can be best understood by introducing a "darkened" layer of glass particles at the base of the bed and observing the displacement of those glass particles during the bubble evolution. This displacement is shown through the time sequence of Lagrangian particle locations in Figure 4.11. The flow pattern is identical to that in the previous Figure 4.10 but we can now observe the marked particles. During the time interval 0 to 1.1 secs, a single gas bubble has formed at the orifice and has risen to the surface of the bed. This gas bubble convects solid particles both in its wake and also in a thin circumferential region around the bubble (in a deeper bed these latter particles would likely rain through the bubble and be convected in the wake). The entrainment of these particles is clearly shown in the trail at time t = 1.1 secs; this wake has the classic pattern observed in many two-dimensional fluidized bed experiments (c.f., Davidson and Harrison, 1971).

The gas flow rate has a strong influence upon the formation and evolution of bubbles in this shallow bed. A comparison of the flow fields for the three problems A, B and C is shown in Figure 4.12; again the flow rate in problem B is the intermediate case which leads to the formation of a succession of bubbles at the orifice. These bubbles, as previously shown in Figures 4.10 and 4.11, rise to the free surface of the bed and produce a dramatic pattern of surface waves as they diffuse through the free surface. If the flow

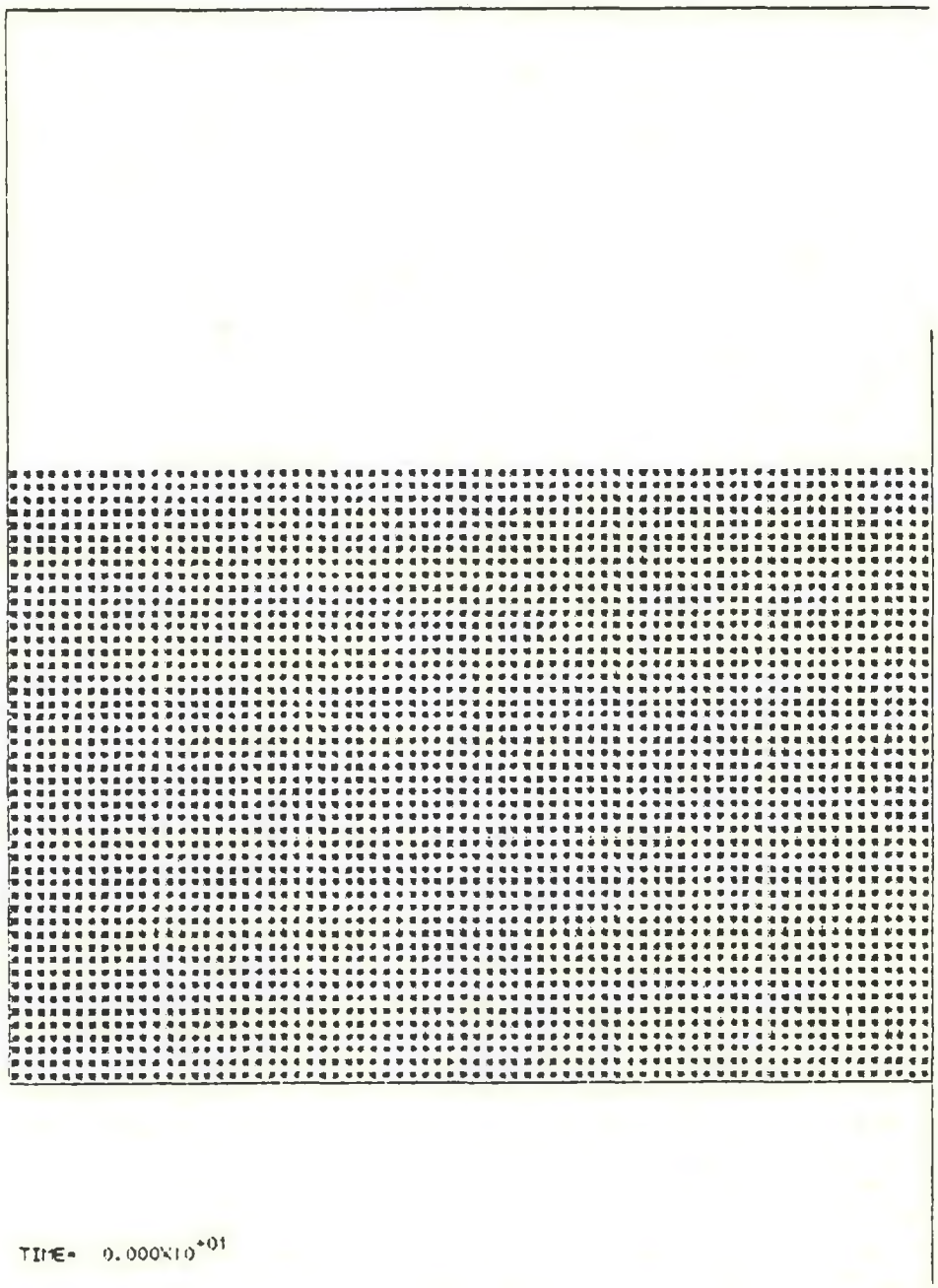

Figure 4.10a. Time history of bubble evolution in a two-dimensional bed, Problem B.

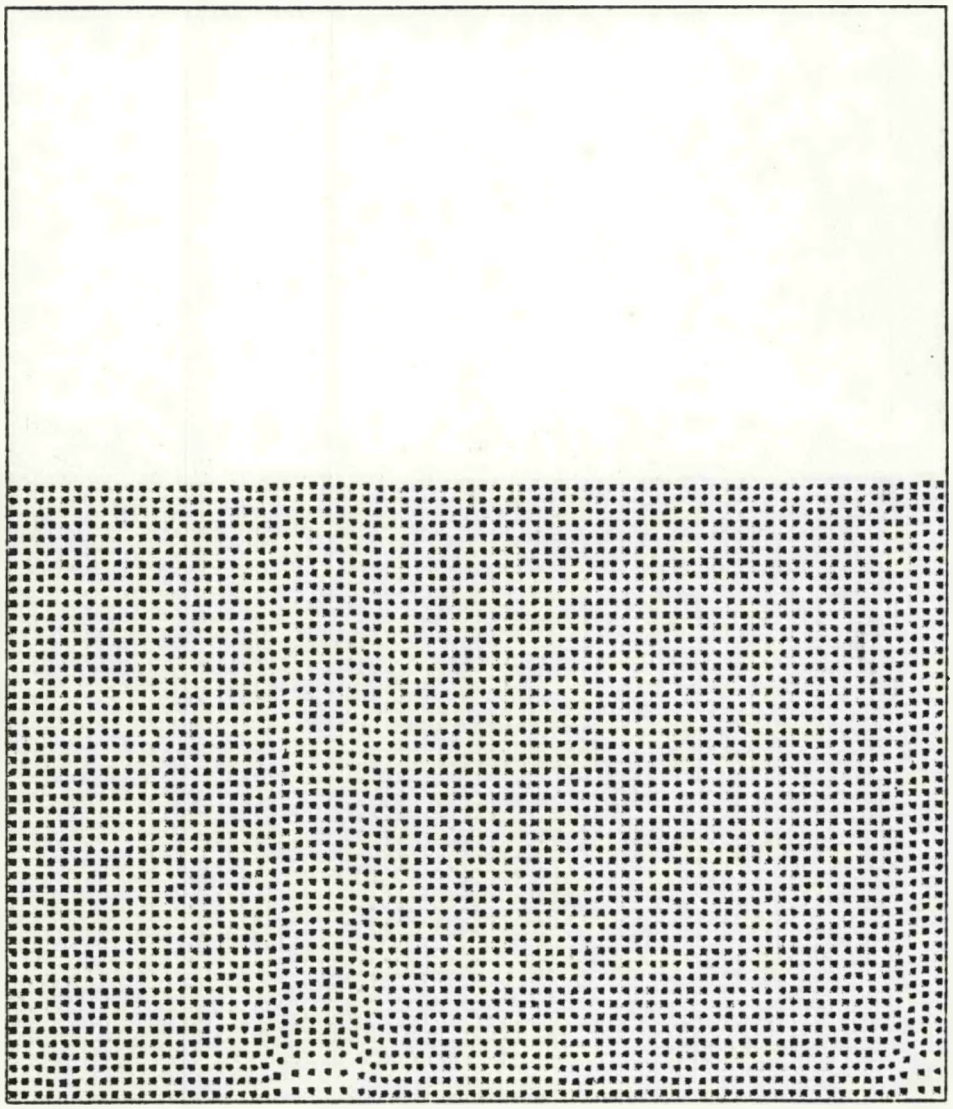

Figure 4.10b.

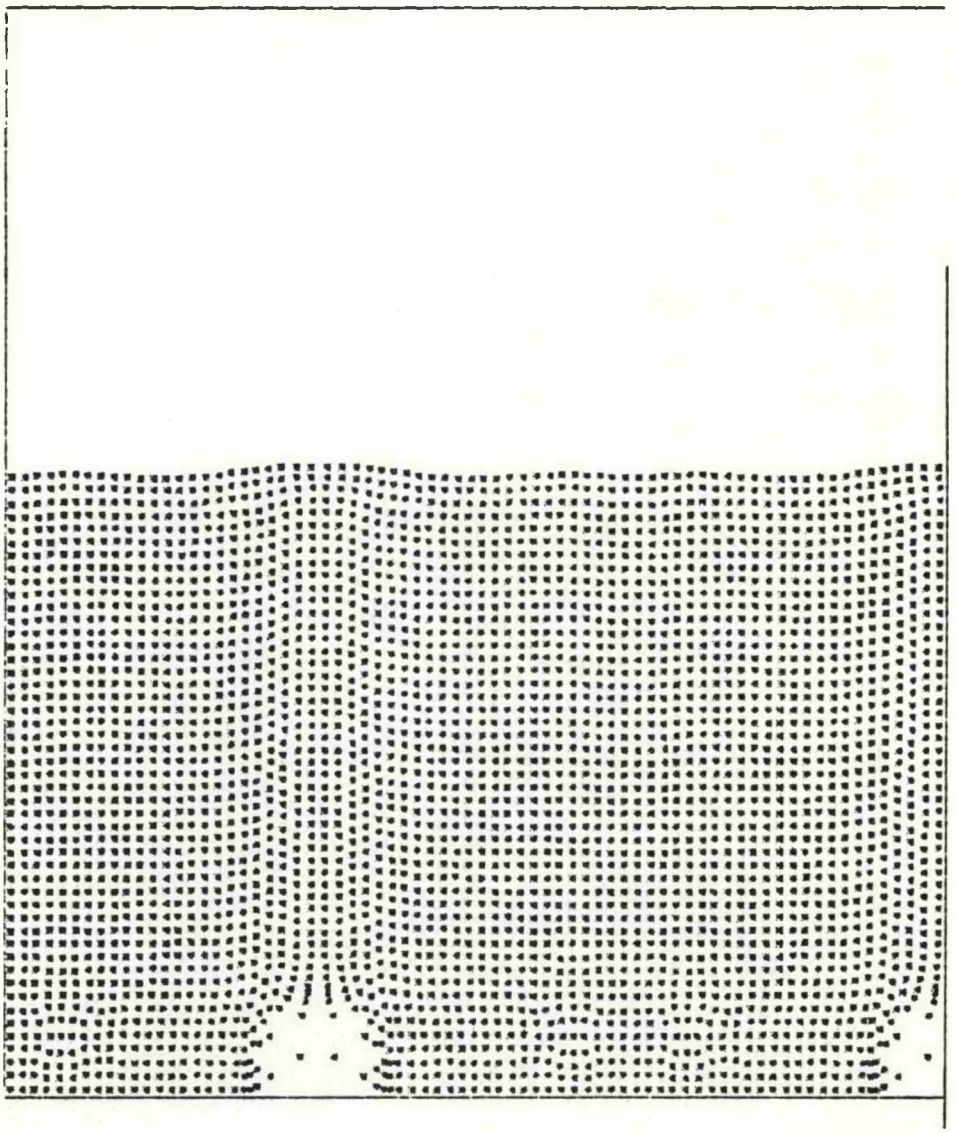

Figure 4.10c

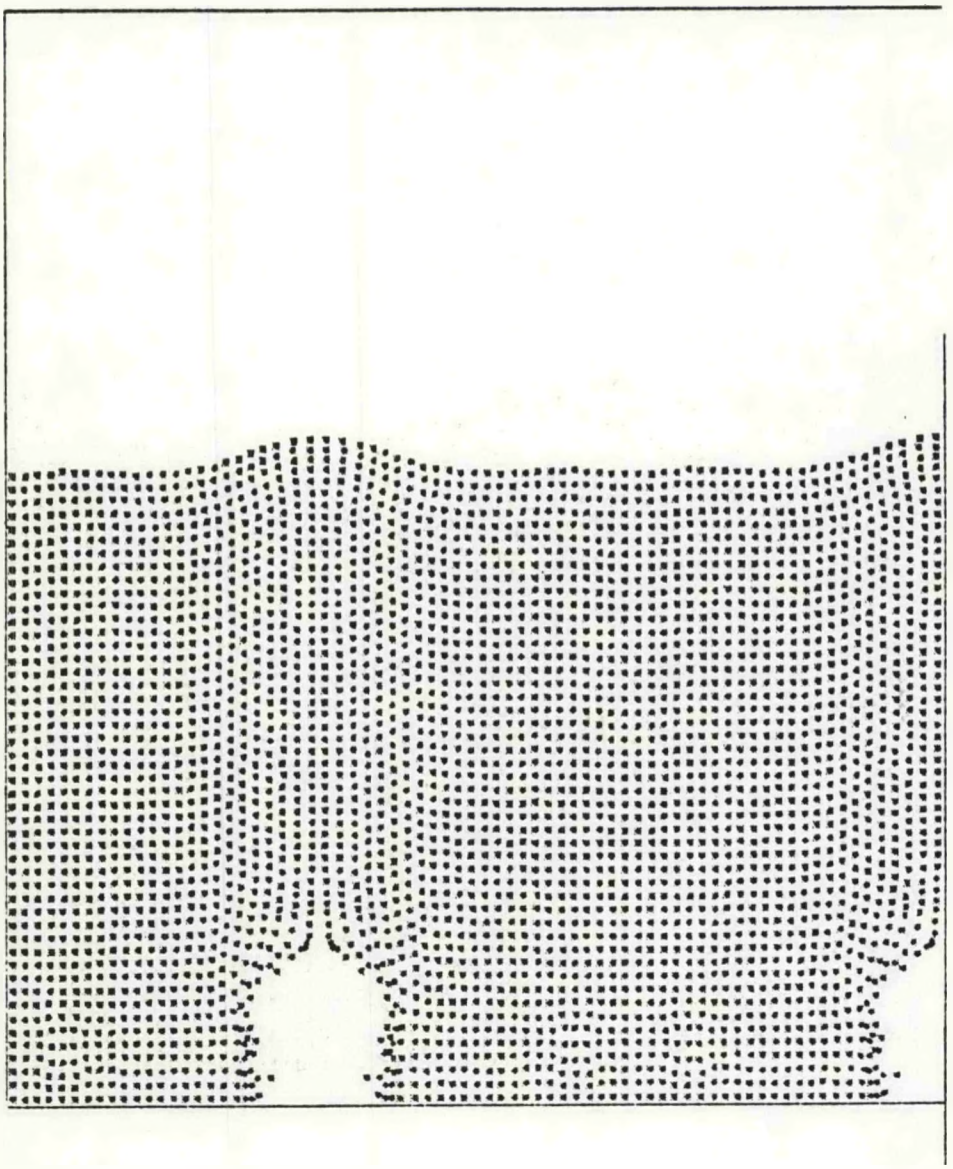

Figure 4.10d.

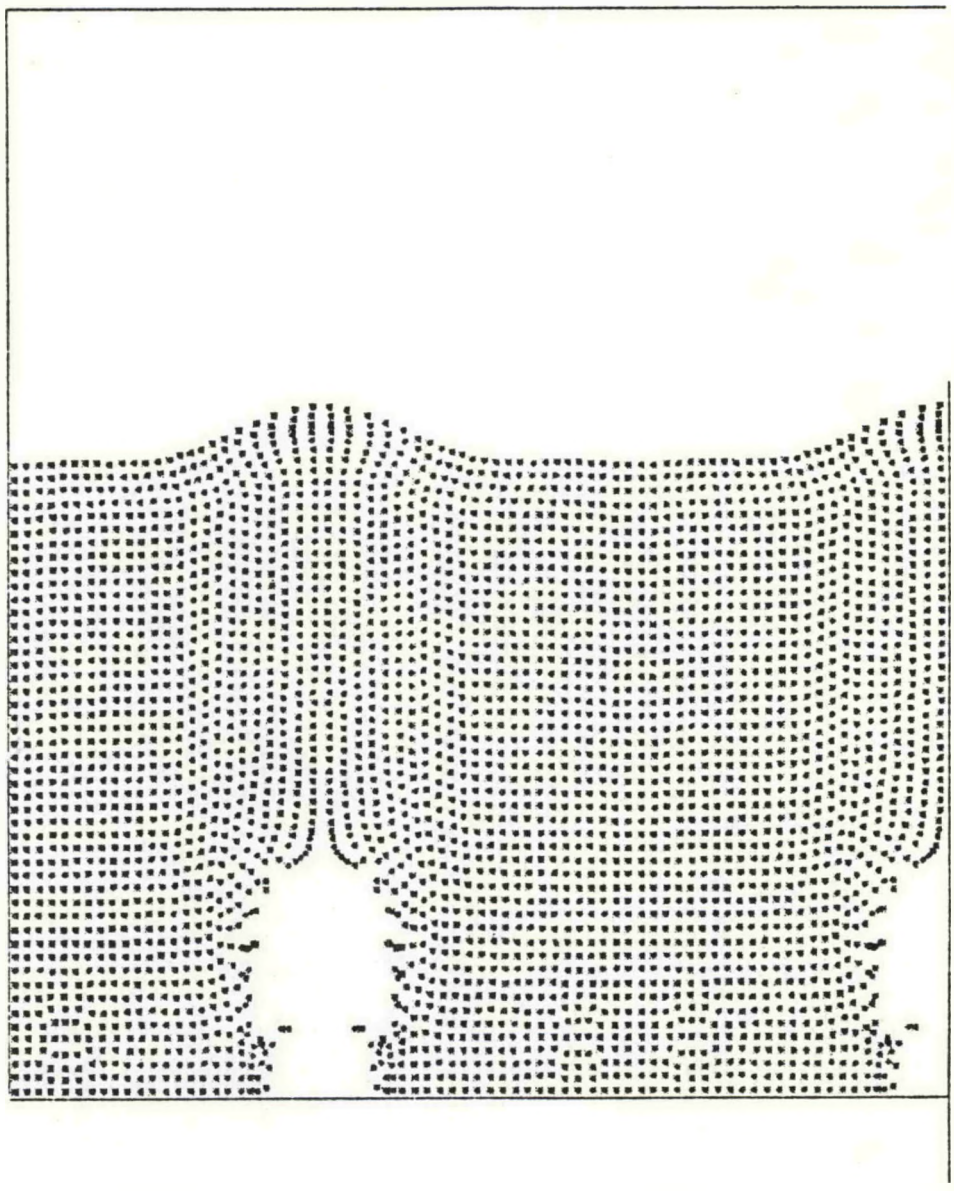

Figure 4.10e.

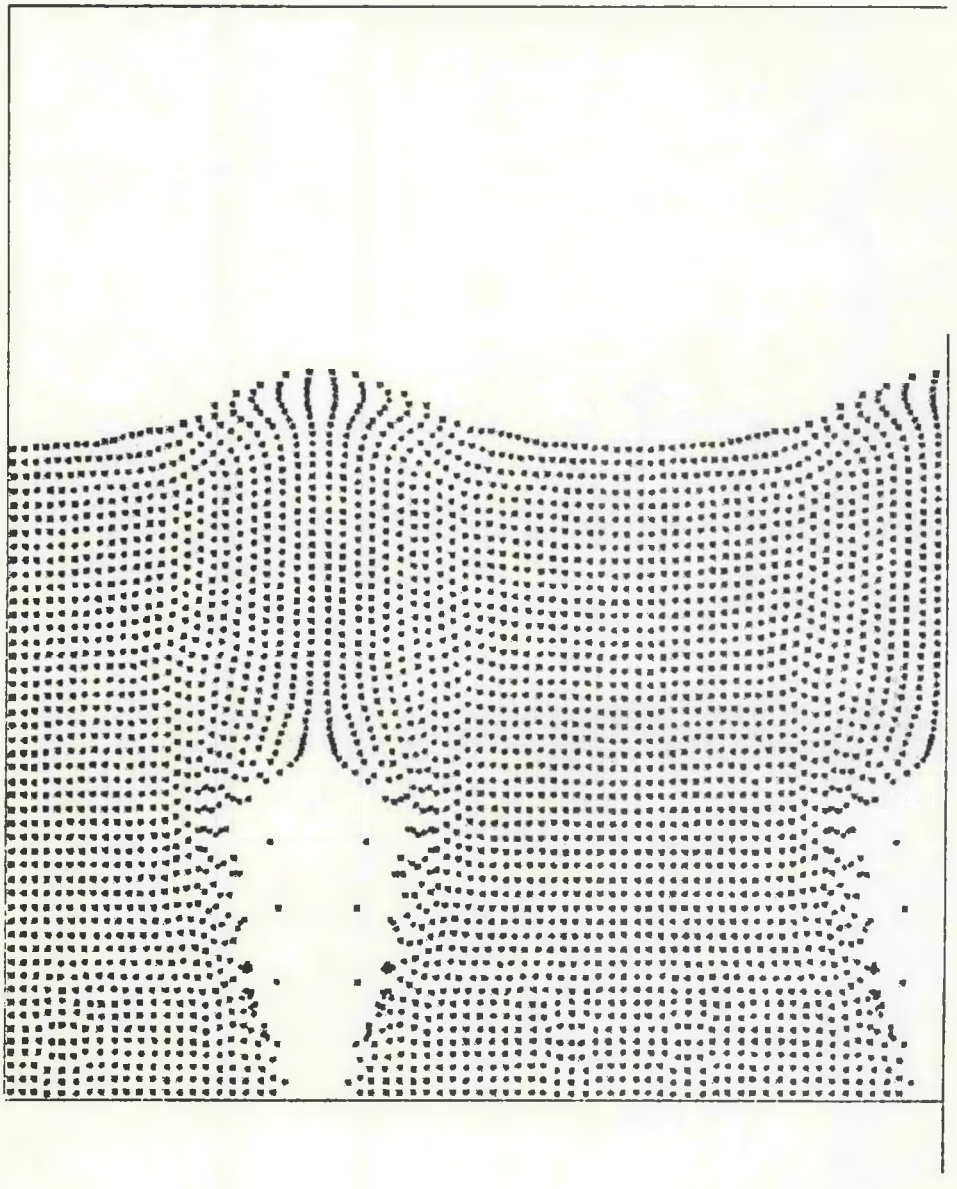

Figure 4.10f.

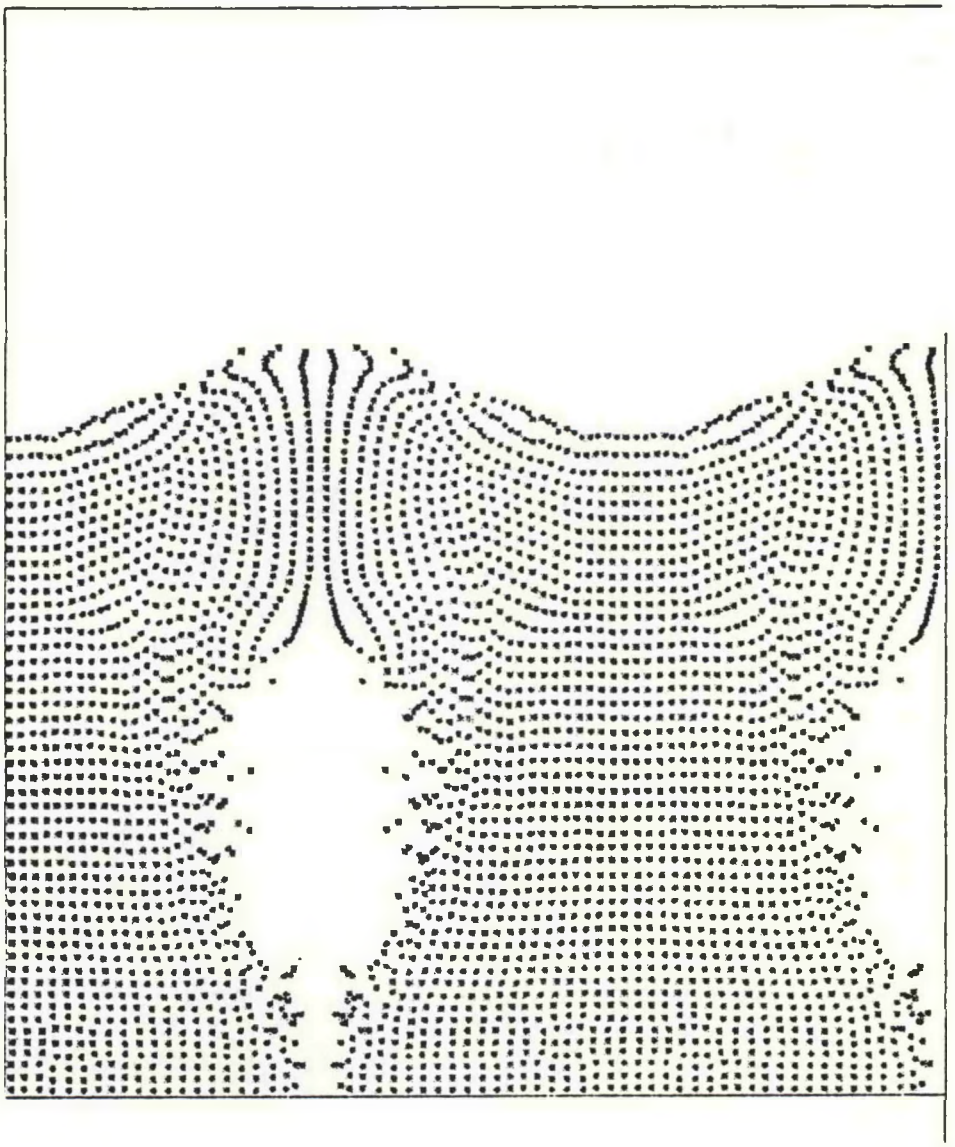

Figure 4.10g.

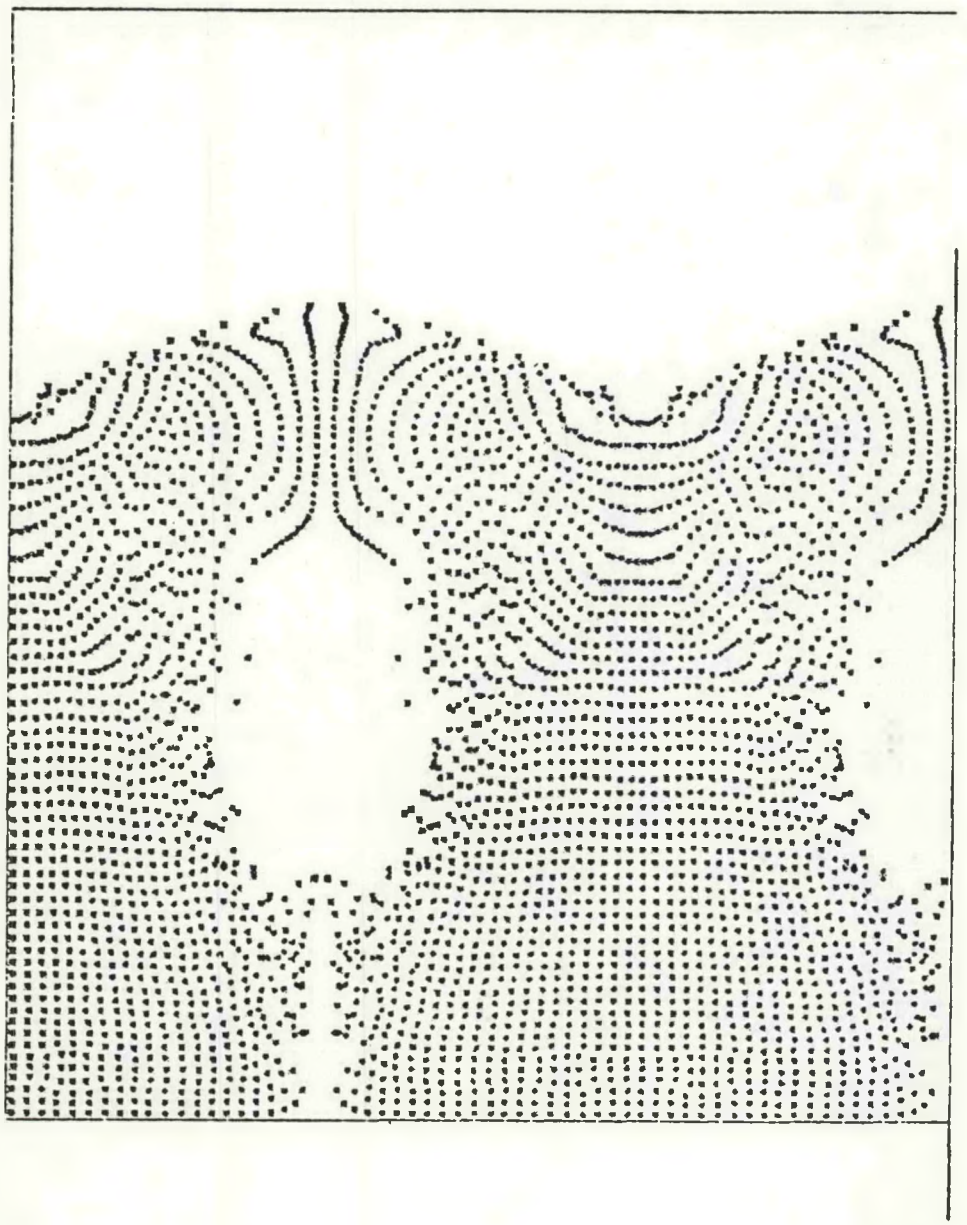

Figure 4.10h.

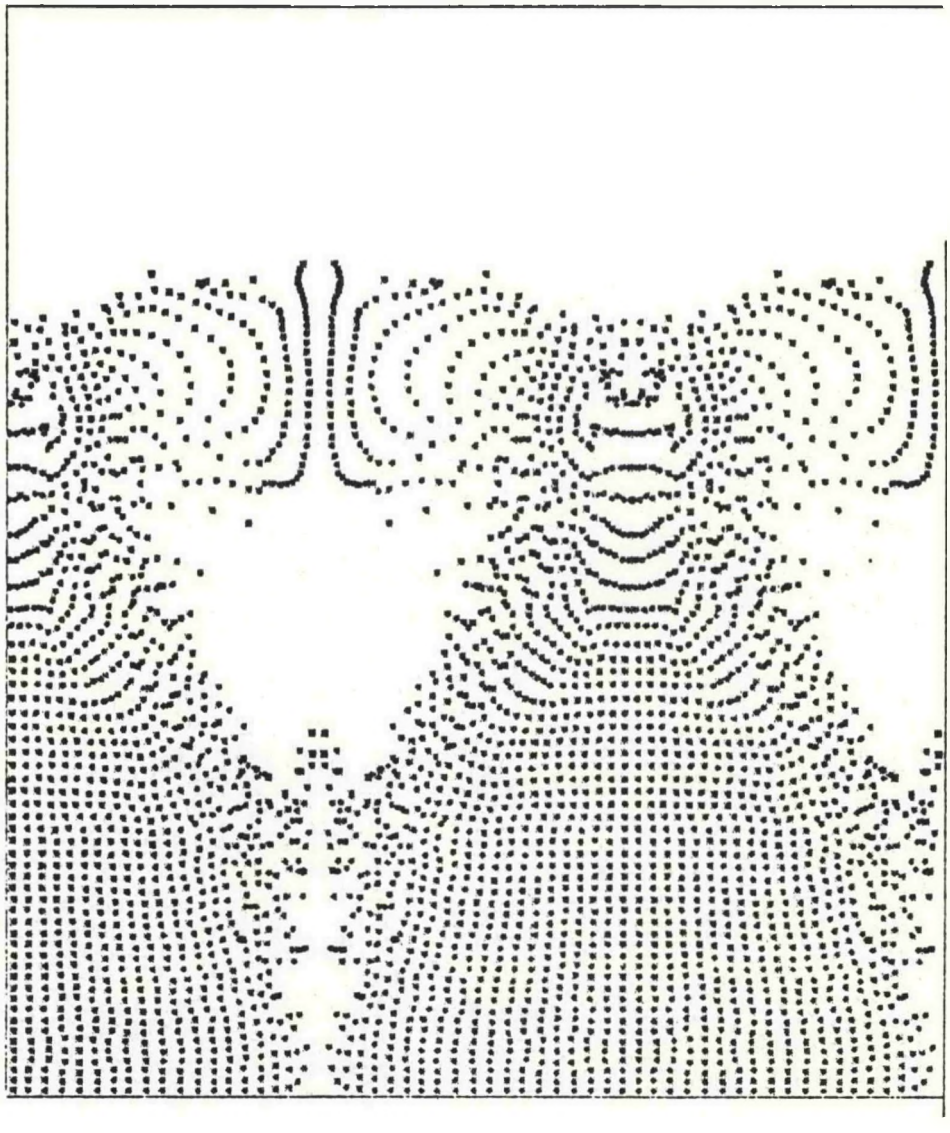

Figure 4.10i.

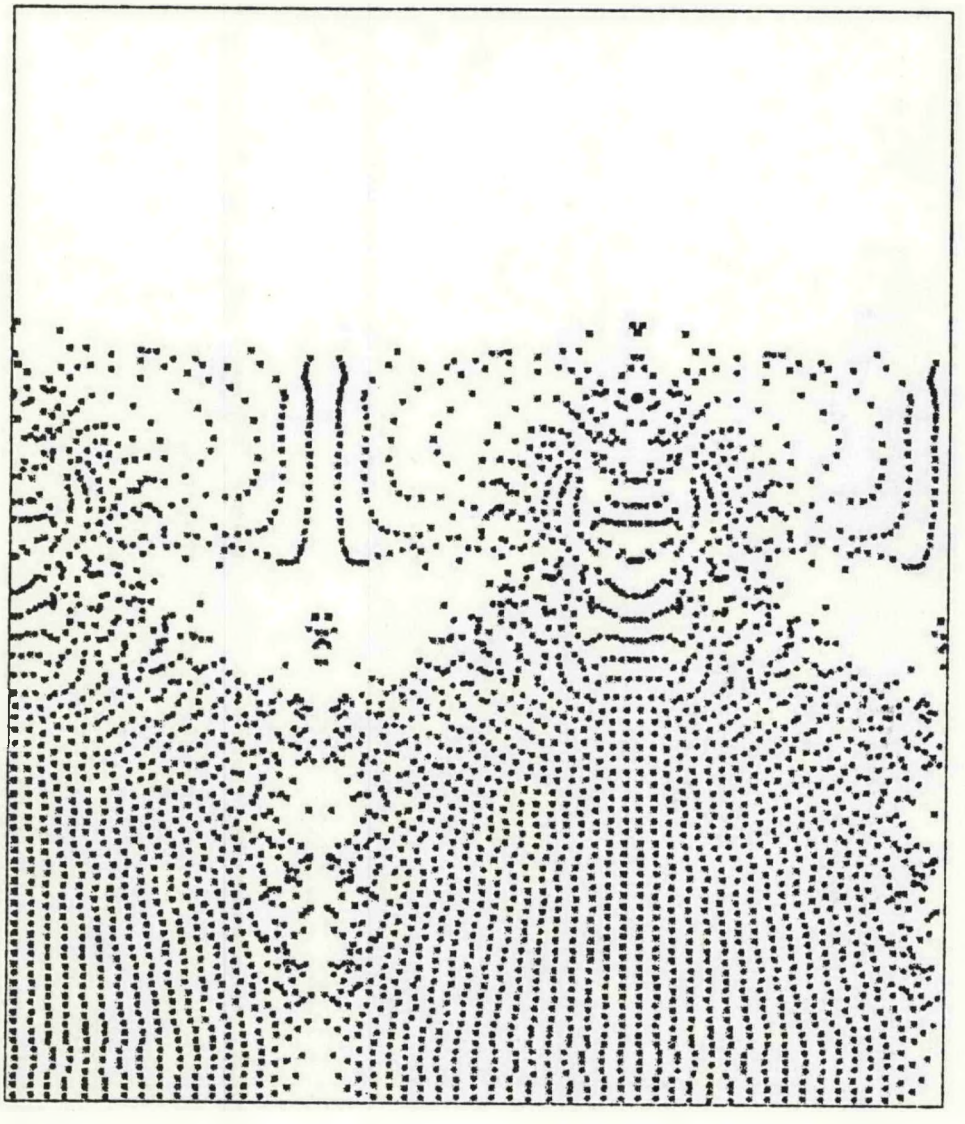

Figure 4.10j.

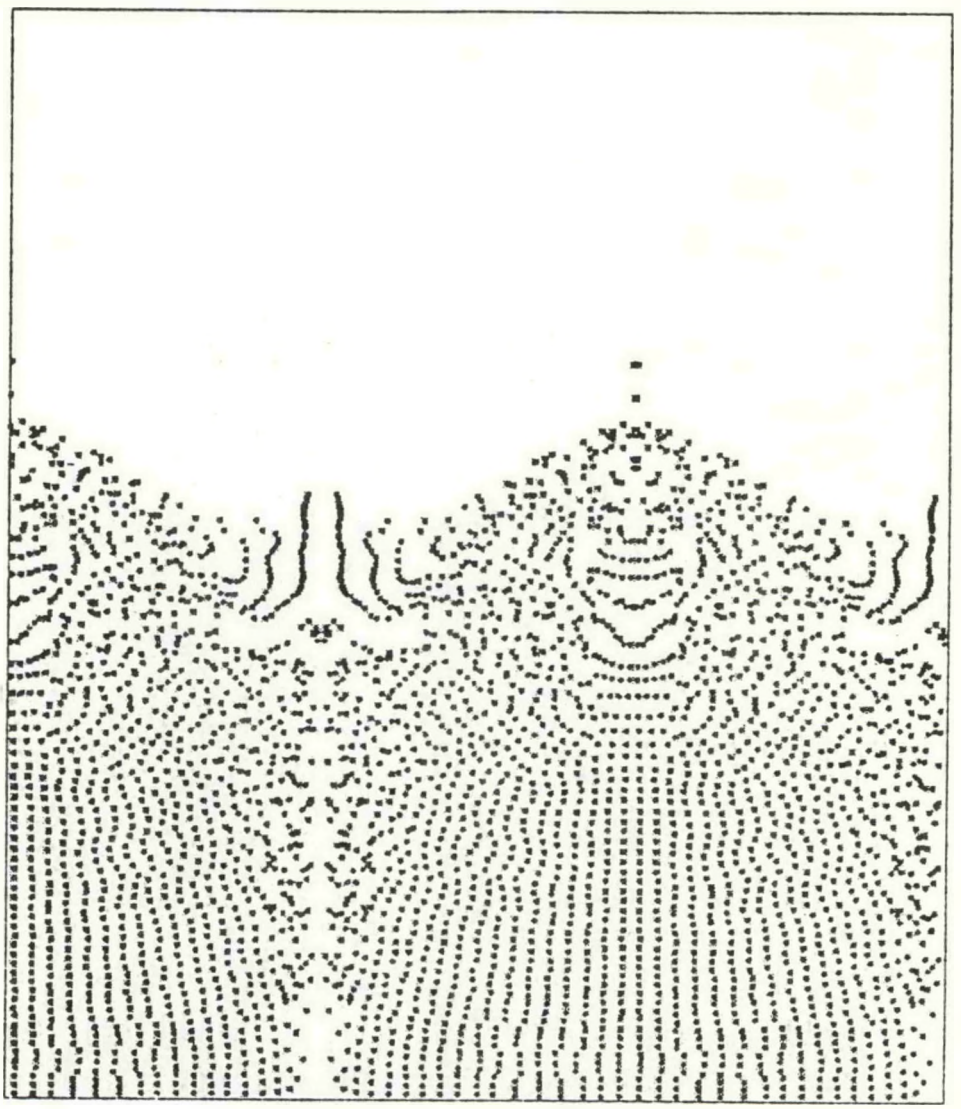

Figure 4.10k.

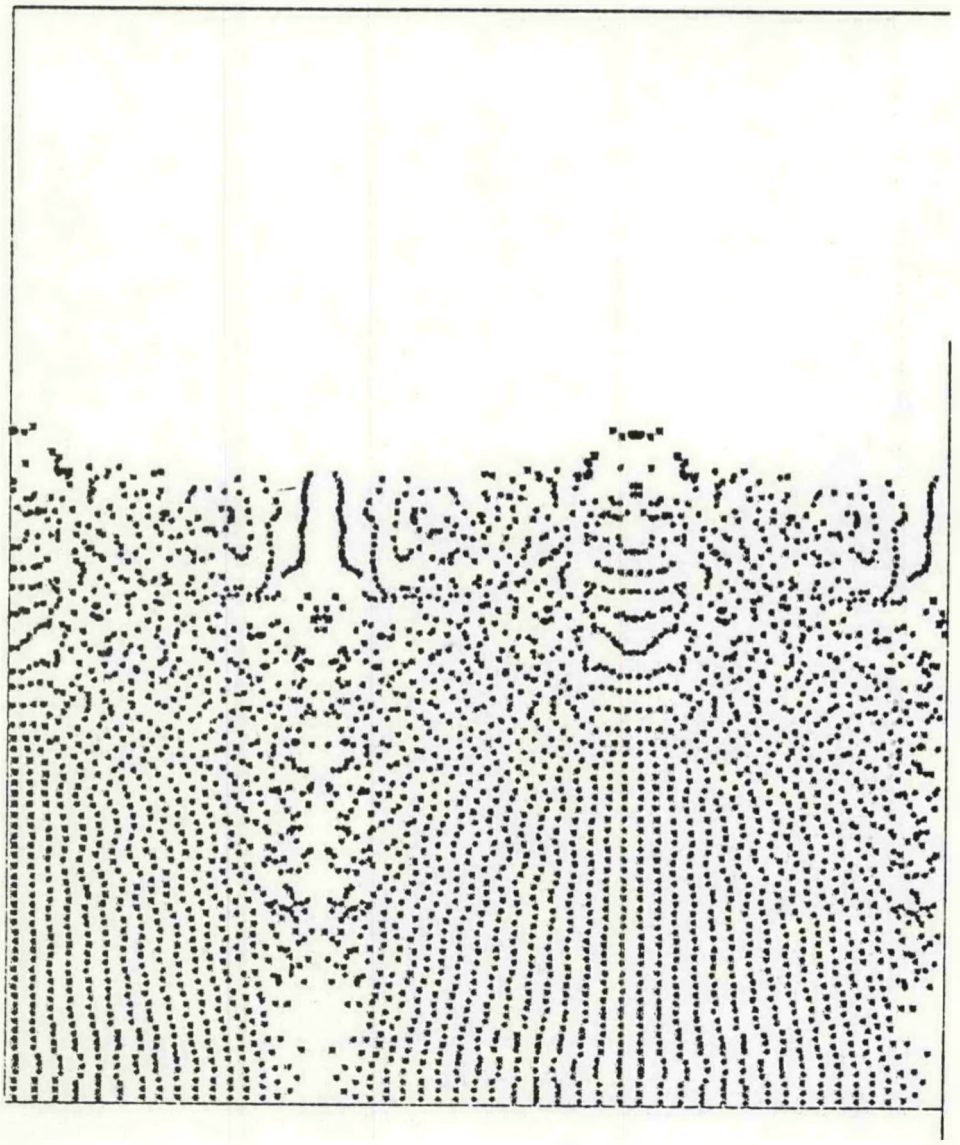

Figure 4.101.

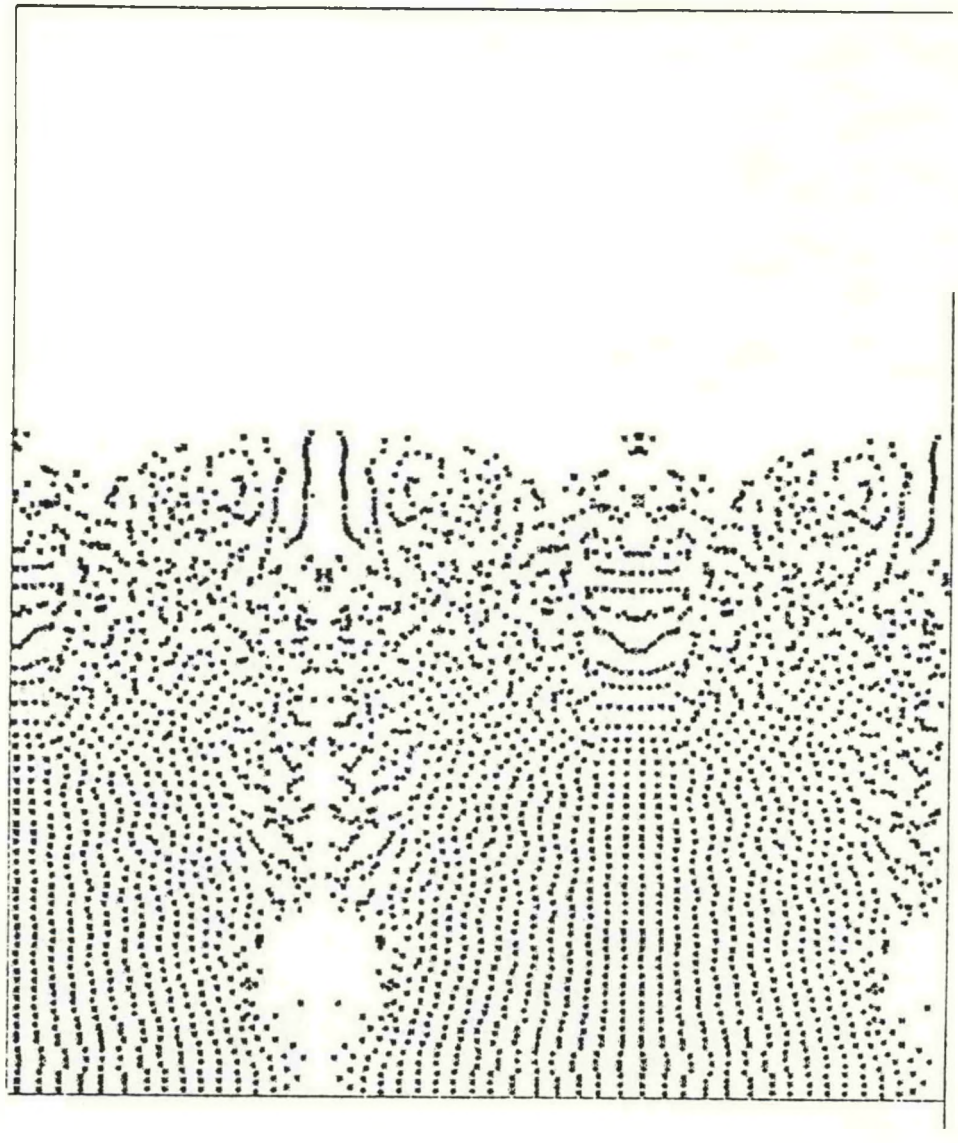

Figure 4.10m.

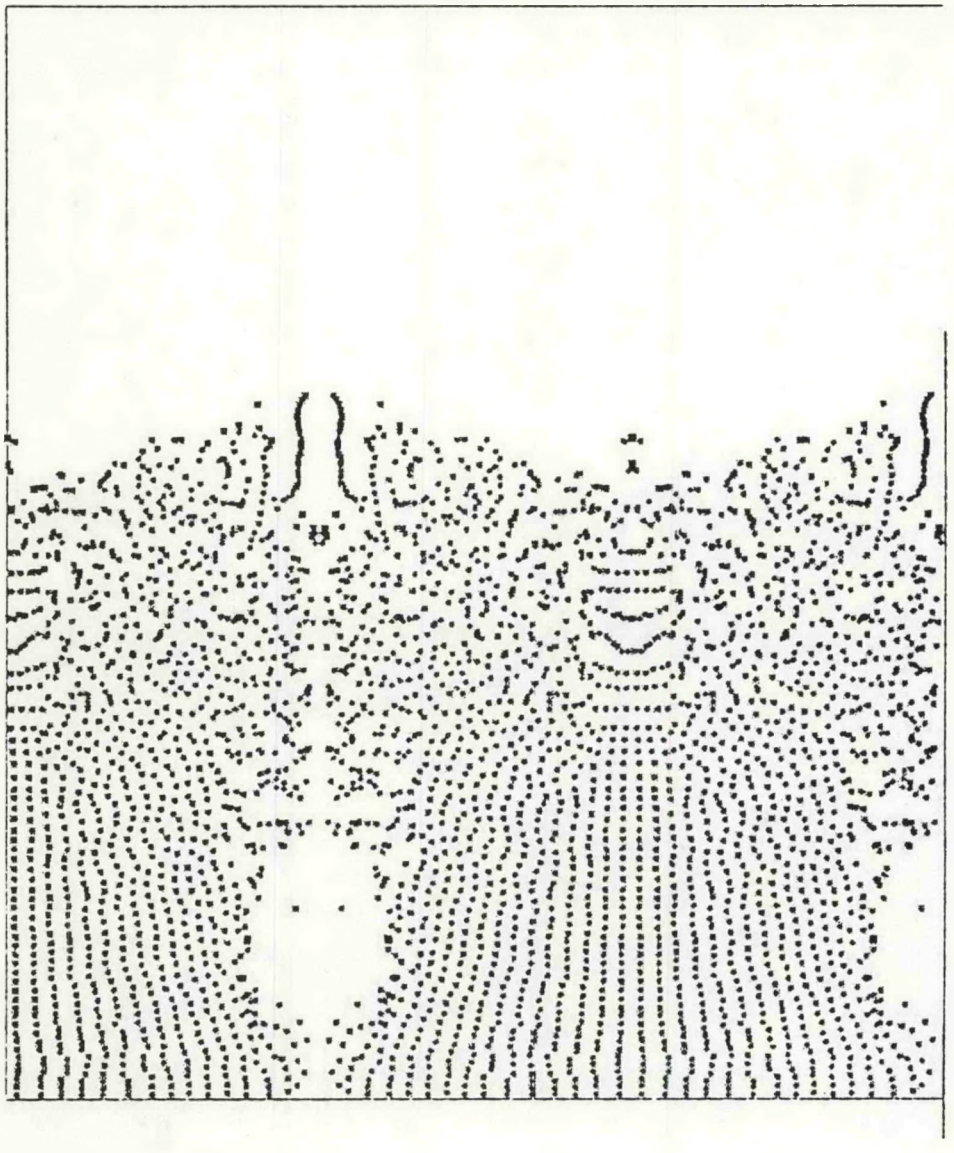

Figure 4.10n.

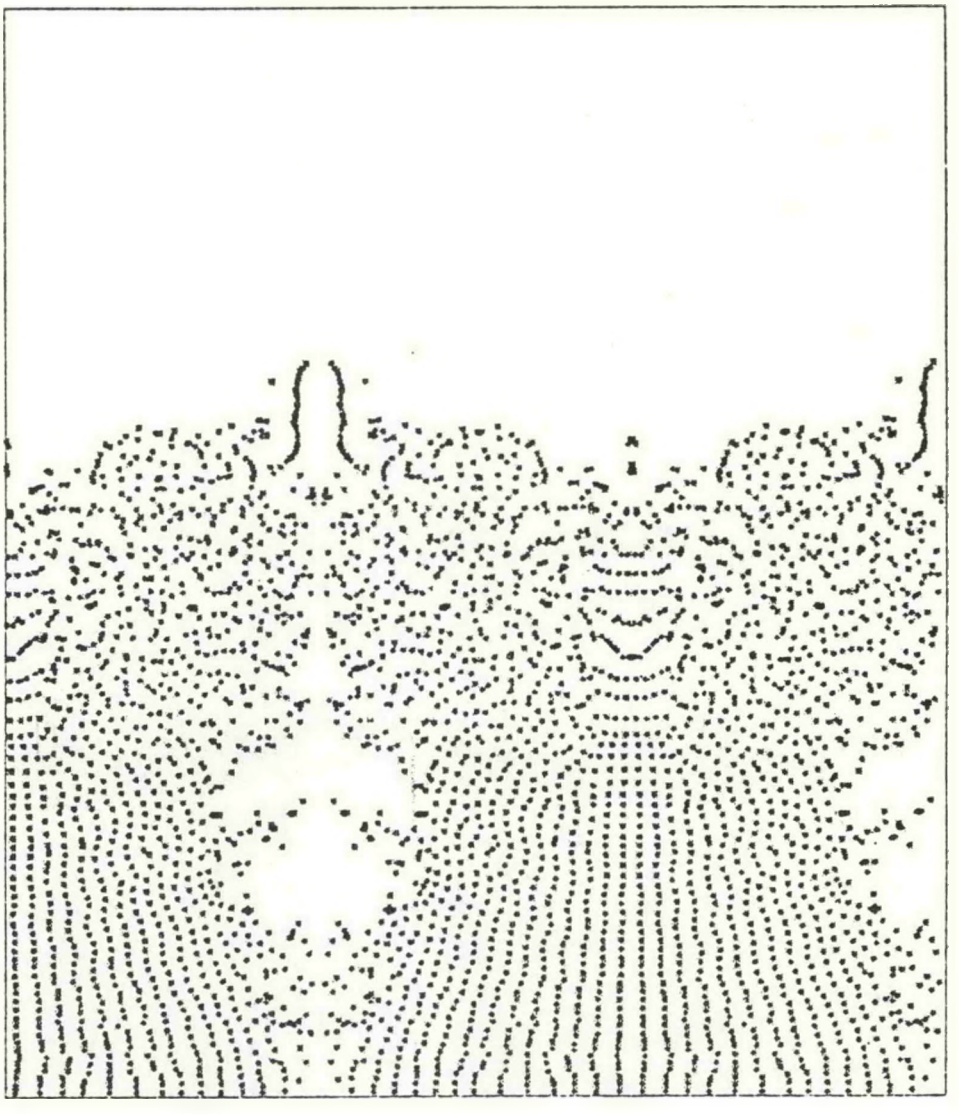

Figure 4.10o.

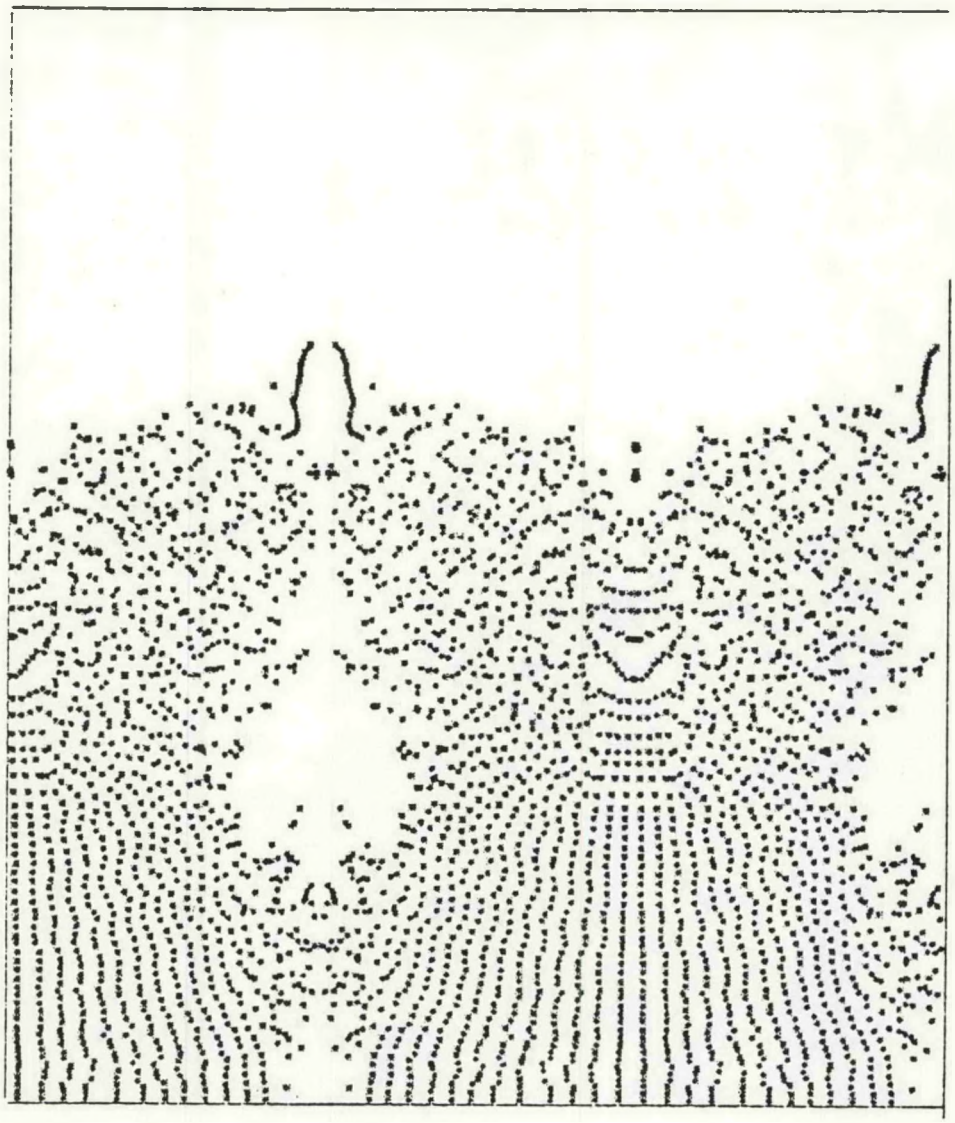

Figure 4.10p.

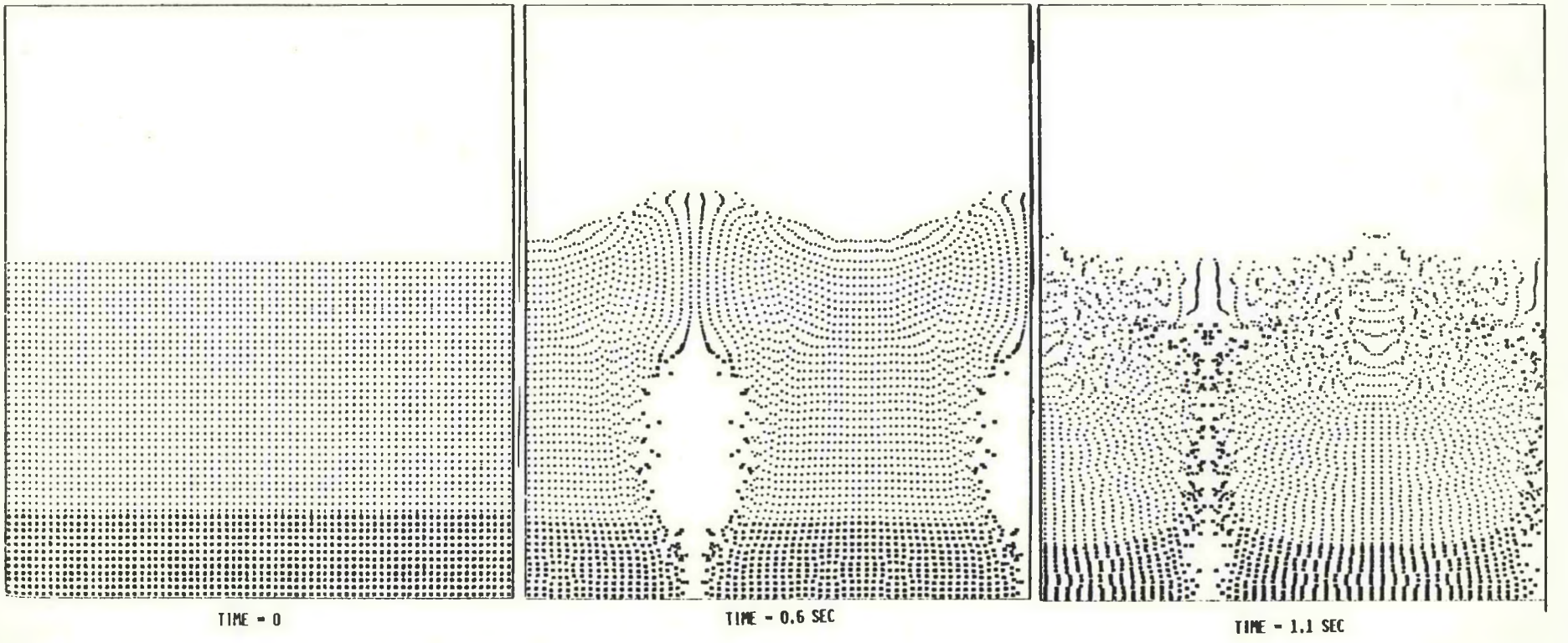

Figure 4.11. Calculations of bubble-induced mixing for Problem B.

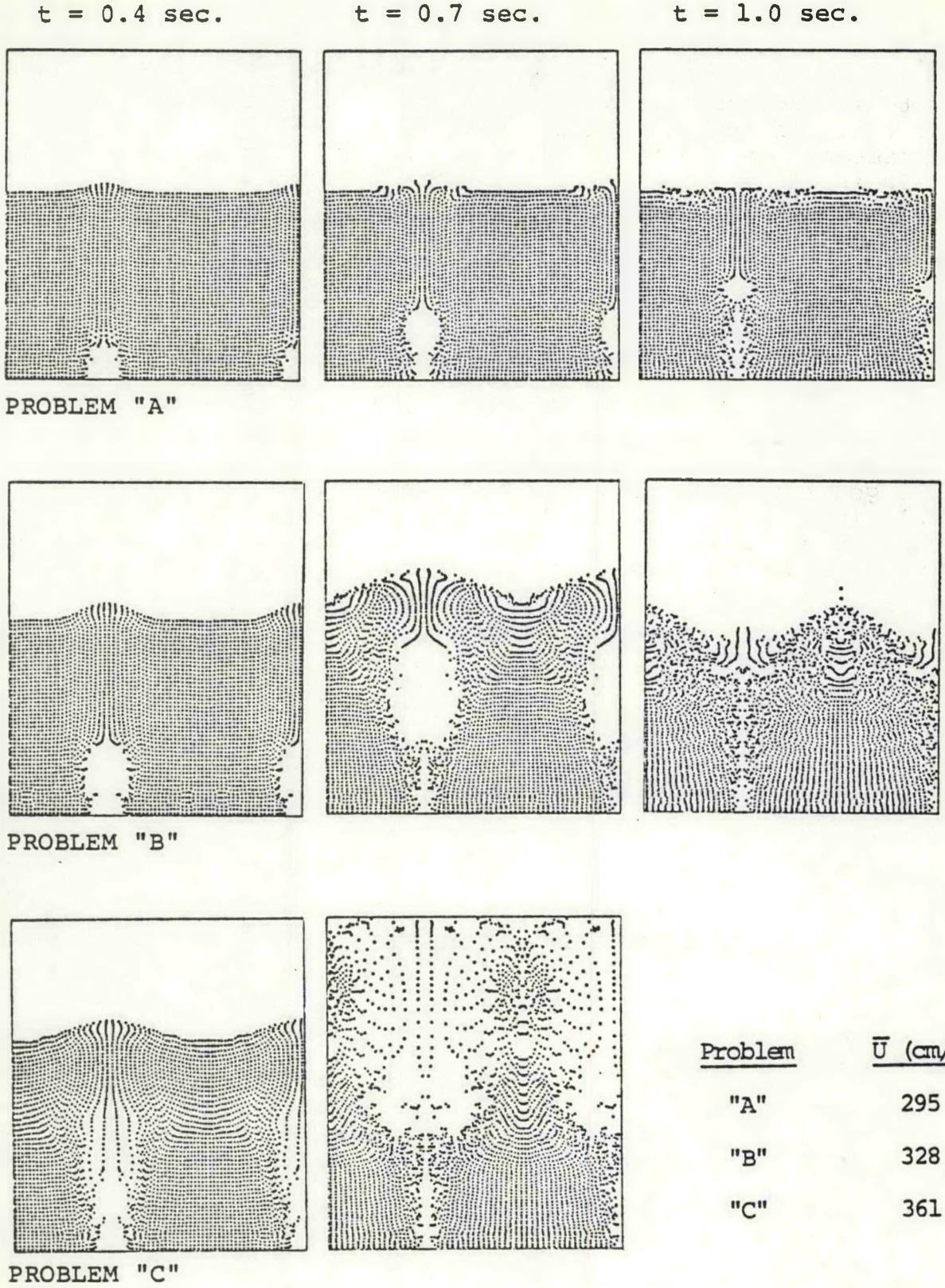

Problem	$\bar{U}$ (cm/sec)
"A"	295
"B"	328
"C"	361

Figure 4.12. Effect of inlet gas flow rate on behavior of fluidized bed.

rate is reduced to that in problem A then the bubbles form at the orifice but rapidly decay as the gas in the bubbles diffuses into the surrounding dense (or emulsion) regions. This is illustrated in the upper time sequence of flow patterns in Figure 4.12. Conversely, if the mass flow rate is too large (problem C) then a "spouted" condition develops with severe channelization occurring in the fluidized bed. For that case we only show the early time behavior in the lower time sequences of Figure 4.12. In the later phase of that flow the solid particles interact with the impermeable (screen) boundary at the top of the figure.

These parametric calculations illustrate some of the immediate applications of the thermohydrodynamic code: namely, the study of solids convection as a function of flow rate, bed geometry and solid particle properties. From such calculations it is also possible to obtain space and time distributions of pressure, temperature, gas velocity and composition and with such distributions, define the gas flow field in the bed.

SECTION 5

CHEMISTRY MODEL

In this section we discuss the development of a computer model representing the chemistry appropriate to coal gasification processes. The research described herein and in the following Section 6 comprised Task Area 04 which has been summarized in Section 2.

5.1 FIRST YEAR OBJECTIVES

The research effort in gasification chemistry involved the formulation of models for coal chemistry and the incorporation of this chemistry in a homogeneous reactor model. This reactor model provides a test bed for the chemistry in a simple flow environment. Further, when the chemistry is incorporated into the thermohydrodynamic computer model during the second year of this program, subroutines in this homogeneous chemical reactor model can be directly used. A particular version of the homogeneous reactor code, which incorporates the chemistry and kinetics appropriate to the CO_2 acceptor process, was developed. This code, based upon the assumption of locally uniform spatial distributions of solid particles, gas composition and thermodynamic properties, represents the gasification processes in a single computational zone in the finite difference computer model of a reactor. Alternatively, it can be used to represent the complete reactor during homogeneous operation; in the latter mode, with gas and solid feed rates appropriate to the Conoco Rapid City Pilot Plant, the code has been used to calculate the startup and time-dependent evolution to steady state of the CO_2 acceptor process. The calculated exit stream flow rates, exit stream compositions and reactor materials inventory, at steady state, are in very good agreement with both direct measurements and estimated data from the pilot plant.

It should be realized at the outset that the chemistry code, when used as a one zone or homogeneous model of a reactor, can only be expected to predict reactor performance with limited precision because the role of inter and intraphase transport is not properly treated. Indeed, one of the main reasons for developing a combined chemistry-thermohydrodynamic reactor model is to make it possible to assess the role of these transport mechanisms in real systems. Despite this limited expectation, we have been able to produce computed results which are in good quantitative agreement with measurements at Rapid City. That is to say, the computer model has been successful beyond reasonable expectations. Even in those few cases of data where agreement is less good, we have been able to account for the discrepancies between calculation and measurement on the basis of minor systems effect which the

model could include, but which it does not include in its present form. When we consider that the CO_2 acceptor process is chemically more complex than most proposed gasification processes, the results of our first year's work lead to the expectation that the chemical part of the model for any gasification process to be considered in this program can be dealt with accurately and precisely. At the same time, we should introduce a note of caution: the chemical processes occurring in any gasification scheme are complex. To date, only partial studies exist for many of the basic processes which occur. Our results suggest some insensitivity of systems performance, both computed and measured, to the precise values of many parameters. However, there remains the possibility that for some specific cases yet to be encountered, there will be parameters not yet subjected to experimental determination which impact significantly upon performance.

We will describe the chemical model in terms of a sequence of basic processes which occur during gasification. For each basic process, we will consider its role vis-a-vis the CO_2 acceptor process in somewhat greater detail. We will indicate in general terms the construction of the computer program which results from this model, although we will not trouble the reader with details of programming. It is worth noting, however, that proper execution of these details is critically important if the program is to function successfully and economically. In the latter regard, the program is still in a state of evolution, and its final form has not been reached. Nevertheless, it already is at a point where extensive parametric study can be carried out at very little computer cost.

5.2 GENERAL DESCRIPTION

The objective of the homogeneous reactor model is to predict the dynamic, i.e., time evolving, variation of chemical composition of the contents of the reactor as well as the physical variables, pressure and temperature. In general the causes for composition variation will be the following:

1. Mass increase due to feed streams.
2. Mass decrease due to exit streams.
3. Chemical reactions between species within the reactor.

5.2.1 Feed Streams

The character of the feed streams depends upon the particular process. Broadly speaking, there will be solid feed streams of coal, lignite, or char; and in the special case of the CO_2 acceptor process an acceptor feed stream. There will also be gas feed streams, which in the main may consist of hydrogen, steam, air, oxygen, or combinations thereof depending upon the particular process. There may additionally exist minor feed streams of other gases which enter the system via purge lines or other sources. For example, in the CO_2 acceptor process, small amounts of a CO_2-N_2 mixture enter the reactor this way.

5.2.2 Recycle Streams

A rather special type of feed stream which may enter the reactor is a recycle stream in which part of the product gas from the reactor is returned to the reactor. Such return may occur either prior to or after process changes applied to the exit stream. Such process changes may involve changes in temperature, pressure, or composition. For the CO_2 acceptor process, for example, approximately 23 percent of the dry product gas produced in the reactor is recycled to the reactor. Unlike "ordinary" feed streams, the composition, temperature, and pressure of a recycle stream is not fixed by controls external to the reactor itself. Instead, for a recycle stream these variables are dynamic functions of the state of the reactor itself and will, accordingly, be modeled in the code on that basis.

5.2.3 Exit Streams

The chemical composition of the exit stream will vary dynamically in proportion to the dynamic variation of the composition at the zone containing the exit orifice. For a homogeneous or single zone model, this composition is assumed to be the same as the composition within the reactor.

5.2.4 Chemical Reactions Between Species Within the Reactor

The rates of change of the amounts of the various chemical species which occur in any reactor is the subject of the science of chemical kinetics. Many variables influence these rates. For solids, important variables include surface area, porosity, and temperature. For gases, important variables include gas partial pressures or densities and temperature. Of additional importance is the presence or absence of catalyst, since many reactions between gas species actually occur through the intermediary of surface reactions on catalysts.

Except for some trivial exceptions, it is not possible to make a priori prediction as to the rate of any chemical reaction under any given set of conditions. It is necessary instead to make experimental measurements of these rates, and to correlate these measurements with important variables using fundamental concepts of chemical kinetics as a guide. To our knowledge, exhaustive measurements do not exist for any of the reactions critical to coal gasification. Fortunately, however, a sufficient body of data exists so as to enable us to estimate the parameters of the correlations between rates and important variables for the critical reactions of coal gasification. The estimation of these rates is a matter of some importance, since errors in these estimations will be reflected by errors in computed predictions of gasifier product compositions. We shall discuss at some length the estimation procedures we have used to date for the CO_2 acceptor process.

To illustrate this one zone calculation of a reactor, consider Figures 5.1 and 5.2. Figure 5.1 is a scale sketch of the gasifier presently being operated by Conoco Coal Development Company at Rapid City, South Dakota. The sketch indicates the basic vertical dimensions of the reactor, and the levels at which various feed and exit streams enter and leave. The product gas exit stream passes out, along with unreacted steam, via the cyclone shown near the top of the reactor. The dipleg from the cyclone returns char fines to the bed, so that it is in effect a recycle stream. In the model as presently developed, this recycle aspect of the cyclone has been ignored, i.e., the char passing through the cyclone is regarded as still being part of the char inventory of the reactor. The small inventory of char within the cyclone and dipleg at any

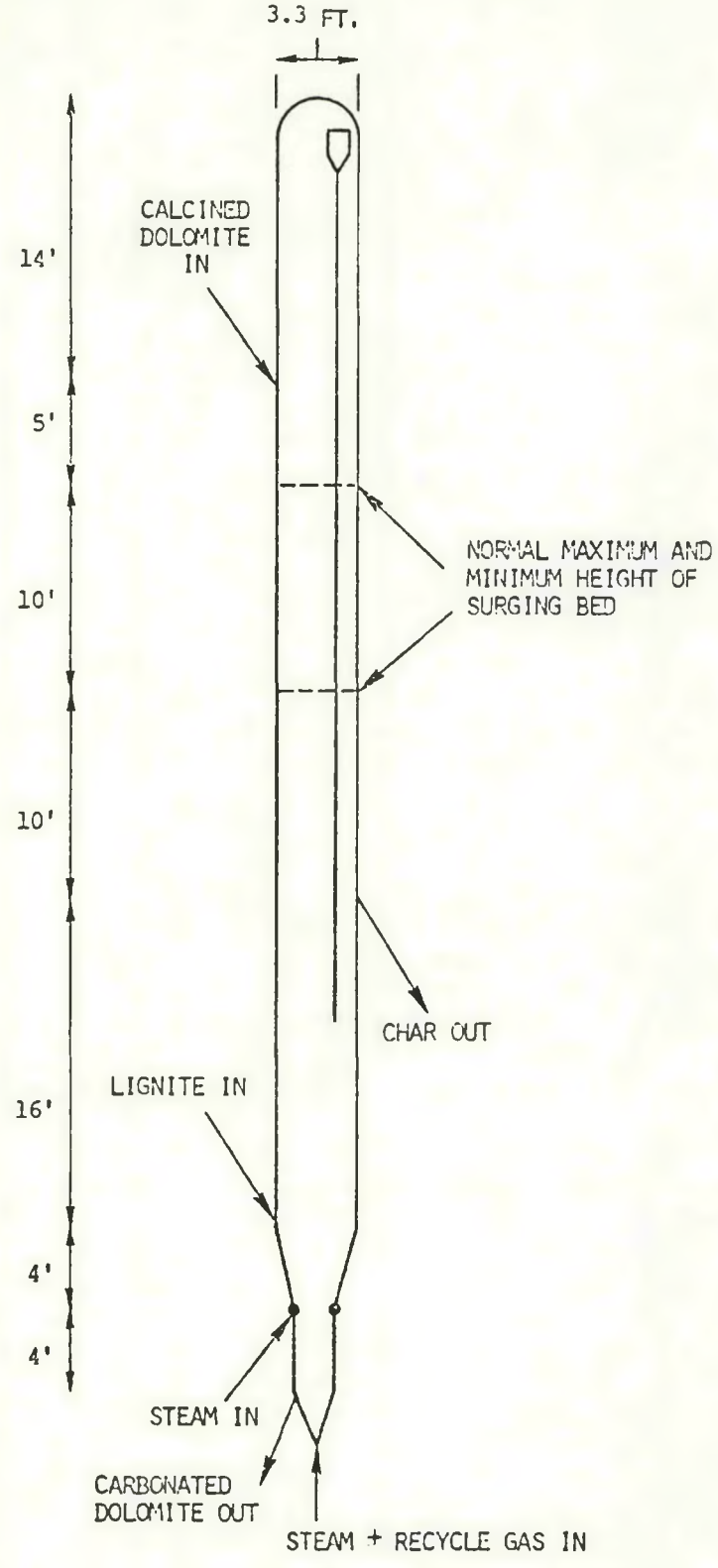

Figure 5.1. Fluidized bed gasifier, Consolidation Coal Company CO_2 acceptor pilot plant, Rapid City, South Dakota.

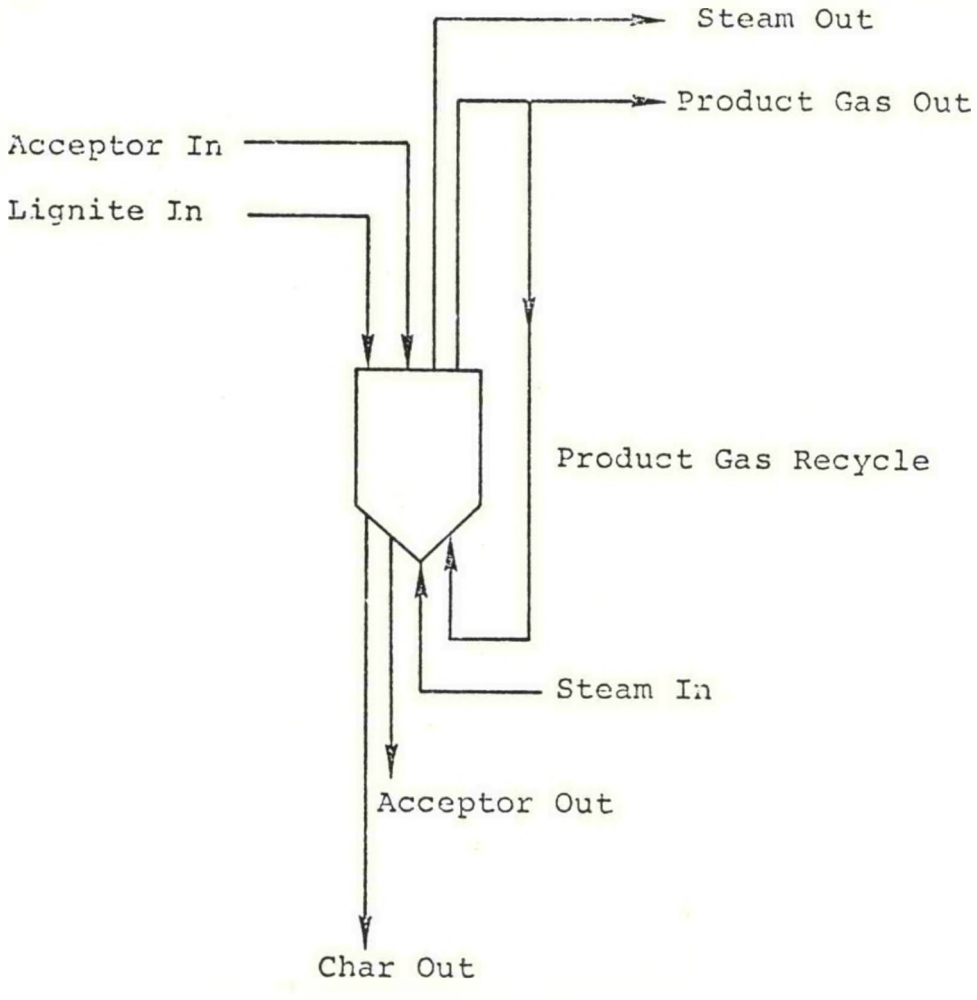

Figure 5.2. CO_2 acceptor process gasifier flows (schematic).

time renders this an excellent approximation. At the same time, the cyclone also is an exit for char since a fraction of the char which enters it does not return to the reactor via the dipleg, but instead passes out the system with the product gas. Thus, in fact, there are two exit streams for char in the pilot plant. In the one zone chemical model we have allowed for only one char exit stream, the total output of which represents the sum of the two physical exit streams.

In the one zone model we have developed, the flows are simplified and schematized as shown in Figure 5.2. There is, however, no physical separation of the flows; instead the feed and exit streams distribute mass homogeneously throughout the reactor.

5.3 CHEMICAL REACTIONS

The chemical reactions which occur in a specific process are to some extent peculiar to that process. Nonetheless, we can classify these reactions in broad terms, and then pick out from these classes the particular reactions which occur in a given process. The appropriate classes are as follows:

1. Devolatilization of Feed Material
    a. Formation of heavy molecules
    b. Formation of light molecules
2. Rapid Rate Methanation of Feed Material
    a. Methanation by reaction with hydrogen from the gas phase
3. Low Rate Gasification of Devolatilized Feed Material
    a. Reactions with steam
    b. Reactions with hydrogen
    c. Reactions with other gases
4. Reactions of Gaseous Species with Each Other (Catalyzed by Solids Present)
    a. Water gas shift reaction
    b. Methane-steam reforming reaction
    c. Other reactions
5. Decomposition Reactions of Gaseous Species
    a. Cracking of heavy molecules to light molecules
    b. Cracking of methane

6. Reactions of Gas Molecules with Feed Material or Devolatilized Feed Materials

   a. Absorption of acid gases by ash

7. Reaction of Gas Molecules with Acceptor

   a. Absorption of acid gases by acceptor

8. Oxidation of Feed Material or Devolatilized Feed Material

   a. Combustion reactions

We will discuss briefly these reactions, with stress on those of particular interest for the CO_2 acceptor process.

5.3.1 Devolatilization of Feed Materials

These reactions consist of partial decomposition of the "molecules" constituting the raw feed materials, leading to the formation of a variety of gaseous substances and a residual solid char. The products formed in these reactions can cover a wide range, with the amounts of the various species which are produced dependent upon many variables: coal type, pretreatment, heating rate, maximum temperature, pressure, etc. Roughly speaking, lower temperatures lead to the production of heavier molecules and higher temperatures lead to the production of lighter molecules, primarily because of the tendency of larger molecules to crack under conditions of elevated temperature. A recent review (Anthony and Howard, 1976) discusses the subject of devolatilization, and provides references to many studies. For purposes of modeling, it is impractical to consider all of the ramifications of devolatilization, mainly because the potential list of products is too extensive. Furthermore, despite much experimental work, a complete characterization of the products of devolatilization in terms of the independent variables listed above is not available. It is, therefore, a practical necessity to restrict consideration to those products of devolatilization where more complete information exists. We have, therefore, limited our model, at least for the present, to representing devolatilization as yielding the following set of gaseous products: H_2, H_2O, CH_4, CO, CO_2, N_2, H_2S. For many processes, including the CO_2 acceptor process, such a list is reasonably adequate. For one thing, the temperature at which devolatilization occurs can be substantially identified with the operating temperature of the reactor, which is in the neighborhood of 1085°K (1500°F). This temperature is sufficiently high so as to lead to the rapid decomposition of larger organic molecules. For another

thing, analytical data on product stream content of other species is unavailable* so that no basis for comparing the model with experiment exists for other species. As a third point, pilot plant and laboratory measurements indicate that other species exist only at low concentrations, so that little error is introduced by omitting them.

For processes other than the CO_2 acceptor process, some modifications of the above list may be needed. Other species which one might contemplate including in the model would be NH_3, COS, C_2H_6, NO, SO_2, O_2, depending on the particular process. In its present form the model does not allow for these species. However, during the first half of the second year of the program, changes will be made in the program so as to allow the user to specify the inclusion or exclusion of a wide range of species, both from among those listed above and others as well. Whether or not inclusion of lesser species can be part of a model program which can be implemented in practice would depend upon the availability of kinetic data on rates of formation of such species. Little such data seems to be available. It is possible, of course, to consider minor species from the point of view of their thermodynamic stability, and options to do so might be made part of the program if it later proves desirable.

The process of devolatilization can be characterized partially in terms of stoichiometry. To achieve this, we describe a coal or lignite feed material in terms of an empirical chemical formula

$$\text{Coal} = C_\alpha H_\beta O_\gamma N_\delta S_\varepsilon A$$

where α, β, γ, δ, ε, indicate the number of gram-atoms ("moles") of each of these elements contained in a unit mass of material.** The letter A in the formula serves as a reminder that in addition to the indicated elements the coal contains a certain amount of ash per unit mass. For a specific coal, the numerical values of the coefficients α, β, γ, δ, ε, are determined by ultimate analysis of a specimen of the material.

---

* NH_3 is an exception to this statement.

**The ash (A) always contains oxygen, and often contains sulfur. The subscripts γ and ε refer only to that part of the oxygen and sulfur which are not retained in the ash during devolatilization.

Devolatilization leads to formation of a char which we similarly characterize by an empirical formula

$$\text{Char} = C_{\alpha'}H_{\beta'}O_{\gamma'}N_{\delta'}S_{\varepsilon'}A$$

The char denoted here, it should be emphasized, is that which forms promptly during devolatilization.* Subsequent gasification of the char will lead to a continual alteration of the numerical values of these coefficients as the char is successively converted to residual ash. We also define the coefficients α', β', γ', δ', ε' as the number of gram-atoms ("moles") of these elements contained in that mass of char formed by the devolatilization of one unit mass of feed coal or lignite. The numerical values of these parameters could be obtained in the laboratory by an ultimate analysis of a devolatilized sample.

We can write a chemical equation for the conversion of feed coal to char:

$$C_\alpha H_\beta O_\gamma N_\delta S_\varepsilon A \rightarrow C_{\alpha'}H_{\beta'}O_{\gamma'}N_{\delta'}S_{\varepsilon'}A + u'H_2 + v'H_2O + (\varepsilon-\varepsilon')\,H_2S + \tfrac{1}{2}(\delta-\delta')N_2 + wCO + xCO_2 + yCH_4 \qquad \text{(R1)}$$

It can be seen from reaction (R1) that the production of H_2S and N_2 is fixed in terms of the ultimate analysis of the coal and char. For the other species, the coefficients u'-u, v'-v, w, x, and y are fixed in part by three elemental mass balances:

Carbon Balance

$$\alpha = \alpha' + w + x + y \qquad (5.1)$$

Hydrogen Balance

$$\beta + 2u = \beta' + 2(\varepsilon-\varepsilon') + 4y \qquad (5.2)$$

Oxygen Balance

$$\gamma = \gamma' + v' + w + 2x \qquad (5.3)$$

*We will use the term "fresh char" in referring to this material.

These stoichiometric relations provide a system of three equations in five unknowns. Two additional relations must be provided in order to obtain a set of solvable relations. One of these relations is closely connected to the subject of "rapid rate methanation", which we discuss next.

5.3.2 Rapid Rate Methanation

The conversion of coal to methane, both in the presence of and in the absence of ambient hydrogen, has been the subject of research going back to the work of Dent, *et al.* (1938), or even earlier. A large number of papers discussing the subject are available, on the basis of which the following general statements may be made:

Devolatilization of coal leads to the formation of some methane. The amount of methane formed is influenced by the presence of hydrogen, with increasing hydrogen pressure favoring increased methane production. At sufficiently high hydrogen pressure, conversion of substantially all of the coal carbon to methane is possible, although such pressures required are too high to be feasible commercially. The rate of production and amount of methane produced also depends upon coal type and temperature.

Various authors have proposed molecular mechanisms for explaining the observed relation between methane production and hydrogen partial pressure. Although no unambiguous evidence exists favoring any one mechanism over another, most mechanisms proposed in the literature to date lead to similar empirical relations between methane production and hydrogen partial pressure. Important summary discussions of this work have been provided both by Zahradnik and Glenn (1971), Zahradnik and Grace (1974), and by Johnson (Pyrcioch, *et al.*, 1972; Johnson, 1974; Johnson, 1975). The consequences of these discussions indicate that a very useful way to correlate methane production and hydrogen partial pressure is by means of the relation

$$y = \alpha\left\{b_1(T) + b_2(T)\ P_{H_2} \Big/ \left[1 + b_3(T)\ P_{H_2}\right]\right\}, \qquad (5.4)$$

where α and y are as defined in the chemical equation (R1), P_{H_2} is the hydrogen partial pressure, and $b_1(T)$, $b_2(T)$, $b_3(T)$ are empirical correlation parameters which are related to the fundamental steps in the gasification process (Zahradnik and Grace, 1974; Johnson, 1975). The latter parameters depend upon temperature and also on coal type. It is necessary, for a particular coal, to evaluate them by means of experimental measurements of methane formation at various pressures and temperatures.

One important aspect of Eq. (5.4) must be discussed: First, the number of experiments performed to date for the purpose of determining the parameters $b_1(T)$, $b_2(T)$, and $b_3(T)$ is quite limited. Many coal or lignite types have not yet been studied, and of those which have, the ranges of pressure and temperature covered are narrow. Therefore, it may be the case with respect to a particular coal type that little data is available in the literature, and parameter values must be secured by estimation processes based upon related materials and similarity hypotheses. In point of fact this is exactly the case we are faced with for the Velva (N.D.) lignite currently in use at the CO_2 acceptor pilot plant in Rapid City, South Dakota. It is useful to rewrite Eq. (R1) in another form, in which it represents the sum of the process of devolatilization and rapid rate methanation:

$$C_\alpha H_\beta O_\gamma N_\delta S_\varepsilon A + uH_2 \rightarrow C_{\alpha'} H_{\beta'} O_{\gamma'} N_{\delta'} S_{\varepsilon'} A + u'H_2 + v'H_2O + (\varepsilon-\varepsilon')\, H_2S + \frac{1}{2}(\delta-\delta')\, N_2 + wCO + xCO_2 + yCH_4 \qquad (R2)$$

This general form includes the possibility of ambient hydrogent entering the rapid rate reaction, as it must in the general case.

All of the studies which lead to the evaluation of the constants $b_1(T)$, $b_2(T)$, $b_3(T)$ seem to have been done under conditions in which the ambient partial pressure of H_2 is maintained constant, e.g., by using a flowing hydrogen stream, and a small coal sample mass. As a result, they provide no data on stoichiometry. Nonetheless, if we hypothesize that under reactor operating conditions not enough hydrogen is removed from or added to the vapor phase so as to change the hydrogen partial pressure to any significant degree, Eq. (5.4) provides a fourth equation to be adjoined to Eqs. (5.1) - (5.3). There then results a set of four equations in five unknowns, the unknowns now being $u'-u$, v', w, x, and y. There still remains the task of finding a fifth equation in order to complete the characterization of the combined processes of devolatilization and rapid rate methanation. Given a fifth equation, we would additionally be able to determine the net hydrogen consumed.

Little is available in the way of guidance in finding this fifth relation beyond the observation that product gases from gasification experiments frequently seem to be at or near water gas shift equilibrium. This is sometimes taken as

suggesting that products of devolatilization themselves satisfy water gas shift equilibrium. This is difficult to verify, and in fact may not matter in the case where the water gas shift reaction occurs subsequent to devolatilization and rapid rate methanation, and at sufficient speed. The latter appears to be the case under the operating conditions at Rapid City, and is almost certainly the case in systems which operate at still higher temperatures (c.f., Von Fredersdorff and Elliot, 1963). In our model, we have introduced the assumption that the ratio x/w of CO_2 to CO produced during devolatilization and rapid rate methanation is proportional to the ambient ratio of hydrogen to steam, i.e.,

$$\frac{xP_{H_2}}{wP_{H_2O}} = \Phi K(T) \qquad (5.5)$$

where P_{H2}, P_{H2O} are the ambient partial pressures, K(T) is the water gas shift equilibrium constant, which is a function of temperature, and Φ is a parameter, yet to be determined. This relation, which is unproven but plausible, closes the equation system provided a value is chosen for Φ (which is a dimensionless constant). To date, we have only calculated using $\Phi = 1$. The more rapid the subsequent water gas shift reaction, the less important is the choice of Φ. Results to date suggest that the choice of Φ is not likely to be important in the CO_2 acceptor process, but the importance of this parameter in models of other processes is an open question at this time.

The result of the above analysis is that we can characterize the combination of devolatilization and rapid rate methanation in terms of "instantaneous" productions of H_2, H_2O, CH_4, CO, CO_2, N_2 and H_2S provided that we have values for the following variables: ultimate analysis of coal or lignite, ultimate analysis of char, partial pressures (instantaneous), estimates of the parametric variation of $b_1(T)$, $b_2(T)$, $b_3(T)$, the equilibrium constant K(T) (which is known on the basis of excellent available thermodynamic data), and an estimate or guess of Φ. It should be appreciated that this means that these gas production rates will be dynamic functions of time as a consequence of the time variation of these parameters, although in the limit of a steady state they all will settle down to constant values.

5.3.3 Low Rate Gasification of Devolatilized Feed Materials

Studies of char gasification with a variety of gases have been the subject of numerous research studies, some of which date back a half-century or more. Principal reactions

of interest in virtually all proposed commercial methods are those with steam and with hydrogen. Secondary interest can be attached to the reaction of char with carbon dioxide, leading to the formation of carbon monoxide

$$\text{Char} + CO_2 \rightleftarrows 2CO + \text{minor species} \qquad \text{(R3)}$$

However, in commercial processes the rate of this reaction is so low that it probably can be ignored. In our study of the CO_2 acceptor process we did ignore this reaction, a step which is amply justified not only by its low rate but by the fact that for this process the ambient CO_2 partial pressure is low.

The oxidation of char also can be thought of as a process of gasification, but we prefer to consider it separately. We will refer to it in Section 5.3.8 below.

The reaction of char with steam is usually referred to as the carbon-steam reaction. Reports of studies of char gasification commonly write this reaction as

$$C + H_2O \rightleftarrows CO + H_2 \ , \qquad \text{(R4)}$$

viewing the char as carbon. At the same time, it is recognized that char is more reactive toward steam than is pure carbon, i.e., either graphite or diamond. It also should be noted that the gasification of char is <u>not</u> a reversible reaction, since carbon monoxide and hydrogen will <u>not</u> react to form a char of the same composition as that produced by devolatilization of coal.

We prefer to write the "carbon-steam" reaction in more detail:

$$\begin{aligned} C_{\alpha'}H_{\beta'}O_{\gamma'}N_{\delta'}S_{\varepsilon'}A + (\alpha'-\gamma')\ H_2O \\ \rightarrow \alpha' CO + \tfrac{1}{2}\,\delta' N_2 + \varepsilon' H_2S \\ + \tfrac{1}{2}\,(\beta'+2\alpha'-2\gamma'-2\varepsilon')\ H_2 + A \end{aligned} \qquad \text{(R5)}$$

This form notes the irreversibility, and also treats correctly the stoichiometry of the nitrogen and sulfur. Kinetic studies of this process frequently express the rate of this reaction

in terms of the fraction of carbon gasified per unit time. These studies correlate these rates with temperature, partial gas pressures, char origin, and extent of previous reaction of the char. The authors usually interpret the derived correlations in terms of reaction (R4), but the form of the published correlations allows interpretation in terms of reaction (R5). We have adopted the latter as our standard procedure.

In a similar fashion, the reaction of char with hydrogen is frequently expressed as

$$C + 2H_2 \rightleftarrows CH_4, \qquad \text{(R6)}$$

which fails to account for the fate of the hydrogen, oxygen, nitrogen, and sulfur species in the char. Here, too, it is not correct to write the reaction as reversible, since cracking of methane does not lead to a solid material which is identical with the char produced by devolatilization of coal. We therefore adopt as a standard expression

$$C_{\alpha'}H_{\beta'}O_{\gamma'}N_{\delta'}S_{\varepsilon'}A + \left(2\alpha' + \varepsilon' + \gamma' - \frac{1}{2}\beta'\right) H_2 \rightarrow \frac{1}{2}\,\delta' N_2 + \varepsilon' H_2S + \gamma' H_2O + \alpha' CH_4 + A \qquad \text{(R7)}$$

which is irreversible, and treats correctly the stoichiometry of all of the elements.

Studies of gasification of char in steam, hydrogen, and steam-hydrogen mixtures indicate that reaction (R7), if it occurs at all, is extremely slow. It turns out, in fact, that conversion of char to methane is strongly influenced by the presence of steam. It has been found in these studies that it is impossible to correlate methane production on the basis of reaction (R7) alone. As a consequence, another reaction is introduced which is written as

$$2C + H_2 + H_2O \rightleftarrows CO + CH_4 \qquad \text{(R8)}$$

It is not contended that reaction (R8) constitutes a real physical process. Instead, use is made of reaction (R8) as a surrogate for a complex of unknown processes, and kinetic data on methane production is correlated on this basis.

Once more, we point out that reaction (R8) is not actually reversible, nor does it account properly for all elements of the char. We therefore have adopted the standard of writing reaction (R8) in the form

$$2C_{\alpha'}H_{\beta'}O_{\gamma'}N_{\delta'}S_{\varepsilon'}A + (\alpha'+2\varepsilon'-\beta'+2\gamma')\ H_2 + (\alpha'-2\gamma')\ H_2O \rightarrow \alpha'CO + \alpha'CH_4 + \delta'N_2 + 2\varepsilon'H_2S + A. \qquad (R9)$$

Reactions (R5), (R7), and (R9) in combination then represent the processes of gasification of char, with the production of CO, CH_4, N_2 and H_2S, and with the production or consumption of H_2 and/or H_2O. Specific expressions for the rates of these processes will be discussed in Section 6.

5.3.4 Reactions of Gaseous Species with Each Other (Catalyzed by Solids Present)

The most important reaction between gaseous species is the water gas shift reaction

$$CO + H_2O \rightleftarrows CO_2 + H_2 \qquad (R10)$$

It is well-known that this reaction does not occur in the gas phase but instead occurs as a surface process upon catalytic surfaces. This reaction is of common use commercially, and several studies exist on the kinetics of the iron oxide catalyzed water gas shift reaction. While none of these studies provides an unambiguous determination as to the mechanism of the reaction, or even as to its order with respect to the species, these studies do provide correlations between reaction rate, temperature, and gas phase partial pressure.

Most coal ash can be expected to act as a catalyst for reaction (R10). The degree of catalytic activity of the ash cannot be determined *a priori*, so that in the absence of experimental measurements on the ash, a certain amount of speculation is needed in order to estimate the catalytic activity. In the case of the CO_2 acceptor process, using Velva (N.D.) lignite, and for many other processes as well, it is found experimentally that the product gas is at, or near, shift equilibrium. This, of course, provides a clue

as to ash activity, in that it sets a lower limit to this activity. In the simulations of the CO_2 acceptor process (c.f., Section 6), we have found that the assumption that ash is 0.5 percent as active as commercial catalysts is sufficient to lead to the establishment of shift equilibrium in the product gas. Such an activity is not out of line with the known iron content of North Dakota lignites.

Another reaction of potential interest in gasification is the methane-steam reforming reaction

$$CH_4 + H_2O \rightleftarrows CO + 3H_2 \qquad \text{(R11)}$$

The reverse of this reaction is employed in a reactor downstream of the gasifier in many proposed high BTU gasification processes. Commercially, this reverse reaction is carried out in a reactor using a nickel catalyst. It is well-known that this catalyst is poisoned by H_2S, so that great care must be exercised to remove H_2S from the gas stream prior to its entering the methanation reactor. In a process such as the CO_2 acceptor process, the product gas is found to have a methane concentration which corresponds to reaction (R11) being shifted strongly to the left. It is possible to account for most of this methane on the basis of that produced during devolatilization, which indicates that reaction (R11) proceeds slowly, if at all, in the gasifier. The presence of H_2S in the gasifier is a virtue, in this respect, in that it likely would poison any material which might otherwise serve to catalyze reaction (R11). In developing our computer program, we have allowed for the possibility of occurrence of reaction (R11), but in all calculations done to date, we have "shut off" this reaction by taking its rate to be zero. Decision as to whether or not it can be similarly "shut off" in other processes will be deferred to such time as specific other processes are modeled.

A variety of other reactions between gas phase species can be contemplated. By way of illustration, hydrogen sulfide and carbon monoxide might react as follows:

$$CO + H_2S \rightleftarrows COS + H_2; \qquad \text{(R12)}$$

nitrogen and hydrogen might react to produce ammonia:

$$N_2 + 3H_2 \rightleftarrows 2NH_3. \qquad \text{(R13)}$$

Because reactions such as (R12) and (R13) produce species which are known to be minor constituents of the gas phase, it is sufficient for most purposes to ignore them completely. This is the point of view we have adopted to date. In the event that interest were to develop in estimating minor species concentrations in our model, we are tempted to believe that equilibrium calculations would suffice. Such calculations are much less expensive and faster on a computer than kinetic calculations, and use only readily available thermodynamic data as input, instead of harder to obtain kinetic measurements. Although thermodynamic calculations are less accurate in their results than careful kinetic calculations, they would likely suffice to provide a general indication of the concentration levels achievable for minor constituents.

5.3.5 Decomposition Reactions of Gaseous Species

If gasification is carried out under mild conditions, i.e., low temperatures, it is possible to produce a variety of heavy hydrocarbons. Under some circumstances these materials may condense as "tar" in cooler parts of a reactor. Such tars are difficult to characterize chemically in detail, since they consist of mixtures of many compounds. If it were to become necessary to model a process in which such tar were formed, considerable complication would ensue. It would probably become necessary to treat the tar empirically, in a manner similar to our treatment of char, by invoking the use of an empirical formula based upon ultimate analysis of the tar.

Under somewhat harsher conditions, such tar would undergo degradation to smaller molecules, possibly with the formation of a residual char. Under still harsher conditions such smaller molecules could crack to still smaller molecules, or undergo other conversion reactions. In the event where good data are available on the production of small molecules, such as C_2H_6 or NH_3, during devolatilization, their inclusion in a kinetic program could be contemplated. Modification of the existing chemical program during Year Two of our project will allow for this possibility. This in turn would likely require the inclusion of cracking reactions, perhaps the simplest of which is

$$C_2H_6 + H_2 \rightleftarrows 2CH_4 \qquad \text{(R14)}$$

A particular cracking process of possible significance is the reaction

$$CH_4 \rightleftarrows C + 2H_2 \qquad \text{(R15)}$$

here written with C taken to represent β-graphite. It is a frequent observation in experimental gasification studies (Dobner, et al., 1975) that the methane content of the product is thermodynamically unstable with respect to reaction (R15). Such in fact is the case in the CO_2 acceptor process. This raises at least the formal possibility of the occurrence of reaction (R15). Whether or not it in fact occurs depends upon temperature and likely also on the existence of surfaces conducive to graphite deposition. In the latter regard we speculate that once the process has been initiated by the formation of an initial layer of graphite,* further reaction proceeds easily. That is to say, the critical step in thermal cracking of methane may be in the formation of condensation nuclei. In the case of the CO_2 acceptor process, the temperatures appear to be too low for reaction (R15) to occur. Processes at more severe conditions may require consideration of this reaction. Programming modifications to accommodate this process will be undertaken in Year Two of the project.

5.3.6 Reaction of Gas Molecules with Feed Material or Devolatilized Feed Material

The most obvious reactions falling into this relatively minor category are the absorption of CO_2 and/or H_2S by lime components of ash:

$$CaO + CO_2 \rightleftarrows CaCO_3 \qquad \text{(R16)}$$

$$CaO + H_2S \rightleftarrows CaS + H_2O \qquad \text{(R17)}$$

$$CaO + SO_2 \rightleftarrows CaSO_3 \qquad \text{(R18)}$$

$$CaO + SO_2 + \tfrac{1}{2} O_2 \rightleftarrows CaSO_4 \qquad \text{(R19)}$$

Reactions (R16) and (R17) are of definite occurrence in the CO_2 acceptor process, where the lignite ash has a high content of CaO. Reactions such as (R18) and (R19) could occur in the combustion region of a steam-oxygen process, following initial conversion of coal sulfur into SO_2.

At present, our model does not include any reactions of the type exemplified by reactions (R16) - (R19). Programming modifications could be carried out so as to include

---

*It is perhaps more appropriate to use here the word "carbon" instead of "graphite", as the deposited solid might well contain enough impurities to have a less definite structure than graphite.

them if sufficient interest were to develop. There is, of course, some question as to the availability of kinetic data for absorption by ash which would have to be resolved prior to realistic inclusion of these reactions. Based upon the availability of data on similar reactions by acceptors, it would appear possible to develop reasonable kinetic expressions for these reactions.

5.3.7 Reactions of Gas Molecules with Acceptor

The reactions (R16) - (R19) listed above also apply to the absorption of these gases by acceptors. It should be understood that the actual sorbent may not simply be CaO, but can be a more complex species, such as half-calcined dolomite $MgO \cdot CaCO_3$ or fully-calcined dolomite $MgO \cdot CaO$.

Reaction (R16) is one of the key reactions of the CO_2 acceptor process, and has been the subject of kinetic investigations which we will discuss in Section 6.4. Although the correlations are not as detailed as we might like, they appear to be more than adequate for modeling the CO_2 acceptor process.

Reaction (R17) has been discussed in the literature (Ruth, et al., 1972; Abel and Fisher, 1975), and some kinetic information is available. Interestingly enough, when the sorbent is fully calcined dolomite $CaO \cdot MgO$ instead of CaO, the reaction is very slow; but following sorption of CO_2 to form $CaCO_3 \cdot MgO$ [c.f., reaction (R16)], subsequent conversion to $CaS \cdot MgO$ with elimination of CO_2 is rapid. The model at present does not allow for sorption of H_2S, although it would not be difficult to add this process to the model.

With respect to reactions (R18) and (R19), many kinetic studies are available. Most of these stem from the potential commercial importance of these processes as means for removing SO_2 from combustion effluent streams. The consequence of this is that a fairly good understanding of the kinetics of these processes can be obtained from the literature, so that their inclusion in the model is possible. At present, however, they are not included in the model.*

5.3.8 Oxidation of Feed Materials or Devolatilized Feed Materials

We indicated earlier that oxidation processes could be thought to be a special case of gasification processes, but that we preferred to think of them separately. Oxidation steps do not occur in the CO_2 acceptor process, and therefore are not

*They do not occur in the CO_2 acceptor process.

presently included in the model. It clearly will be necessary to add them in order to apply the model to steam-oxygen gasification processes. It would appear to be quite straightforward to represent the combustion of coal by the expression

$$C_\alpha H_\beta O_\gamma N_\delta S_\varepsilon A + \frac{1}{2}\,\delta'' N_2 + \left[\alpha+\frac{1}{2}(\beta-\gamma+\delta+\delta''+\delta''')+\varepsilon\right]O_2$$

$$\rightarrow \alpha CO_2 + \frac{1}{2}\,\beta H_2O + \frac{1}{2}\,\delta''' N_2 + (\delta+\delta''-\delta''')NO + \varepsilon SO_2 + A \qquad \text{(R20)}$$

A similar expression would represent char combustion. As written, reaction (R20) considers formation of NO, which typically accompanies combustion at elevated temperatures. Free nitrogen is written on both sides of the equation since its presence influences the amount of NO formation, while at the same time it may be released from the coal during combustion. Correlations are available in the literature relating the amount of NO produced to temperature, oxygen and nitrogen partial pressure, and fuel nitrogen content. Production of NO is likely to be small in gasification processes, and in any event NO may be reduced by other reactions at later stages of the gasification process.

The most important part of reaction (R20) is the oxidation of the coal. Studies of combustion kinetics abound in the literature. For purposes of modeling gasification, kinetic information on reaction (R20) is likely to be unnecessary, since relative to other reactions and to fluid mechanical processes, combustion is very rapid. Thus, it would probably suffice to treat reaction (R20) in a manner similar to devolatilization and rapid rate methanation, i.e., by means of stoichiometric relations and the assumption that the process is infinitely rapid. The "effective" rate of reaction would be controlled by the rates of interdiffusion of gaseous reactants and products in the region surrounding a burning coal particle.

SECTION 6

RATE CONSTANTS FOR THE CO_2 ACCEPTOR PROCESS/SAMPLE CALCULATIONS

In reviewing the nature of the feed, recycle, and exit streams for a "general" gasification process (c.f., Section 5), we frequently mentioned specific considerations appropriate to the CO_2 acceptor process. We will briefly summarize these here, and indicate our sources for kinetic data, as used in Year One of the project, in modeling the CO_2 acceptor process. This effort is part of Task Area 04 as summarized in Section 2.

The chemical reactions of significance for the CO_2 acceptor process are:

1. Devolatilization and rapid rate methanation of lignite feed [reaction (R2)].

2. Low rate gasification of char [reaction (R5), (R7), (R9)].

3. Water gas shift reaction [reaction (R10)].

4. Absorption of CO_2 by acceptor* [reaction (R16)].

6.1 DEVOLATILIZATION AND RAPID RATE METHANATION OF FEED LIGNITE

As discussed in Sections 5.3.1 and 5.3.2, these processes are partially characterized by stoichiometry, i.e., by elemental mass balances, provided that we have available ultimate analyses of both lignite and the char produced by devolatilization. Such analyses for the lignite have been carried out by Conoco Coal Development Company (CCDC), and the data have been provided to us (Curran, 1976). Table 6.1 gives both the ultimate and proximate analysis for the Velva (N.D.) lignite used in process tests at the Rapid City, South Dakota, pilot plant.

Ultimate analysis of the char was available only indirectly. Char samples have been recovered at the pilot plant both from the char stream which feeds to the plant regenerator and from char fines which escape through the

*The acceptor used in the commercial process is a fully-calcined dolomite $CaO \cdot MgO$, which absorbs CO_2 to form $CaCO_3 \cdot MgO$. At process conditions, the MgO thus acts as an inert, passive diluent, and does not enter into the reaction. Its presence does effect reaction kinetics, however, because of its effect on particle grain structure.

TABLE 6.1

PROXIMATE AND ULTIMATE ANALYSIS OF VELVA (N.D.) LIGNITE*

Proximate Analysis (Dry Lignite as Fed to Gasifier)

Moisture	0.00 Weight Percent
Volatiles	42.18 Weight Percent
Fixed Carbon	50.98 Weight Percent
Ash	6.84 Weight Percent

Ultimate Analysis (Dry Basis)

Carbon	66.16 Weight Percent
Hydrogen	4.59 Weight Percent
Oxygen	20.86 Weight Percent
Nitrogen	1.00 Weight Percent
Sulfur	0.54 Weight Percent
Ash	6.84 Weight Percent

*G. P. Curran (private communication), 23 January 1976.

cyclone. Analyses of these samples, as provided to us by CCDC (Curran, 1976), are given in columns a and b of Table 6.2. Neither of these analyses provides directly the data we need. The reason that they do not is that they give analyses of char residues which have undergone low rate gasification as well as devolatilization and rapid rate methanation.

It is necessary to estimate the ultimate analysis of freshly produced char. Information supplied by CCDC indicated that 16 percent of the dry coal mass was volatile carbon, so that after devolatilization of one gram of coal, the remaining char would contain 0.6616-0.1600 = 0.5016 grams of carbon. Since the total weight of this char would be 1 - 0.4218 = 0.5782 grams, the fresh char should have an ultimate analysis showing 86.75 weight percent carbon and 11.83 percent ash. Adding the latter two figures together leaves 100 - 11.83 - 86.75 = 1.42 weight percent of the char unaccounted for. This latter mass must be due to the hydrogen, oxygen, nitrogen and sulfur content of the char. In order to estimate these quantities, we have assumed that during subsequent low rate gasification the relative atomic ratios H/C, O/C, N/C, and S/C of the char remain unchanged. The data in Table 6.2, columns a and b, allow us to assess the validity of this assumption.* To do this, we recalculate the weight percentages of the elements C, H, O, N, S on an ash free, CO_2 free, CaO-CaS free basis. We also estimate the percentage of total carbon burnoff for the three specimens as follows:

Let: f_0 = weight fraction of ash in feed lignite

f_1 = weight fraction of ash in char (ex CO_2 and CaO-CaS)

a = weight of ash per unit mass of feed lignite

x_0 = weight of volatiles and fixed carbon per unit weight of feed lignite

x_1 = weight of fixed carbon per unit weight of char (ex CO_2 and CaS-CaO)

*There is a study (Wen, Mori, Gray, and Yavorsky, 1975) of char gasification using Illinois #6 coal as a char source, in which it is shown that this assumption is only approximate. No equivalent study is available for Velva (N.D.) lignite.

TABLE 6.2

ULTIMATE ANALYSES OF VELVA (N.D.) LIGNITE CHAR[†]

	Weight Percent		
	a	b	c
Carbon	59.10	73.29	86.75
Hydrogen	0.78	0.83	0.99
Oxygen	0.00	0.00	0.00
Nitrogen	0.22	0.36	0.43
Sulfur	0.00	0.00	0.00
Ash	33.05	18.70	11.83
CO_2	6.36*	6.75*	---
CaS-CaO	0.49*	0.07*	---

a. Experimental values, based upon measurements of char fines lost via cyclone.

b. Experimental values, based upon measurements on char samples from gasifier exit stream which feeds to plant regenerator.

c. Computed values which are used to estimate composition of freshly devolatilized char (see text).

*The weight of CO_2 in the experimental samples, as indicated here, is due to CO_2 absorbed by the lime in the ash. The CaS-CaO component arises from H_2S absorbed by the lime in the ash (see Section 5.3.6 of text).

[†]G. P. Curran (private communication), 23 January 1976.

Then, assuming no loss of ash during reaction, we have the relations

$$f_0 = a/(x_0 + a) \tag{6.1}$$

$$f_1 = a/(x_1 + a) \tag{6.2}$$

Eliminating a from Eqs. (6.1) and (6.2) leads to

$$100\left(1 - \frac{x_1}{x_0}\right) = \frac{100(f_1 - f_0)}{f_1(1-f_0)} \ . \tag{6.3}$$

The quantity $100(1-x_1/x_0)$ is the percentage of total carbon burnoff for a sample with an ash weight fraction f_1. From Table 6.1, the value of f_0 is fixed at 0.0684 for Velva (N.D.) lignite. Calculations using Eq. (6.3) lead to results shown in Table 6.3. We have used the figures in Table 6.3, column b, to provide estimates of the H/C, O/C, N/C, and S/C ratios (ex ash, CO_2 and CaO-CaS) of fresh char. This then leads, in combination with the data in Table 6.1, to an estimated ultimate analysis of fresh char as shown in Table 6.2, column c. The data in the latter column were used in all subsequent calculations. Because of the small H and N content of the char, errors introduced by this assumption should be very small.

Calculation of the parameters α, β, γ, δ, ε, and α', β', γ', δ', ε' is straightforward once the data in Tables 6.1 and 6.2 are available. Table 6.4 gives the values of the parameters α, β, ..., γ', ε' for Velva (N.D.) lignite.

As discussed in Sections 5.3 and 5.3.2, it is also necessary to specify the ratio of CO_2 to CO produced during devolatilization. We have used Eq. (5.5), as discussed previously.

Also needed are the temperature dependent correlation parameters $b_1(T)$, $b_2(T)$, $b_3(T)$, for use in Eq. (5.4). Zahradnik and Glenn (1971) have discussed the experiments of several authors on methane production during devolatilization and rapid rate methanation. They presented models which lead to selection of Eq. (5.4) as the correlating relation between methane yield and hydrogen partial pressure. None of the experiments they discuss were on Velva (N.D.)

TABLE 6.3

CALCULATED WEIGHT PERCENTAGES OF ELEMENTS (ex CO_2, ASH, and CaO-CaS) AND CALCULATED PERCENTAGE OF TOTAL CARBON BURNOFF

	a	b
C	98.34%	98.40%
H	1.30%	1.12%
O	0.00%	0.00%
N	0.36%	0.48%
S	0.00%	0.00%
Burnoff	86.6%	70.8%

a. Based on measurements on char fines lost via cyclone.

b. Based on measurements on char samples from gasifier exit stream which feeds to plant regenerator.

TABLE 6.4

STOICHIOMETRIC PARAMETERS FOR VELVA (N.D.) LIGNITE AND VELVA (N.D.) LIGNITE CHAR (BASIS: ONE GRAM OF FEED LIGNITE)

$\alpha = 0.05509$	$\alpha' = 0.04176$
$\beta = 0.04554$	$\beta' = 0.00568$
$\gamma = 0.01304$	$\gamma' = 0.00000$
$\delta = 0.00071$	$\delta' = 0.00018$
$\varepsilon = 0.00017$	$\varepsilon' = 0.00000$

lignite, although experiments by Glenn, Donath, and Grace (1967), on a lignite identified as from Mercer County, N.D., were included in the analysis.

The experiments analyzed by Zahradnik and Glenn covered methane production at a variety of pressures and temperatures. These are summarized in Table 6.5. The experiments on bituminous coals show that $b_1(T)$, $b_2(T)$ and $b_3(T)$ have an Arrhenius form of temperature dependence

$$b_i(T) = a_i \exp(-c_i/T) \qquad (6.4)$$

We hypothesize that the temperature dependent term $\exp(-c_i/T)$ is the same for all coals, but that the coefficient a_i is material-dependent. With this hypothesis, we can utilize the data of Lewis, et al. (1967), at 725°C and that of Moseley and Paterson (1967) at 850°C on subbituminous coal to deduce values for c_1, c_2, and c_3. The results are

$$c_1 = -1197\ (°K)^{-1}$$

$$c_2 = 6491\ (°K)^{-1}$$

$$c_3 = 6164\ (°K)^{-1}$$

The results of Glenn, et al. (1967), on Mercer County (N.D.) lignite then allow us to evaluate the constants a_1, a_2 and a_3. The results are

$$a_1 = 0.02520$$

$$a_2 = 1.2513$$

$$a_3 = 1.0350$$

TABLE 6.5

EXPERIMENTAL STUDIES USED IN DEVELOPING METHANE CORRELATION PARAMETERS $b_1(T)$, $b_2(T)$, $b_3(T)$

Material	H_2 Partial Pressure Range	Temperature	Reference
Mercer County, N.D. Lignite	15-30 atm	950°C	a
Elkol, Wyoming Sub-bituminous	10-20 atm	950°C	a
High Volatile 902 Bituminous	50-500 atm	850°-950°	b
High Volatile A Pittsburgh Bituminous	30-100 atm	725°C	c

References: a. Glenn, Donath, and Grace, 1957.
b. Lewis, Friedman, and Hiteshue, 1967.
c. Moseley and Paterson, 1967.

We have assumed that Velva lignite is similar enough to Mercer County lignite so as to allow the use of the correlation parameters so derived for purposes of modeling gasification of Velva lignite. The assumed correlations thus are:

$$b_1(T) = 0.0252\exp(1197/T) \tag{6.5}$$

$$b_2(T) = 1.2513\exp(-6491/T) \tag{6.6}$$

$$b_3(T) = 1.035\exp(-6164/T) \tag{6.7}$$

Equations (6.5) - (6.7) have been used in all calculations performed to date.

6.2 LOW RATE GASIFICATION OF CHAR

As discussed in Section 5.3.3, the low rate gasification of char can be modeled by the chemical reactions (R5), (R7), and (R9). Two convenient sources of kinetic correlations for these reactions are available. The first of these sources is in a group of papers by Johnson (Pyrcioch, et al. 1972; Johnson, 1974; Johnson, 1975). The second is in a set of CCDC reports prepared by Curran and associates (Curran, 1970; Curran, et al., 1970).

In Johnson's work, he develops correlating expressions for the rates of reactions (R5), (R7), (R9) by utilizing data on various chars studied both at the Institute of Gas Technology (IGT) and at Consolidation Coal Research Division (the corporate predecessor of CCDC). He develops expressions correlating the rates for all chars, irrespective of source, which are multiplied by scale factors to account for the varying reactivity of chars derived from different sources.

The work of Curran, et al. (1970) involved experimental measurements on a variety of Western lignite chars, which were being considered as feedstocks for the CO_2 acceptor process. Since the materials studied by Curran, et al. were more closely related to Velva (N.D.) lignite than the materials correlated by Johnson, it is appropriate to make use of Curran's correlations in simulation calculations of the Rapid City, S.D., pilot plant.

The correlations due to Curran, et al. were derived on the basis of a simple unpublished steady state analysis of a set of hypothesized basic reactions. The correlations take the form

$$\Gamma_1 = \frac{k(P_{H_2O} - K^{-1}P_{H_2}P_{CO})}{(1 + K_1P_{H_2O} + K_2P_{H_2} + K_3P_{CO})^2} \qquad (6.8)$$

and

$$\Gamma_2 = \frac{k'(P_{H_2O}P_{H_2} - K'^{-1}P_{CO}P_{CH_4})}{(1 + K_1'P_{H_2O} + K_2'P_{H_2} + K_3'P_{CO} + K_4'P_{CH_4})^2} \qquad (6.9)$$

In these expressions, Γ_1 is the rate of reaction (R4) (reaction (R5) as modified by us) and Γ_2 is the rate of reaction (R8) (reaction (R9) as modified by us), each expressed in units of grams of carbon gasified per gram of carbon in the reactor per unit time. Unlike Johnson's correlation, this correlation does not make use of the direct methanation reaction (R6) (or (R7)).

The subscripted P's in Eqs. (6.8) and (6.9) are the partial pressures of the components of the gas phase. The K_i's and K_i''s and k, k' are kinetic parameters related to the fundamental steps of the reaction model developed by CCDC. As deduced by the reaction model, the constants K and K' should be the equilibrium constants for reactions (R4) and (R8), respectively. However, in correlating experimental data, Curran and Gorin found that better agreement with data was obtained when the value of K was considerably smaller than the equilibrium value. For K' an accurate assessment of value was not possible, because the term $P_{CO}P_{CH_4}/K'$ containing it was too small under experimental conditions, relative to the term $P_{H_2}P_{H_2O}$, to allow evaluation of K'. It was therefore assumed that K' was best represented by its equilibrium value.

The correlation parameters in Eqs. (6.8) and (6.9) each are dependent upon temperature, the specific lignite being gasified, and the extent to which gasification has proceeded. With respect to the latter dependence, it is a common observation during char gasification that the reactivity of the char varies as the char burns off. The studies by Curran and Gorin found that for some lignites reactivity decreased steadily with burnoff, while for others reactivity first increased with burnoff and then decreased.

The CCDC study did not include kinetic measurements on Velva (N.D.) lignite, but did include measurements on Husky lignite, whose kinetic behavior is believed to be similar.* We have used the CCDC data on Husky lignite

*G. P. Curran (private communication).

(Curran, et al., 1970) in our simulation calculations of the Rapid City, South Dakota, pilot plant. The Husky lignite data were obtained under two different sets of conditions: (1) 1144°K (1600°F) at 25 percent to 48 percent carbon burnoff; (2) 1089°K (1500°F) at 39 percent to 56 percent carbon burnoff. During gasifier operation, there is within the gasifier at any point in time a distribution of char particles which have experienced varying degrees of burnoff. In steady state operation, this distribution will achieve some limiting form. It is presently difficult to determine the form of this steady state distribution (work in Year Two of the program will study the distribution). However, it seems reasonable to estimate that kinetic parameters corresponding to some average burnoff would represent the average reactivity of the steady state char inventory of the reactor. Since the Husky char kinetic data falls into a burnoff range which probably is average for a reactor at steady state, we have used these data directly.

The experiments of Curran and Gorin (1970), being at two different temperatures, allow us to estimate the temperature dependences of the correlation parameters. To do so, we have assumed each parameter to have an Arrhenius temperature dependence, i.e., $k = A\exp(-B/T)$, where A and B are constants and T is the absolute (Kelvin) temperature. In Table 6.6 we give the values for the parameters of Eqs. (6.8) and (6.9), expressed in terms of respective constants A and B. The constant K' is obtained as the value of the equilibrium constant for reaction (R8), where C is taken to represent β-graphite. In our computer programs, this constant is calculated from tabulated temperatures dependent values for the free energies of formation of the various species which appear in reaction (R8). It is perhaps worthy to note that under typical operating conditions of temperature and pressure, the rate Γ_1 is about ten times as large as the rate Γ_2, so that most char gasification occurs via the carbon-steam reaction.

6.3 WATER GAS SHIFT REACTION

This reaction is frequently utilized in the chemical process industry. It occurs rapidly at elevated temperatures in the presence of suitable catalysts. Common commercial catalysts include chromia-promoted iron oxides. In commercial processes, the shift reaction usually is carried out at temperatures in the range 575°K-775°K, which is considerably lower than the operating temperatures of coal gasification processes. Because of commercial interest, kinetic studies (Bohlbro, 1961; Moe, 1962) typically are carried out at lower temperatures. As a consequence, estimation of the rate of this reaction under gasifier operating conditions requires

TABLE 6.6

KINETIC PARAMETERS FOR LOW RATE GASIFICATION KINETICS

Constant	A (units)	B($°K^{-1}$)
k	4.146×10^{18} atm^{-1} min^{-1}	51128.
K	1.169×10^{14} atm	33717.
K_1	3.456×10^{12} atm^{-1}	36456.
K_2	2.000×10^{-1} atm^{-1}	0.
K_3	1.597×10^{-5} atm^{-1}	-12395.
k'	1.996×10^{15} atm^{-2} min^{-1}	45776.
K'	Computed from thermodynamic equilibrium data	
K'_1	1.235×10^{3} atm^{-1}	11571.
K'_2	5.523×10^{-10} atm^{-1}	-22217.
K'_3	2.734×10^{4} atm^{-1}	11303.
K'_4	4.543×10^{4} atm^{-1}	12676.

a double extrapolation. On the one hand, we must extrapolate kinetic measurements over a rather wide temperature range; on the other hand, we must utilize the idea that data on commercial shift catalysts can be "scaled". Under appropriate conditions, these extrapolations, although severe, may not introduce errors of consequence. In particular, if the reaction occurs with sufficient rapidity that it leads to the occurrence of shift equilibrium essentially throughout the reactor, then any kinetic correlation, even one that is inaccurate in an absolute sense, may suffice, provided only that the correlation leads to a prediction of essentially the same equilibrium.

In our model, we have utilized a simple correlation (Moe, (1962)) according to which the rate of the shift reaction is given by the expression

$$\Gamma_3 = k_s(T)\left[P_{CO}P_{H_2O} - P_{CO_2}P_{H_2}K_{wgs}^{-1}\right] \tag{6.10}$$

where the P's are partial pressure, K_{wgs} is the equilibrium constant for the shift reaction, and $k_s(T)$ is a rate parameter. This parameter, which has been evaluated by measurements on commercial iron catalysts, is of Arrhenius form:

$$k_s = 3.586\times10^5\exp(-4895/T) \tag{6.11}$$

where T is the Kelvin temperature. The units of k_s in Eq. (6.11) are mole atm^{-2} min^{-1} gm^{-1}, that is to say, this expression gives the chemical rate per unit mass of catalyst.

We have hypothesized that coal ash has a temperature dependent activity with an activation energy (4895(°K)) identical to that given in Eq. (6.11). Because of its open structure, we can anticipate that for ash the active surface area is proportional to mass. Under these two assumptions, ash would be identical in catalytic properties to commercial catalyst, a highly unlikely circumstance. We therefore introduce a factor β which expresses the activity of ash relative to commercial catalyst. Thus, we hypothesize that for ash Eq. (6.11) is replaced by

$$k_s = 3.568\times10^5\beta\exp(-4895/T) \tag{6.12}$$

Evaluation of β or verification of the value assumed for the activation energy would require experimental measurements which are not available. It thus becomes necessary to try to fix the value of β by studying how predictions of process results at Rapid City for varying β values compared with observations. Clearly, the variable to be studied this way is the shift ratio of the reactor contents at steady state, which should be close to its equilibrium value. Such a study was made, varying β in the range $0.001 \leq \beta \leq 1$. The value $\beta = 1$ corresponds to ash which acts as a commercial catalyst and leads to the prediction of shift equilibrium at steady state, as it should. What is gratifying is that over the wide range of values $0.0035 \leq \beta \leq 1$ essentially the same result is obtained. Only when β is taken to be less than about 0.0035 does calculation lead to a prediction of a steady state gas composition not at shift equilibrium.

The previous result, obtained in several preliminary calculations with our computer program, can be stated in form that "even if ash is as little as 0.0035 times as active as a commercial catalyst, this would still be sufficient activity to assure that the steady state gas composition in the reactor essentially displays shift equilibrium". Inasmuch as typical North Dakota lignites ash show Fe_2O_3 content ranging between 5 percent and 10 percent by weight, an activity ratio of 0.0035 (or even much higher) is eminently plausible. For purposes of calculation, we have for the present standardized on $\beta = 0.005$, which would seem then to be a very conservative estimate of ash catalytic activity.

Despite the rationale of the above argument, and the computational results to which it leads (see Section 6.6 below) it is worth noting that some caution is called for. The potential significance of the water gas shift reaction is so great for all gasification processes that direct experimental data on the catalytic activity of the ash, and even of precursor coal or char, would appear to be desirable. We can well contemplate the occurrence of situations in which ash catalytic activity is marginal at best, in which case predictions based on calculations will be sensitive to the activity. In such a case, good fortune may not prevail, and the absence of direct measurements may hinder the valid application of computer prediction methodology.

6.4 ABSORPTION OF CO_2 BY ACCEPTOR

Kinetic studies of acceptor recarbonation, reaction (R16), were carried out by the same group at CCDC that studied low-rate gasification kinetics, and the results of these studies were published in the same reports (Curran and Gorin, 1970; Curran, et al., 1970), and also elsewhere (Curran, et al., (1967).

Samples studied had been freshly prepared by calcination of commercial dolomites or limestones. These were then recarbonated under conditions of constant temperature and CO_2 partial pressure. A thermobalance measured the sample mass as a function of time during recarbonation. The results of these experiments suggest that recarbonation of individual acceptor particles can be modeled as a "shrinking core" process. For such a process, the mass fraction x of acceptor which has reacted with CO_2 varies in time t according to the equation

$$1 - (1-x)^{1/3} = kt \tag{6.13}$$

In Figure 6.1 we show plots of $1 - (1-x)^{1/3}$ against t for five different experimental runs published by Curran, et al., 1967.* From this figure we can see that the shrinking core model holds well for values of x at least as high as 0.99.

Direct application of Eq. (6.13) to model absorption of CO_2 in a reactor is not possible. Three difficulties ensue.

1. It is observed in pilot plant and laboratory studies, in which acceptor is continuously recycled between the gasifier and a calcining regenerator, that the capacity of the acceptor to absorb CO_2 slowly declines. Typically, following 20 or more cycles of carbonation and calcination, only about one-third of the original acceptor charge retains its ability to absorb CO_2.

2. In continuous operation, there is a feed stream of calcined acceptor and an exit stream of partially carbonated acceptor. Because the latter continuously withdraws a "random" sample of the gasifier acceptor inventory, there gradually builds up within the gasifier a distribution of acceptor particles, each characterized at a given point in time by its own value of the parameter x. The net rate of carbonation at a given time then depends on this distribution of x-values.

3. The parameter k in Eq. (6.13) is a function both of the ambient CO_2 partial pressure, and also of the equilibrium partial pressure $P^0_{CO_2}(T)$ of CO_2 in the three phase chemical reaction

$$CaO + CO_2 \rightleftarrows CaCO_3 \tag{R16}$$

*This plot was prepared for us by Professor C. Y. Wen.

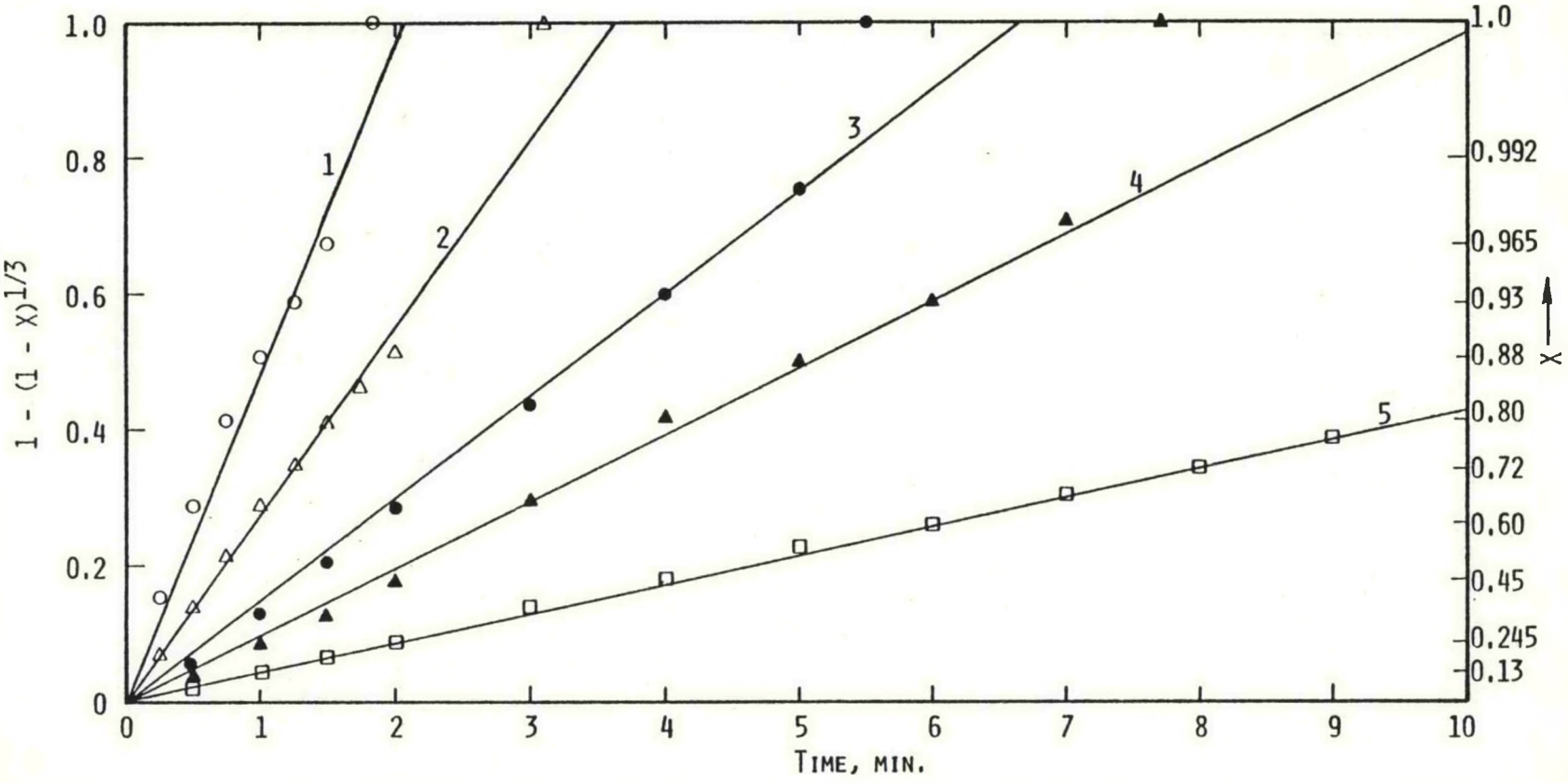

Figure 6.1. Mass fraction of acceptor carbonated versus time. Points are based upon data of Curran, Fink and Gorin [1967]. Straight lines are predictions of shrinking core model. Process conditions for curves are as follows: (1) T = 859°C, P_{CO_2} = 0.972 atm; (2) T = 813°C, P_{CO_2} = 0.456 atm; (3) T = 881°C, P_{CO_2} = 0.953 atm; (4) T = 850°C, P_{CO_2} = 0.630 atm; (5) T = 887°C, P_{CO_2} = 0.857 atm.

The form of this pressure dependence has heretofore not been well-known, and must be treated approximately.*

Responses to these three difficulties are available.

1. Experimental measurements on specific acceptors can be performed which measure the fraction of the acceptor which remains active following repeated calcination. Included in such measurements are effects due to the fact that plant operation requires a steady makeup stream of fresh, 100 percent active acceptor, to compensate for various system losses. With data available on this "limiting activity" we can model the carbonation reaction by assuming that a fraction Θ_a of the acceptor particles remains active and reacts in accordance with a shrinking core model, and that a fraction $1-\Theta_a$ are nonreactive. Needless to say, such an assumption is an oversimplification of a complex situation. The true causes of activity loss would appear to be loss of pore volume, increase of crystallite size, and perhaps interference with pore diffusion due to formation of surface layers of material derived from minor components of the acceptor. Such factors should affect all particles to some degree, but not enough is known as yet to allow for a detailed description of this.

2. The distribution of x-values which is achieved in steady state operations can be dealt with precisely, and in fact simplifies the modeling of the carbonation process. To do this, imagine the active acceptor particles each to have a mass m_0 of active CaO prior to carbonation. Let m be the mass of active CaO remaining at some intermediate level of carbonation. The following relation then holds between m, m_0, and x:

$$x = 1 - (m/m_0) \tag{6.14}$$

Equation (6.13) arises from integration of the differential equation

$$\frac{dm}{dt} = -3km_0^{1/3}m^{2/3} \tag{6.15}$$

*Subsequent to the completion of the calculations described in this report, G. P. Curran developed a correlation which describes well all of the experimental data. This new correlation arrived too late to be included in the present work, but it will be incorporated in further studies.

with boundary conditions $m = m_0$ at $t = 0$. In a reactor in which there are many particles of acceptor, with a distribution of values of m, the quantities of interest are not the m values of the individual particles, but instead the value of the total mass M of active but unreacted acceptor, and the total rate of reaction of this mass, dM/dt. At steady state there will be some distribution of individual masses $N(m)$ such that $N(m)dm$ is the total number of acceptor particles for which the amount of unreacted mass is between m and $m + dm$. The total mass M is then given by

$$M = \int_0^{m_0} mN(m)\,dm \tag{6.16}$$

The total rate of reaction similarly is

$$\frac{dM}{dt} = -3km_0^{1/3} \int_0^{m_0} m^{2/3} N(m)\,dm \tag{6.17}$$

If we assume for sake of argument that $N(m)$ is a uniform distribution, i.e., that $N(m) \equiv 2M/m_0^2$ for all m in the range $0 \leq m \leq m_0$, we then obtain for the total rate of reaction $d\bar{M}/dt$

$$\frac{dM}{dt} = -3km_0^{1/3} \int_0^{m_0} \frac{2M}{m_0^2} m^{2/3} dm = -\frac{18}{5} kM. \tag{6.18}$$

Equation (6.18) shows that the total rate of reaction for a uniform mass distribution is proportional to the total mass of active but unreacted acceptor. Furthermore, from Eq. (6.15), the reaction rate for a group of N_1 particles, all of which are initially of mass m_0, is given by

$$\frac{d}{dt}(N_1 m) = -3km_0^{1/3} N_1^{1/3} (N_1 m)^{2/3} \tag{6.19}$$

But for such particles $N_1 m$ is the total mass and $N_1 m_0$ is the initial total mass. Writing $M_1 = N_1 m$ and $M_{10} = N_1 m_0$, Eq. (6.19) becomes

$$\frac{dM_1}{dt} = -3kM_{10}^{1/3} M_1^{2/3} \tag{6.20}$$

We can express Eqs. (6.18) and (6.20) in terms of reaction per unit mass

$$M^{-1} dM/dt = -\frac{18}{5} k \tag{6.21}$$

$$M_1^{-1} dM_1/dt = -3k(M_{10}/M_1)^{1/3} \tag{6.22}$$

There will be a value of the ratio M_1/M_{10} for which $M^{-1} dM_1/dt = M^{-1} dM/dt$. Numerically, this value is

$$\frac{M_1}{M_{10}} = \left(\frac{5}{6}\right)^3 \simeq 0.5787 \tag{6.23}$$

Equation (6.23) indicates that the rate constant which determines the fractional mass loss rate for a system with a uniform distribution of masses can be obtained from experiments on a system with a single particle size by using as the rate constant the numerical value of the measured slope $m^{-1} dm/dt$ evaluated where $m/m_0 = 0.5787$.

If the limiting distribution is not uniform, a similar conclusion can be reached. For example, if the distribution were of the form $N(m) = 6M(m_0 - m)/m_0^3$, we would obtain

$$\frac{dM}{dt} = -3km_0^{1/3} \cdot 6Mm_0^{-3} \int_0^{m_0} (m_0 - m) m^{2/3} \, dm = -\frac{81}{20} kM \tag{6.24}$$

The corresponding value of the ratio M_1/M_{10} is

$$\frac{M_1}{M_{10}} = \left(\frac{20}{27}\right)^3 \simeq 0.4064 \qquad (6.25)$$

Work is underway in Year Two of the program which will determine a realistic form for the distribution N(m), but the results quoted here are sufficient to establish that the reactivity per unit mass for a distribution of particles is that for uniform particles at a time at which they have achieved an intermediate x value. There is reason to believe that the steady state distribution N(m) would be biased in favor of smaller values of m, so that the distribution used to obtain Eq. (6.25) is more realistic than that used to obtain Eq. (6.23). For purposes of computation, we in fact have used $M_1/M_{10} = 0.3403$, which corresponds roughly to a distribution proportional to $(m_0-m)^{3/2}$. With this value of M_1/M_{10} it can be shown that a distribution of acceptor masses would react 90 percent to completion in the same time as a uniform set of particles all of initial mass m_0.

3. The functional dependence of the reaction rate upon the CO_2 partial pressure has only recently been established,* too late for inclusion in the present work, although the computer program will be modified to include this new correlation. It has turned out that the rate can be correlated with the 4/3 power of the pressure difference $P_{CO_2}-P^0_{CO_2}$, where $P^0_{CO_2}$ is the equilibrium partial pressure of CO_2 above a mixture of CaO and $CaCO_3$ which is at phase equilibrium. The value of $P^0_{CO_2}$ is a function of temperature, and in fact is the reciprocal of the equilibrium constant for reaction (R16). Its value can easily be computed from empirical expressions for the standard free energies of formation of the species in reaction (R16).

As an approximation to the acceptor kinetics, we have assumed for purposes of calculation that the reaction rate was proportional to the first power of the pressure difference $P_{CO_2}-P^0_{CO_2}$. If we write the rate equation

$$\frac{dM}{dt} = -\ell k M \qquad (6.26)$$

---

*G. P. Curran (private communication).

with the constant ℓ chosen so that the equivalent mass M_1/M_{10} is equal to 0.3403 (see above) then values for the product ℓk can be extracted from the experimental data of Curran, Fink and Gorin. These values, when divided by $P_{CO_2} - P^0_{CO_2}$ for each experiment, should be independent of $P_{CO_2} - P^0_{CO_2}$ if the rate was linear in $P_{CO_2} - P^0_{CO_2}$. In fact, the resulting ratio varies by a factor of two as $P_{CO_2} - P^0_{CO_2}$ varies by a factor of five. To reconcile this difficulty, we have utilized the <u>average</u> value of $\ell k/(P_{CO_2} - P^0_{CO_2})$, averaged over all the experiments. The resulting expression for the rate of the carbonation reaction is

$$\Gamma_5 \equiv \frac{dM}{dt} = -k_c M(P_{CO_2} - P^0_{CO_2}) \qquad (6.27)$$

with the numerical value of k_c being $k_c = 4.3\ \text{atm}^{-1}\ \text{min}^{-1}$. There is also the possibility of some variability in k_c with temperature. The quoted numerical value represents that for an average temperature in the range of the experiments. Fortunately, this average temperature is sufficiently close to the operating temperature at the Rapid City pilot plant that neglect of temperature effects (other than those upon $P^0_{CO_2}$) should not lead to serious error.

Despite the difficulty in arriving at a precise expression for the kinetics of acceptor carbonation, it is possible to show that no serious computational errors are induced thereby. The reasoning is similar to that used in connection with the water gas shift reaction. Process conditions at the Rapid City pilot plant are such that the space time for the acceptor is long compared to the time required to complete the recarbonation of an acceptor particle. This means that, in steady state, operation essentially is influenced only by the stoichiometry of reaction (R16), taken to completion, and the time required to completely carbonate a freshly introduced acceptor particle. We have carefully chosen the effective rate expression, Eq. (6.26), so that this total time coincides with what has been measured experimentally, although details of the rate as a function of time are not quite correct. The stoichiometry of the reaction is, of course, trivially correct. As a consequence, we can state that the important aspects of the reaction rate are modeled correctly, although some details are in error. Such an approach should suffice as long as we are not considering transients which occur over times small compared to the time required to completely carbonate a fresh acceptor particle. The latter time is of the order of five minutes, as can be deduced from the experimental kinetics. The improved correlation now available, will when installed in the computer program in Year Two, will allow us also to

deal with transient chemical phenomena on time scales short compared to five minutes.

6.5 CONSTRUCTION OF THE MODEL FROM THE KINETIC RATE EXPRESSIONS

A one zone model for a well-stirred chemical reactor consists of a set of coupled ordinary differential equations, in which the dependent variables are the masses (or number of moles) of the various chemical species contained in the reactor, all as functions of the time t. Other possible dependent variables include pressure and temperature. Up to the present, the computer program we have written to implement the model has been set up and operated in an isothermal mode, with the reactor temperature held constant at the experimental steady state value of the CO_2 pilot plant. During Year Two, non-isothermal operation of the program will be undertaken. The choice of isothermality corresponds to choosing a particular rate of heat transfer through the reactor walls, and this rate of heat transfer can be calculated as an auxiliary variable using thermodynamic data on the chemical species in the system. Up to the present program operation has also been in a constant pressure mode, because program checking is easier in this mode.

Under conditions of constant pressure and temperature, the chemical model takes the form

$$\frac{dm_i}{dt} = S_i + R_i - N_i + C_i \qquad (6.28)$$

where the m_i's are the masses of the species contained in the reactor, the S_i's are source terms, e.g., those due to feed streams, the R_i's are rates of changes due to chemical reactions, the N_i's are sink terms, representing the exit streams and the C_i's are recycle terms. The index i denotes the species and t is time, for which we adopt 1 minute as the unit. For the CO_2 acceptor process, the species we have included are the following:

Gases: H_2, H_2O, CH_4, CO, CO_2, N_2, H_2S

Acceptor: $CaO \cdot MgO$ and $CaCO_3 \cdot MgO$

Lignite: Feed $C_\alpha H_\beta O_\gamma N_\delta S_\varepsilon A$;
Fresh Char $C_{\alpha'} H_{\beta'} O_{\gamma'} N_{\delta'} S_{\varepsilon'} A$
Ash A

Not all of these require a differential equation for their description: Thus, since the change in the number of moles of $CaCO_3 \cdot MgO$ per unit time is the negative of that for $CaO \cdot MgO$, only one of these needs to be followed in time. A similar consideration applies to the ash. Also, if we assume that the time required to devolatilize feed lignite is extremely small, we can conceptualize the lignite feed stream as being a char feed stream, plus a gas feed stream which provides gaseous species according to the discussion in Section 5.3. Thus, we are left with a set of nine dependent variables, i.e., the seven gaseous species, unreacted acceptor, and char. We adopt the convention that the subscript i identifies these species according to Table 6.7.

Source Terms

Feed streams at the CO_2 acceptor pilot plant provide lignite and steam. Because the latter devolatilizes and undergoes rapid rate methanation virtually instantaneously upon introduction to the reactor, there are "equivalent" feed streams for most species due to the physical lignite feed stream. These actual and "equivalent" feed streams provide sources of mass S_i in Eq. (6.28).

If r is the mass rate of feeding lignite to the reactor, then we have for the char

$$S_8 = (1-x_v)r = 0.5782r \tag{6.29}$$

where x_v is the weight fraction of volatiles in the lignite (the numerical value is for Velva lignite, see Table 6.1).

The source term for methane S_3, is obtained from the discussion in Section 5.3.1 and 5.3.2 as

$$S_3 = r\alpha M_3 \left\{ b_1(T) + b_2(T)P_{H_2} \Big/ \left[1 + b_3(T)P_{H_2} \right] \right\} , \tag{6.30}$$

where M_3 is the molecular weight of methane. The hydrogen partial pressure P_{H_2} is obtained from the expression

$$P_{H_2} = \frac{m_1 M_1^{-1}}{\sum_{i=1}^{7} m_i M_i^{-1}} P \tag{6.31}$$

TABLE 6.7

INDEXING OF SPECIES

Index	Species
1	H_2
2	H_2O
3	CH_4
4	CO
5	CO_2
6	N_2
7	H_2S
8	C_α-H_β-O_γ-N_δ-S_ε-A
9	CaO·MgO (active part only)

where the M_i's are the molecular weights of the gaseous species. By combining Eqs. (6.30) and (6.31), S_3 is a specific function of P, T, and the masses of the seven gaseous species contained in the reactor. Since the latter vary in time, S_3 is itself a function of time.

The source terms for the other gases can be related to S_3 by making use of Eqs. (5.1), (5.2), (5.3), and (5.5). Following some algebra, we obtain

$$S_1 M_1^{-1} = r\left\{\frac{1}{2}(\beta-\beta') - (\varepsilon-\varepsilon') - (\gamma-\gamma')\right\} - 2S_3 M_3^{-1} + \frac{\left[r(\alpha-\alpha') - S_3 M_3^{-1}\right]\left(m_1 M_1^{-1} + 2\Phi K m_2 M_2^{-1}\right)}{m_1 M_1^{-1} + \Phi K m_2 M_2^{-1}} \tag{6.32}$$

$$S_2 M_2^{-1} = r(\gamma-\gamma') - \frac{\left[r(\alpha-\alpha') - S_3 M_3^{-1}\right]\left(m_1 M_1^{-1} + 2\Phi K m_2 M_2^{-1}\right)}{m_1 M_1^{-1} + \Phi K m_2 M_2^{-1}} + r\xi_2 \tag{6.33}$$

$$S_4 = \frac{m_1 M_1^{-1}\left[r(\alpha-\alpha') - S_3 M_3^{-1}\right] M_4}{m_1 M_1^{-1} + \Phi K m_2 M_2^{-1}} \tag{6.34}$$

$$S_5 = \frac{\Phi K m_2 M_2^{-1}\left[r(\alpha-\alpha') - S_3 M_3^{-1}\right] M_5}{m_1 M_1^{-1} + \Phi K m_2 M_2^{-1}} \tag{6.35}$$

$$S_6 = r(\varepsilon-\varepsilon')M_6 \tag{6.36}$$

$$S_7 = \frac{1}{2} r(\delta-\delta')M_7 \tag{6.37}$$

In these expressions K denotes the equilibrium constant for the water gas shift reaction (see Eq. (5.5)). The term $r\xi_2$ in Eq. (6.33) represents the steam feed stream to the reactor, the parameter ξ_2 being the ratio of the mass feed rates of steam to lignite.

Finally, the mass feed rate of acceptor is a specified parameter. We can write this rate as the product $r\xi_9$, where ξ_9 is the ratio of the mass feed rates of steam to lignite. For computational purposes, it is necessary to divide this accept mass into two parts, $\Theta_a r\xi_9$ capable of absorbing CO_2 and $(1-\Theta_a)r\xi_9$ which is unreactive and incapable of absorbing CO_2, as discussed in Section 6.4. Then we use

$$S_9 = \Theta_a r\xi_9 \tag{6.38}$$

to define the source term for active acceptor.

Chemical Reaction Terms

The chemical rate of formation of species i can be written in the form

$$R_i = \sum_{j=1}^{5} \nu_{ij}\Gamma_j \tag{6.39}$$

where ν_{ij} is the stoichiometric coefficient, i.e., it is the number of moles of species i formed (or destroyed)* per one equivalent of reaction j. Here Γ_j is the rate of reaction j, with the index j identified with reactions as indicated in Table 6.8. The rates of these reactions are expressed by Eqs. (6.8), (6.9), (6.10), and (6.27), respectively. At present, we use $\Gamma_4 = 0$. Numerical values for all parameters which appear in these equations are specified in Sections 6.2, 6.3, and 6.4. The various partial pressures P_i which appear in these equations can be expressed in terms of the species masses by

$$P_i = \frac{P\left(m_i M_i^{-1}\right)}{\sum_{j=1}^{7} m_j M_j^{-1}} \tag{6.40}$$

*A standard convention is to make ν_{ij} positive for products of a reaction, and negative for reactants.

TABLE 6.8

INDEXING OF REACTIONS

Index	Reaction
1	Modified Carbon-Steam Reaction (R5)
2	Low Rate Methanation Reaction (R9)
3	Water Gas Shift Reaction (R10)
4	Methane Steam Reforming Reaction (R11)
5	CO_2 Acceptor Reaction (R14)

Sink Terms

The exit streams provide the sink terms in Eq. (6.28). Determination of appropriate sink terms is somewhat difficult because of inadequate descriptive information as to the controls on exit flows at the pilot plant. As a model description, we have taken each sink term to be proportional to the corresponding mass in the reactor, i.e., of the form

$$N_i = a_i m_i \tag{6.41}$$

For the gaseous species this is equivalent to taking the exit flow rates to be proportional to the gas pressure. For the gases it is clearly the case that the value of the "choking constant" a_i should be the same for all gases. It is difficult to know a priori what numerical value should be assigned to this common a_i until we know in detail how the exit flows are controlled. However, what we can do is use trial and error procedures to find that value of a_i which leads to the volume (pressure) in a constant pressure (volume) calculation which in the steady state limit is equal to the measured volume (pressure) of the actual reactor. The result of such an approach should be the same as what we would obtain from a detailed knowledge of the exit flow controls.

The determination of the sink terms for the solid species also is difficult because of a lack of detailed information on flow controls on char and acceptor exit streams. However, there is an indirect procedure here, too, which provides the needed information. For the case of the acceptor, this procedure involves setting up and solving a system of three coupled differential equations describing the flows of unreacted reactive acceptor, reacted reactive acceptor, and unreactive acceptor. Solution of this system of equations in the steady state limit leads to the result

$$a_9 = \frac{r\Theta_a}{S_0}\left[1 + \Theta_a \rho_0 (M_c - M_a) M_a^{-1}\right] , \tag{6.42}$$

where M_c is the molecular weight of reacted acceptor, M_a is the molecular weight of unreacted acceptor, ρ_0 is the fraction of active acceptor which is carbonated during passage through the reactor, and S_0 is the acceptor inventory in the reactor at startup. All of these parameters either are known or can be estimated on the basis of pilot plant information, so that numerical evaluation of a_9 can be carried out.

Estimation of the constant a_8 is based on the idea that at steady state the ash inventory in the reactor will have a constant value, and that the ratio of the ash removal rate per unit mass of ash is the same as the ratio of the fixed carbon removal rate per unit mass of fixed carbon. This leads to

$$a_8 = \frac{rx_a}{W_a} \tag{6.43}$$

where x_a is the weight fraction of ash in the feed (see Table 6.1 for a numerical value) and W_a is the steady state ash inventory. The latter number can be estimated by combining data in the ash content of measured char samples (see Table 6.2) with an estimate of the total char inventory of the reactor at steady state. From information supplied to us by CCDC, the latter inventory is estimated to be 2.8141×10^5 grams.

Recycle Terms

Gas recycle at the pilot plant returns a fraction Θ_c of the dry exit gas stream to the gasifier. This fractional return rate is measured and known. The recycle stream terms are then given by

$$C_i = \Theta_c a_i m_i \quad (i = 1,3,4,5,6,7) \tag{6.44}$$

There is no recycle for i = 2 (H_2O) since the recycle returns dry gas to the reactor.

6.6 TEST RUN

Equations (5.1) - (5.5), (6.4), (6.8) - (6.10), (6.12), (6.27) - (6.44) completely define the chemical model in its present form. These equations were programmed in FORTRAN for the UNIVAC 1108 computer, using Gear's method (1969, 1971) to integrate the differential equations. Numerous trial runs were performed to check out the operation of the program. As discussed previously, lack of information on two parameters, Θ, the catalytic activity factor for ash; and a_1 (= a_2 = a_3 = a_4 = a_5 = a_6 = a_7), the exit rate parameter for gas flow, made it necessary to determine these factors by trial and error procedures involving repeated applications of the program.

In order to provide an indication of the quality of the results which are obtained by use of the computer program, we present now a specific computer simulation of the operation of the Rapid City, South Dakota pilot plant.

In Table 6.9 we list parameter values for this run, other than those which have been cited previously. To begin operation of the program, we must specify a starting state, i.e., a set of boundary conditions for the differential equation system. We have utilized various starting states. In all cases final convergence was to the same steady state, as we should expect. For illustrative purposes, we show results for a particular starting state in which the inventories of char and acceptor are approximately at their steady state values, the latter having been estimated from data supplied by CCDC. For this case, the gas phase is started as pure steam at the reactor operating pressure and temperature. Enthalpy calculations show that the reactor would operate endothermically for only about 21 secs after such startup, and that it would operate exothermically thereafter. Startup conditions are specified in Table 6.10.

Following startup, the reactor inventories vary in time as shown in Figure 6.2. Steam content of the reactor (which starts out offscale) drops to a steady state limit in about one minute. At the same time the other gas inventories rise, and following some damped oscillations reach steady state after about 10 minutes, except for H_2. The latter gas continues a slow increase which only levels off after about 100 minutes. (Note in viewing this graph that after about 2 minutes the M's representing methane are not seen because they coincide in locations with the C's representing CO. That is, to the scale available in this computer generated plot, the inventories of CO and CH_4 are the same at steady state.) The plots do not show N_2 and H_2S because the inventories are zero relative to the scale available in the plot.

Figure 6.3 shows the variation in time of the dry product gas from the reactor, expressed as mole fractions of the species. The points prior to 0.001 minute should be ignored, as they are numerical artifacts of the method of computation. Beyond this time, we see some oscillations which finally settle down to a uniform product gas composition about 10 minutes after startup. Again, H_2S and N_2 do not appear because they lie below the lower x-axis of the plot.

TABLE 6.9

SOME PARAMETERS OF A TEST RUN OF THE COMPUTER PROGRAM

Lignite Heat of Combustion	6310 cal/g (measured HHV at 60°F)
Char Heat of Combustion	6659 cal/g (estimated HHV at 60°F)
Lignite Feed Rate to Gasifier, r	18522 g/min
Steam Feed Rate Ratio, ξ_2	1.07 g/g lignite
Acceptor Feed Rate Ratio, ξ_9	3.59 g/g lignite
Steam Feed Temperature	1066°K
Acceptor Feed Temperature	1278°K
Lignite Feed Temperature	478°K
Reactor Operating Temperature, T	1085°K
Reactor Operating Pressure, P	9.3 atm (absolute)
Ash Catalytic Activity Factor, Θ	0.005
Acceptor Activity Factor, Θ_a	0.37
Acceptor Utilization Factor, ρ_0	0.99
Gas Exit Rate Parameter, a_1	1.7320 min^{-1}
Recycle ratio, Θ_c	0.2323
Char Exit Rate Parameter, a_8	4.5020×10^{-3} min^{-1}
Acceptor Exit Rate Parameter, a_9	3.3693×10^{-3} min^{-1}

TABLE 6.10

STARTUP CONDITIONS FOR A TEST RUN OF THE COMPUTER PROGRAM

Reactor Inventory	
H_2, CH_4, CO, CO_2, N_2, H_2S	0 moles
H_2O	1116 moles
Char	1.361×10^6 grams
Acceptor (active fraction 99 percent carbonated)	1.957×10^6 grams

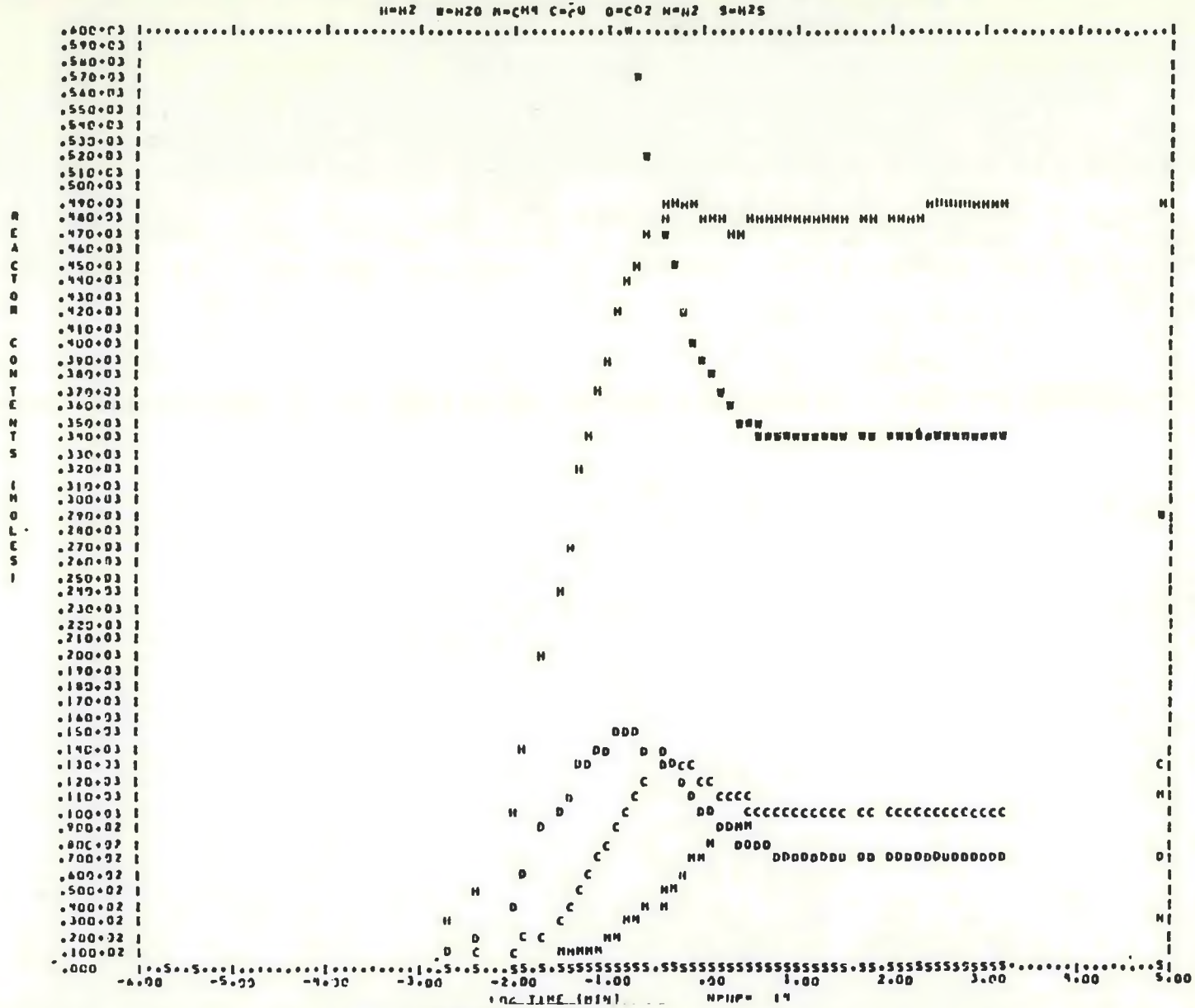

Figure 6.2. Computer generated plot of gas inventories of CO_2 acceptor pilot plant gasifier, plotted versus logarithm of time since startup. The symbols H, W, M, C, D refer to H_2, H_2O, CH_4, CO, CO_2, respectively.

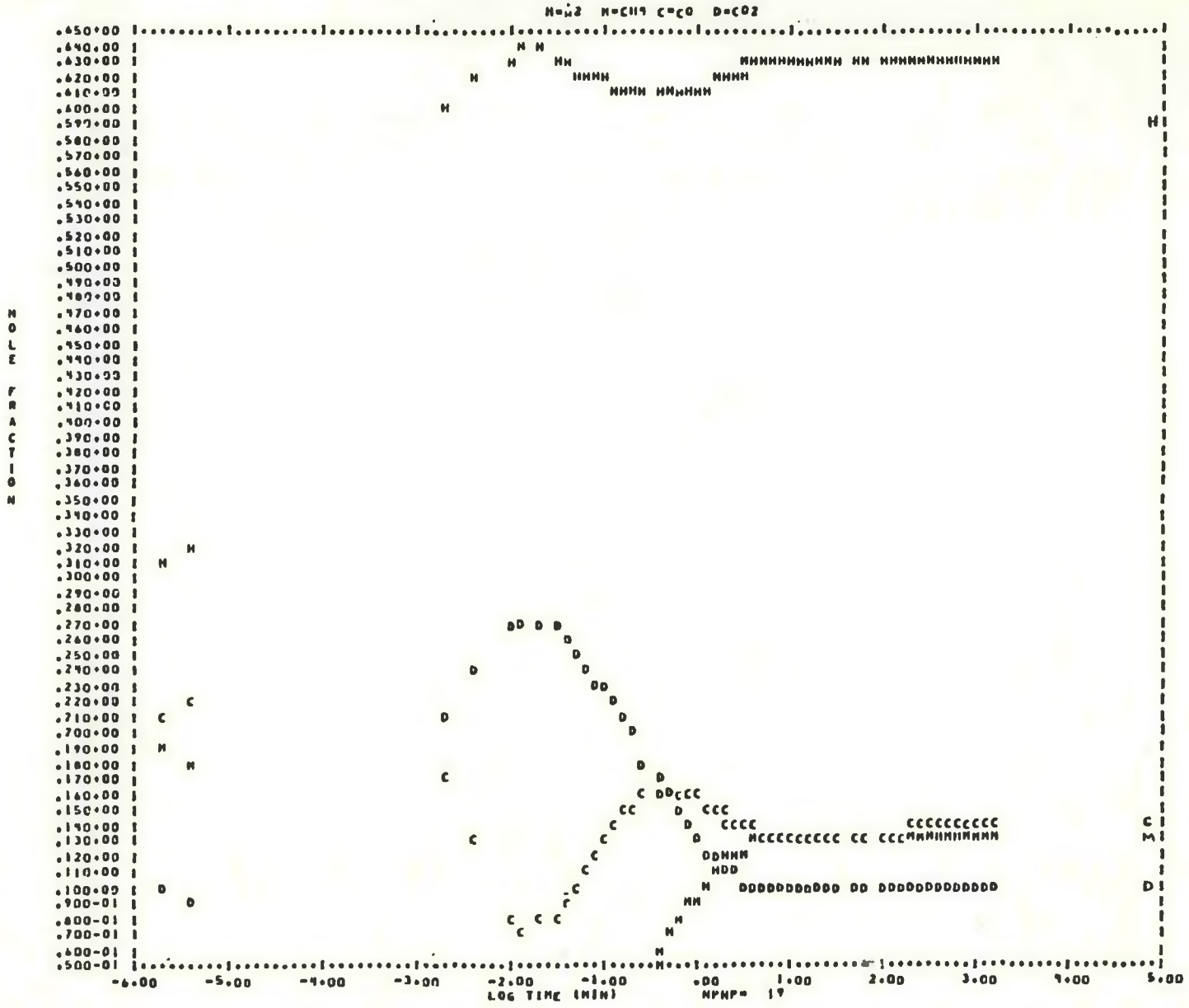

Figure 6.3. Computer generated plot of the composition of the product gas from the CO_2 acceptor pilot plant gasifier (dry basis). Symbols H, M, C, D refer to mole fractions of H_2, CH_4, CO and CO_2, respectively.

Figure 6.4 shows the inventories of char and acceptor in the reactor plotted versus time. We see that the acceptor inventory remains virtually unchanged. This is because the initial charge had a level of carbonation of its active component virtually identical to that found experimentally in the exit feed stream of the pilot plant. The char inventory increases and acquires a steady value about 300 minutes after startup.

We can examine the thermodynamic stability of the product gas (wet basis) or of the reactor contents in terms of several interesting thermodynamic ratios. Three of particular interest are:

(1) The water gas shift ratio, defined by

$$Q_W = \frac{P_{CO_2} P_{H_2}}{P_{CO} P_{H_2O} K_W} \tag{6.45}$$

(2) The methane-steam reforming ratio, defined by

$$Q_H = \frac{P_{CH_4} P_{H_2O} K_H}{P_{CO} P_{H_2}^3} \tag{6.46}$$

(3) The methane-hydrogen cracking ratio, defined by

$$Q_G = \frac{P_{CH_4}}{P_{H_2}^2 K_G} \tag{6.47}$$

In these three expressions, K_W is the equilibrium constant for the water gas shift reaction (R10), K_H is the equilibrium constant for the methane-steam reforming reaction (R11), and K_G is the equilibrium constant for the formation of methane from β-graphite and hydrogen (R6). These ratios are defined so that they are equal to one at equilibrium, are greater than one for a system in which the composition is shifted to the right of equilibrium, and are less than one for a system in which the composition is shifted to the left of equilibrium.

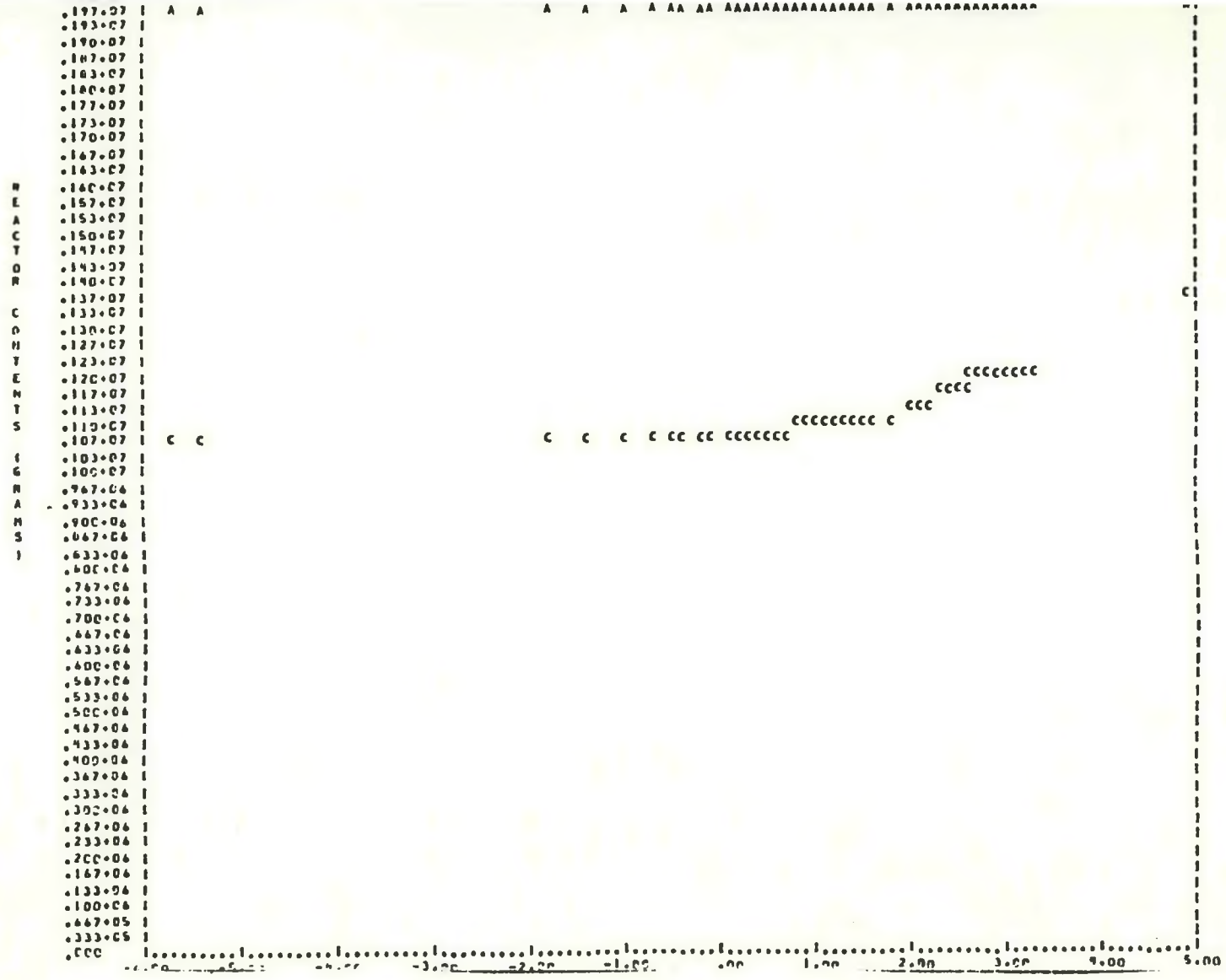

Figure 6.4. Reactor inventory of char (C) and acceptor (A) versus logarithm of time since reactor startup.

Figure 6.5 shows the variation in time of the three ratios, Q_W, Q_H, and Q_G. We see that Q_W achieves its equilibrium value of unity about 0.016 minute (1 second!) following startup, and remains at that value thereafter. This shows that even with the low assumed value $\Theta = 0.005$ of the ash catalysis factor Θ used in this run, that water gas shift equilibrium is for all practical purposes achieved instantaneously.

The ratio Q_H starts offscale and then passes through damped oscillations, finally stabilizing about 100 minutes after startup. The steady state value is about $Q_H \cong 9.3$, showing that the product gas is thermodynamically unstable with respect to the steam reforming of methane. The ratio Q_G also passes through a damped oscillation and settles down to a steady value at about one minute after startup. At steady state, its value is $Q_G \cong 1.26$, showing the system is also thermodynamically unstable with respect to cracking of methane to the elements.

The exit stream flow rates are among the most important parameters a model must predict. In Figure 6.6 we show plots of stream flow rates as functions of the logarithm of the time (in minutes) following startup. The exit mass flow rate for the acceptor is not shown on the graph because it is off scale. Numerically, its value is 7.575×10^4 gm/min,* commencing at startup, and it has virtually no variation in time. The char flow rate shows a slight upward drift following startup, and reaches a steady value about 200 minutes after startup. The steam flow rate starts offscale at about 3.5×10^4 g/min, but by about one minute after startup is nearly steady. There is a further slow decrease with a final steady value achieved after about 300 minutes. The flow rate of dry product gases starts at zero, becomes noticeable at about 2.5 seconds after startup, surges to a peak value about 12 seconds after startup, then undergoes an oscillating decay to a steady state value which is reached about 250 minutes after startup.

An interesting interpretation can be made of the results shown in Figure 6.6. The rapid changes in the flow rates which occur within the first several seconds after startup reflect the influence of the rapid processes which are taking place, primarily devolatilization, rapid rate methanation, water gas shift equilibrium, and CO_2 absorption. The slower changes over the next 250 minutes reflect the gradual onset of steady state with respect to the low rate

*This is the total mass of the acceptor stream, including inactive acceptor, inert impurities, and absorbed CO_2.

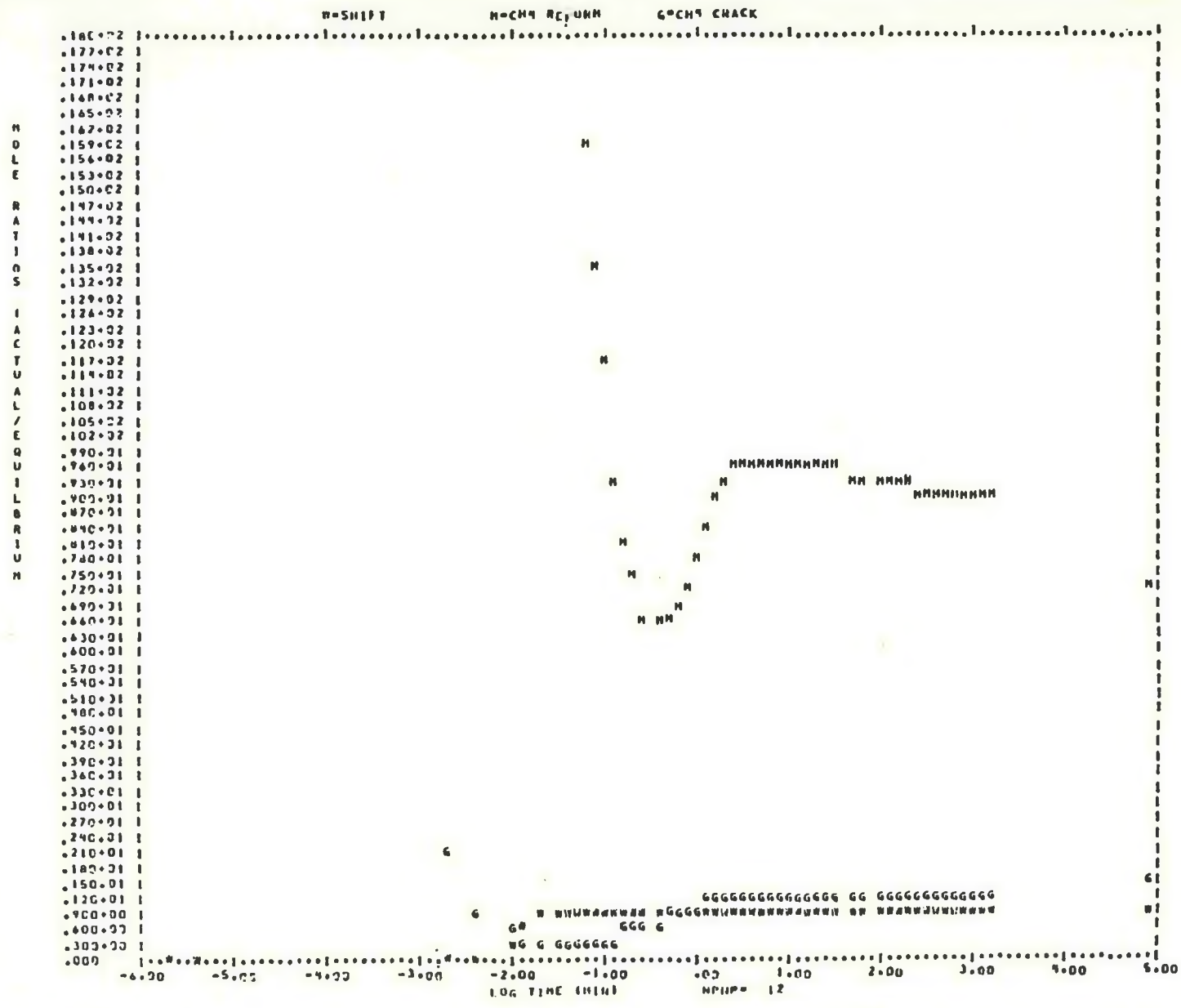

Figure 6.5. Time evolution of thermodynamic ratios for CO_2 acceptor process. W = Q_W (Eq. (6.45)); H = Q_H (Eq. 6.46)); G = Q_G (Eq. (6.47)).

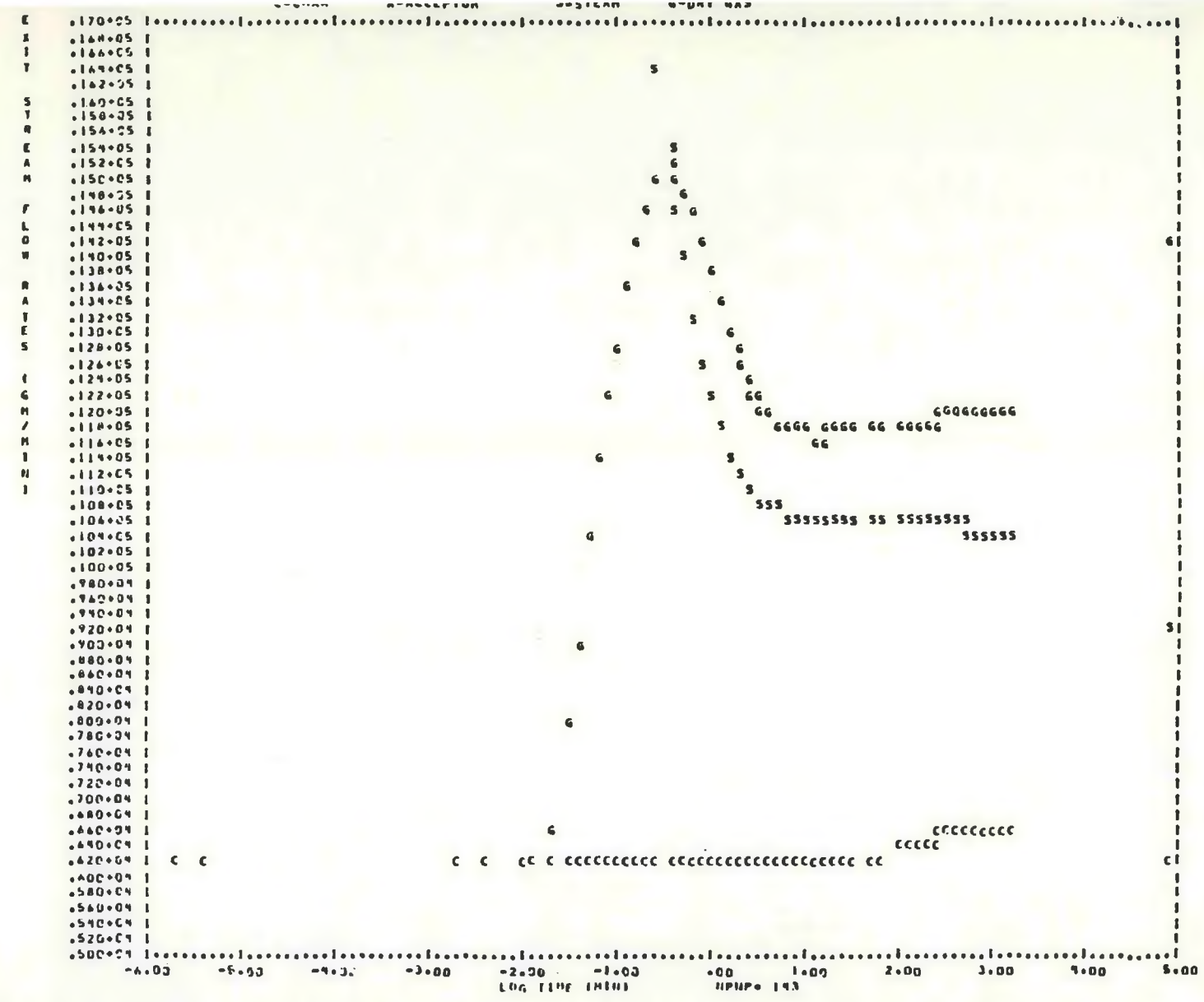

Figure 6.6. Exit stream mass flow rates (g/min) versus log of time (minutes). C = char stream; A = acceptor stream; S = unreacted stream; G = product gas (dry basis).

gasification processes. One can think of the system as having two characteristic chemical times: one for rapid processes of roughly 10 seconds duration, and one for slow processes of roughly 200 minutes duration.

There is interest in the chemical composition of the solids exit streams. In Figure 6.7 we show the time variation of the exit acceptor stream composition. In this plot, the M values denote the weight percent of MgO. The curves labeled C and D give the CaO* and absorbed CO_2 content of the stream. The absence of any observable timewise variation is a reflection of a fortuitous choice of boundary conditions for this run: the initial charge of acceptor in the system was taken to be about 0.990_a carbonated, which turns out to virtually coincide with the steady state value of the carbonation level.

In Figure 6.8 we show the variation of the product char composition, broken down into four components: carbon (C), hydrogen (H), nitrogen (N), and ash (A). In a manner similar to that for the acceptor, the composition of the initial charge was similar to that for the steady state, so that there are only small variations in composition with time. On the scale of the computer generated plot, this shows as a small jump at about 20 minutes, but as seen on computer generated data tabulations, there is a small variation in time which achieves a final steady state value after about 200 minutes. The time needed to achieve this steady state reflects the influence of the low rate gasification reactions.

Steady State Values

In the computer simulation run we are describing, calculations proceeded until a real time of 1700 minutes; i.e., about 28 1/2 hours, by which time all variables had long settled down to steady values.** The steady state values which are computed are of considerable interest, since they can be compared to measured or estimated steady state data from the Rapid City pilot plant.

In Table 6.11 we show computed steady state inventories of the various species in the reactor. We also show estimated values for the pilot plant, based upon data supplied to us by

---

* The CaO curve includes 7.93 weight percent inert materials, e.g., SiO_2, etc.; the actual CaO content is lower than shown in the graph by this amount.

** Only about 7 seconds of computer time are needed to achieve this.

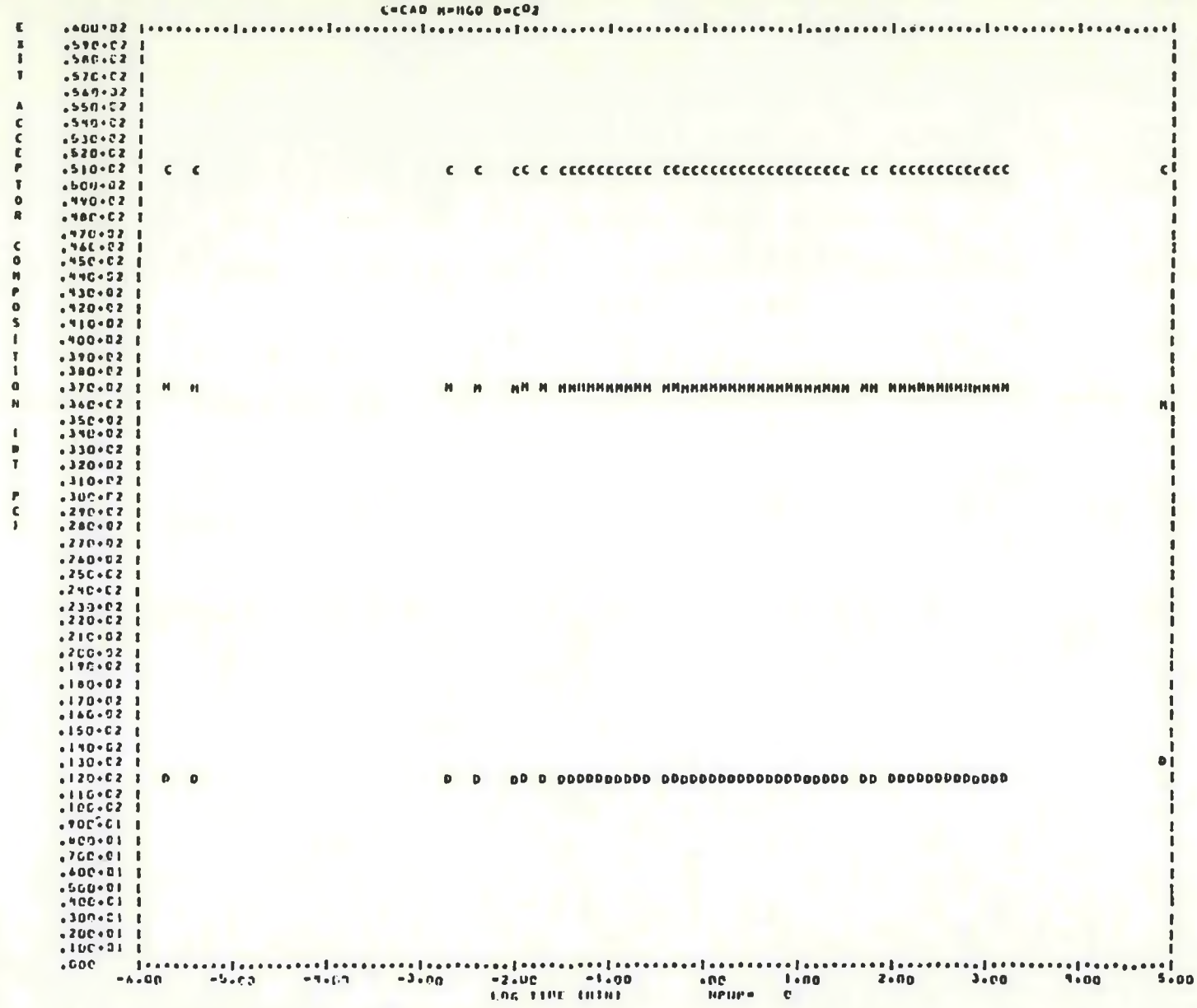

Figure 6.7. Acceptor exit stream composition (weight percent). C = CaO + inert ingredients, e.g., SiO_2; M = MgO; D = absorbed CO_2.

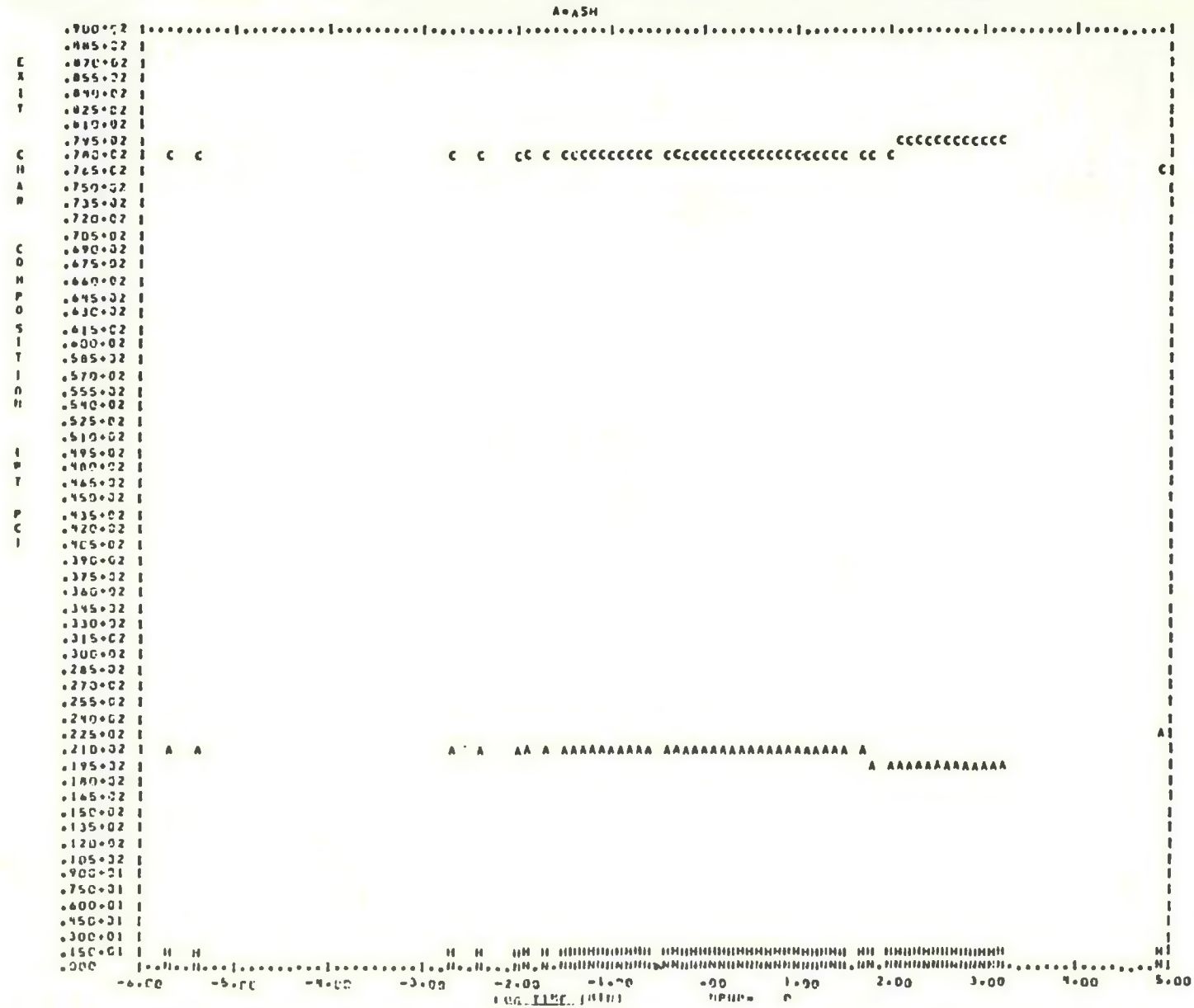

Figure 6.8. Ultimate analysis of product char stream for the CO_2 acceptor process, as a function of time following startup. C denotes carbon; H denotes hydrogen; N denotes nitrogen; A denotes ash. Units: Weight percent versus log time in minutes.

TABLE 6.11

MATERIALS INVENTORIES IN THE REACTOR IN STEADY STATE OPERATION

Material (Units)	Computed	Estimated, Pilot Plant
Hydrogen (moles)	486	490
Steam (moles)	336	286
Methane (moles)	98	113
Carbon Monoxide (moles)	105	127
Carbon Dioxide (moles)	75	75
Nitrogen (moles)	5	26
Hydrogen Sulfide (moles)	2	1
Ammonia (moles)	0	6
Acceptor (grams)*	1.95×10^6	1.96×10^6
Char (grams)	1.48×10^6	1.36×10^6

*Total mass, including absorbed CO_2.

CCDC.* Agreement is excellent in the major species. It is worth noting that relative to the pilot plant values, the computed values are a little too low for product gas species and a little too high for char and steam. This suggests that the kinetic parameters utilized in the calculation are a little smaller than the correct values, perhaps by about 10 percent. We will return to this point shortly.

The differences between computed and observed values for the two minor components, N_2 and H_2S, are worth noting. For N_2, the discrepancy is due to the fact that the pilot plant utilizes about 900 gms/min of N_2, in a purge stream which enters the gasifier. This small feed stream was neglected in our model. Its inclusion, which would not be difficult, would correct virtually all of the discrepancy shown in Table 6.11 for nitrogen. For H_2S, the discrepancy is due to the fact that our model does not include reaction (R17), which operates in the real gasifier, and which reduces the H_2S level. Inclusion of this minor reaction would lower the computed H_2S level and improve the agreement between computed and estimated inventories. The absence of the minor component NH_3 in the inventory is because we did not allow for its formation in our model. Its inclusion in the model would be possible, as mentioned previously.

Table 6.12 shows the values of the thermodynamic ratios Q_W, Q_H, and Q_G at steady state. As discussed previously, both observation and computation show that the system is at shift equilibrium, and that it is thermodynamically unstable with respect to methane loss both via steam reforming and cracking to the elements. The fact that the methane does not actually react by these or other reactions indicates the absence of kinetically available decomposition pathways at operating conditions.

Table 6.13 compares computed and observed steady state stream flow rates. The char rate indicated as observed is the sum of two rates, the first that through the main exit channel which feeds to the regenerator, the second stream being the char fines lost via the cyclone. As discussed previously, the computer model combines these two streams into one, so that the computed value represents the sum of the two streams.

Agreement is excellent. As noted previously, relative to the observations, the computations give char and unreacted steam exit flow rates which are about 10 percent too high, and a product gas rate which is too low by about the same amount.

---

*G. P. Curran (private communication).

TABLE 6.12

COMPUTED AND OBSERVED THERMODYNAMIC RATIOS
IN STEADY STATE OPERATION

Reaction	Ratio	Computed	Observed, Pilot Plant
Water Gas Shift	Q_W	0.99	0.96
Methane Steam Reforming	Q_H	9.01	7.28
Methane Cracking	Q_G	1.26	1.45

TABLE 6.13

COMPUTED AND OBSERVED EXIT STREAM FLOW RATES
AT STEADY STATE

Material (Units)	Computed	Observed, Pilot Plant
Char (g/min)	6648	6123
Acceptor (g/min)*	75750	76100
Unreacted Steam (g/min)	10490	9223
Product Gas (dry basis) g/min	11970	14290

*Includes absorbed CO_2.

This suggests that the parameters defining the gasification kinetics as used in the program are slightly too low in value. In view of the extreme difficulty associated with measurements of kinetic data, plus the complexities of our analysis of the data so as to provide parameters appropriate to modeling the Rapid City pilot plant, the agreement shown in Table 6.13 is remarkably good. Furthermore, we have the option of studying how much adjustment of our parameters would be needed to bring about closer agreement; and more importantly, we can determine which parameters affect the computed results most. Such information may enable us to improve our estimates of kinetic parameters. We plan to exploit this capability in Year Two of the program.

Table 6.14 compares composition data on the acceptor and char exit streams. Agreement is excellent. The fact that the carbon content of the char as computed is a little higher than as observed and that the ash content of the char as computed is a little lower than as observed is another reflection of the fact that the kinetic parameters used in the model are slightly too low in value. A similar comment can be made concerning the CO_2 content of the acceptor.

Table 6.15 compares computed and observed composition data on the product gas (dry basis). Agreement is excellent. The discrepancies noted for the minor constituents, N_2, H_2S, and NH_3 originate for the same reasons that we discussed above for the gasifier inventories of these species.

6.7 SUMMARY COMMENT

By way of summary, we can state again that the agreement between calculation and observation is excellent, particularly when we consider the as-yet not finalized state of the program. On the basis of these comparisons, we are optimistic that modifications, additions, and improvements planned for Year Two of the program, most particularly the coupling of the chemistry and thermohydrodynamics, will lead to the development of a valuable predictive tool for use in modeling fluidized bed gasification.

TABLE 6.14

COMPUTED AND OBSERVED COMPOSITION OF ACCEPTOR AND CHAR EXIT STREAMS OF THE CO_2 ACCEPTOR PILOT PLANT OPERATING AT STEADY STATE

Acceptor	Computed	Observed, Pilot Plant
CaO (weight percent)	43.2	43.5
MgO (weight percent)	36.7	36.0
Inert (weight percent)	7.9	7.9
CO_2 (weight percent)	12.2	12.6
Char	**Computed**	**Observed,* Pilot Plant**
C (weight percent)	79.6	76.5
H (weight percent)	0.9	0.9
O (weight percent)	0.0	0.0
N (weight percent)	0.4	0.4
S (weight percent)	0.0	0.0
Ash (weight percent)	19.1	22.2

*Weighted average of char stream to regenerator and char fines lost via cyclone.

TABLE 6.15

PRODUCT GAS COMPOSITION (DRY BASIS) OF THE CO_2 ACCEPTOR PILOT PLANT OPERATING AT STEADY STATE

Component (Units)	Computed	Observed, Pilot Plant
H_2 (mole percent)	63.1	59.0
CH_4 (mole percent)	12.7	13.5
CO (mole percent)	13.6	15.2
CO_2 (mole percent)	9.7	9.0
N_2 (mole percent)	0.6	3.2
H_2S (mole percent)	0.3	0.1
NH_3 (mole percent)	0.0	0.5

SECTION 7

CONCLUSIONS

The first year goals in this three year research effort were accomplished. This is evident from the satisfaction of the following milestones within the reporting period.

- One dimensional thermohydrodynamic code was developed and parametric calculations performed which provided good quantitative agreement with data.

- Chemistry code was developed and used in a homogeneous, constant temperature, steady flow calculation of CO_2 acceptor process gasifier. Good quantitative agreement between the calculation and the Rapid City Pilot Plant data was obtained.

- Two dimensional, thermohydrodynamic code was developed and limited parametric calculations were performed to study bubble formation, surface waves and solid convection. Qualitative comparisons with data have been made, showing that code results are representative of measurements.

In the second year of this project we will be combining the chemistry and thermohydrodynamic codes, together with descriptions of interphase transport, to model reactive flows in fluidized bed coal gasification. We expect to obtain preliminary calculations of such flows for comparison with experimental measurements.

During the second year we will also extend the chemistry code to include a representation of the chemistry for steam oxygen gasification processes. A theoretical description of the relative motion between different size solid particles will be formulated.

A continuing effort will be the optimization of the numerical formulations to insure that the code development provides the most economical computational method for the solution of reactive flows in fluidized beds.

ACKNOWLEDGEMENTS

Professor C. Y. Wen of West Virginia University has made many important contributions to this research effort. We would like to thank G. P. Curran of Conoco Coal Development Company for invaluable assistance in our development of a chemistry model for the CO_2 acceptor process.

PARTIAL LIST OF SYMBOLS

$B(\phi)$ = local mean drag function

C_V = specific heat of gas

C_V^S = specific heat of solid

d = particle diameter

$e(e^S)$ = specific internal energy in gas (solid) phase

$P^S(\phi)$ = interparticle "pressure" of solid

g_x = gravity acceleration in x-direction

g_y = gravity acceleration in y-direction

$G(\varphi)$ = elastic modulus = $- d/d\theta\ [\theta f(\theta)]$

$H(H^S)$ = volumetric rate of heat generation in gas (solid) phase

$k(\phi)$ = local permeability of the solid phase

N = Reynolds number (3.54)

P = gas pressure

$q_i(q_i^S)$ = heat flux vector in gas (solid) phase

Q = rate of interphase heat exchange

R = Reynolds number (3.49)

S = rate of interphase mass exchange

T = absolute temperature

t = time

u_i = solid velocity vector

v_i = gas velocity vector

x = horixontal direction

y = vertical direction

α = $\kappa/\rho^S c_v^S$

ϕ = porosity = gas volume fraction

θ = "solidity" = solid volume fraction = 1 - porosity

ρ^s = density of a solid particle (a constant)

ρ = gas density

σ_{ij} = stress tensor in gas phase

$\kappa(\theta)$ = thermal conductivity of solid-gas mixture

κ^s = thermal conductivity of solid

κ^f = thermal conductivity of gas

λ^s = effective "bulk viscosity" for the solid phase

μ^s = effective "shear viscosity" for the solid phase

ν = $\lambda^s + 4/3\ \mu^s$

ν' = $d\nu/d\theta$

μ = gas viscosity

ψ = friction factor (3.48)

Γ = shape factor

REFERENCES

Abel, W. T., and E. P. Fisher, 1975, "Limestone to Remove Hydrogen Sulfide from Hot Producer Gas," Morgantown Energy Research Center, Energy Research and Development Administration, Report No. ERDA MERC/RI-75/3.

Anderson, T. B., and R. Jackson, 1967, "Fluid Mechanical Description of Fluidized Beds, Equations of Motion," Ind. Eng. Chem. Fund., 6, pp. 527-539.

Anthony, D. B., and J. B. Howard, 1976, "Coal Devolatilization and Hydrogasification," A.I.Ch.E. Journal (to be published).

Avedesian, M. M., and J. F. Davidson, 1973, "Combustion of Carbon Particles in a Fluidized Bed," Trans. Instn. Chem. Eng., 51, pp. 121-131.

Bakker, P. J., and P. M. Heertjes, 1960, "Porosity Distributions in a Fluidized Bed," Chem. Eng. Sci., 12, pp. 260-271.

Bear, J., 1972, Dynamics of Fluids in Porous Media, Elsevier, New York.

Blake, T. R., and S. K. Garg, 1976, "On the Species Transport Equation and Flow in Porous Media," Water Resources Research, 12 , pp. 748-750.

Bohlbro, H., 1961, "The Kinetics of Water Gas Conversion at Atmospheric Pressure," Acta Chem. Scandinivica, 15, p. 502.

Bond, J. W., K. W. Watson, and J. A. Welch, 1965, Atomic Theory of Gas Dynamics, Addison Wesley, Reading, Massachusetts.

Curran, G. P., C. E. Fink, and E. Gorin, 1967, "CO_2 Acceptor Gasification Process. Studies of Acceptor Properties," Advances in Chemistry, 69, p. 141.

Curran, G. P., C. E. Fink, and E. Gorin, 1970, "Phase II, Bench-Scale Research on CSG Process. Operation of the Bench-Scale Continuous Gasification Unit," Office of Coal Research R&D Report No. 16, Interim Report No. 3, Book 3, January (GPO Catalog No. 163.10:16/Int. 3/ Book 3).

Curran, G. P., and E. Gorin, 1970, "Phase II, Bench-Scale Research on CSG Process. Laboratory Physico-Chemical Studies," Office of Coal Research R&D Report No. 16, Interim Report No. 3, Book 2, January (GPO Catalog No. 163.10:16/Int. 3/Book 2).

Davidson, J. F., and D. Harrison, editors, 1971, Fluidization, Academic Press, New York.

Dent, F. J., W. H. Blackburn, and H. C. Millett, 1937-38, 1938-39, "41st Report of the Joint Research Committee. The Investigation of the Use of Oxygen and High Pressure in Gasification. Parts II and III. Synthesis of Gaseous Hydrocarbons at High Pressure," Trans. Inst. Gas. Eng., 87, p. 231, 88, p. 150.

Dobner, S., R. A. Graff, and A. M. Squires, 1975, "Analysis of Trials of Synthane Steam Oxygen Fluid Bed Gasification Processes," presented at 68th Annual Meeting of the American Institute of Chemical Engineers, Los Angeles, California, 16-20 November.

Ergun, S., 1952, "Fluid Flow Through Packed Columns," Chem. Engn. Prog., 48(2), pp. 89-94.

Garg, S. K., and J. W. Pritchett, 1975, "Dynamics of Gas-Fluidized Beds," Jour. of Appl. Phys., 46, pp. 4493-4500.

Gear, C. W., 1969, "The Automatic Integration of Stiff Ordinary Differential Equations," Information Processing 68, North Holland Publishing Company, Amsterdam, Netherlands, pp. 187-193.

Gear, C. W., 1971, "The Automatic Integration of Ordinary Differential Equations," Communication of the Association of Computing Machinery, 14, p. 187.

Gelperin, N. I., and V. G. Einstein, 1971a, "Heat Transfer in Fluidized Beds," in Fluidization, J. F. Davidson and D. Harrison, editors, Academic Press, London and New York, pp. 471-540.

Gelperin, N. I., and V. G. Einstein, 1971b, "The Analogy Between Fluidized Beds and Liquids, in Fluidization, J. F. Davidson and D. Harrison, editors, Academic Press, London, pp. 541-568.

Gidaspow, D., and C. W. Solbrig, 1976, "Transient Two Phase Flow Models in Energy Production," presented A.I.Ch.E., 81st National Meeting, Kansas City, April 11-14.

Glenn, R. A., E. E. Donath, and R. J. Grace, 1967, "Gasification of Coal under Conditions Simulating Stage 2 of the BCR Two-Stage Super-Pressure Gasifier," Advances in Chemistry, 69, p. 81.

Harlow, F. M., and A. A. Amsden, 1975, "Numerical Calculation of Multiphase Fluid Flow," Jour. Comp. Phys., 17, pp. 19-52.

Institute of Gas Technology, 1976, Coal Conversion Systems Technical Data Book.

Ishida, M., and C. Y. Wen, 1968, "Effectiveness Factors and Instability in Solid-Gas Reactions," Chem. Eng. Sci., 23, p. 125.

Johnson, J. L,, 1974, "Kinetics of Bituminous Coal Char Gasification with Gases Containing Steam and Hydrogen," Advances in Chemistry, 131, p. 145.

Johnson, J. L., 1975, "Gasification of Montana Lignite in Hydrogen and in Helium During Initial Reaction Stages," Div. of Fuel Chemistry, American Chemical Society, Chicago, August 24-29; preprints, Vol. 20, No. 3, pp. 61-87.

Landau, L. D. and E. M. Lifshitz, 1959, Fluid Mechanics, Addison Wesley, Reading.

Leva, M., M. Weintraub, M. Grunner, M. Pollchik, and H. H. Storch, 1951, "Fluid Flow Through Packed and Fluidized Systems," Bu Mines Bulletin 504.

Leva, M., 1959, Fluidization, McGraw Hill, New York, New York.

Lewis, P. S., S. Friedman, and R. W. Hiteshue, 1967, "High BTU Gas by Direct Conversion of Coal," Advances in Chemistry, 69, p. 50.

Matsen, J. M., S. Hovmand, and J. F. Davidson, 1969, "Expansion of Fluidized Beds in Slug Flow," Chem. Eng. Sci., 24, p. 1743.

Moe, J. M., 1962, "Design of Water Gas Shift Reactors," Chem. Eng. Progress, 58, p. 33.

Moseley, F., and D. Paterson, 1967, "The Rapid High-Temperature Hydrogenation of Coal Chars." Part 1: "Hydrogen Pressures up to 100 Atmospheres," J. Inst. Fuel, 38, p. 13; Part 2: "Hydrogen Pressures up to 1,000 Atmospheres," J. Inst. Fuel, 38, p. 378; "The Rapid High Temperature Hydrogenation of Bituminous Coal," J. Inst. Fuel, 40, p. 523.

Murray, J. D., 1965, "On the Mathematics of Fluidization, Part I. Fundamental Equations and Wave Propagation," Jour. Fluid Mech., 21, Part 3, pp. 465-493.

Penner, S. S., 1957, Chemistry Problems in Jet Propulsion, Pergammon Press, New York.

Pyrcioch, E. J., H. L. Feldkirchner, C. L. Tsaros, J. L. Johnson, W. G. Bair, B. S. Lee, F. C. Schora, J. Huebler, and M. R. Linden, 1972, "Production of Pipeline Gas by Hydrogasification of Coal," Institute of Gas Technology Research Bulletin, No. 39, pp. 92-117, Chicago, Illinois.

Rehmat, A., and S. C. Saxena, 1976, "Single Nonisothermal Non-catalytic Solid-Gas Reaction. Effect of Changing Particle Size," I. and E.C. Process Des. Dev., 15, pp. 343-349.

Richardson, J. F., 1971, "Incipient Fluidization and Particulate Systems," in Fluidization, J. F. Davidson and D. Harrison, editors, Academic Press, London and New York.

Richtmyer, R. D., and K. W. Morton, 1967, Difference Methods for Initial Value Problems, 2nd Edition, Interscience, New York.

Rietema, K., and S. M. P. Mutsers, 1973, "The Effect of Interparticle Forces on the Expansion of a Homogeneous Gas-Fluidized Bed," Chem. Engn. Science, 28, pp. 1493-1497; "An Investigation into the Occurrence of Elastic Phenomena in Homogeneous Gas-Fluidized Beds," Inst. of Chem. Engineers Research Meeting, Bradford; "On the Elasticity of Gas-Fluidized Systems," International Fluidization Conference, Asilomar, June 15-20.

Ruth, L. A., A. M. Squires, and R. A. Graff, 1972, "Desulfurization of Fuels with Half-Calcined Dolomite: First Kinetic Data," Environmental Science and Technology, 6, pp. 1009-14.

Schügerl, K., 1971, "Rheological Behavior of Fluidized Systems," pp. 261-292, in Fluidization, J. F. Davidson and D. Harrison, editors, Academic Press, London.

Vennard, J. K., 1946, Elementary Fluid Mechanics, John Wiley, New York.

VonFredersdorff, C. G., and M. A. Elliott, 1963, Coal Gasification," in Chemistry of Coal Utilization, Supplementary Volume, H. H. Lowry, editor, John Wiley, New York, pp. 892-1022.

Wen, C. Y., S. Mori, J. A. Gray, and P. M. Yavorsky, 1975, "Hydrogasification of Hydrane Char in Fluidized and Moving Beds," Div. of Fuel Chem., A.C.S., Chicago, Illinois, August 24-29; preprint 20, No. 4, pp. 155-206.

Zahradnik, R. L., and R. A. Glenn, 1971, "Direct Methanation of Coal," Fuel, 50, p. 77.

Zahradnik, R. L., and R. J. Grace, 1974, "Chemistry and Physics of Entrained Coal Gasification," Advances in Chemistry, 131, p. 126.

*U.S.GOVERNMENT PRINTING OFFICE:1977 -740 -062/ 71 REGION NO. 4